Investigations on the Applicability of Pressure Slip Casting and 3D Printing for Alumina (Al_2O_3) and Aluminum Titanate (Al_2TiO_5) Systems

A dissertation work

submitted in partial fulfilment of the requirements for the award of the degree of

DOCTOR OF PHILOSOPHY

in

METALLURGICAL AND MATERIALS ENGINEERING

By

P RAJU

(Roll No:718052)

Under the guidance of

Dr. M. Buchi Suresh, Scientist "E"
Centre for Advanced Ceramic Materials
International Advanced Research Centre for Powder Metallurgy and New Materials,
Hyderabad.

Dr. Asit Kumar Khanra, Professor
Department of Metallurgical and Materials Engineering
National Institute of Technology
Warangal.

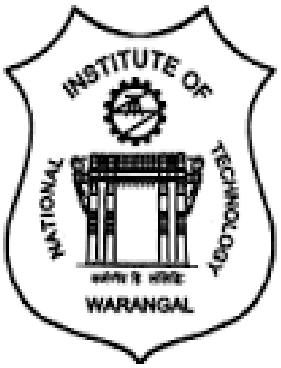

DEPARTMENT OF METALLURGICAL AND MATERIALS ENGINEERING

NATIONAL INSTITUTE OF TECHNOLOGY WARANGAL

MARCH-2023

Dedicated to

My Family and Friends

Thesis Approval for Ph.D.

The thesis entitled "Investigations on the Applicability of Pressure Slip Casting and 3D Printing of Alumina (Al_2O_3) and Aluminum Titanate (Al_2TiO_5) Systems" is submitted by Mr. P. Raju (Roll No.718052) is approved for the degree of Doctor of Philosophy in Metallurgical and Materials Engineering.

Examiner(s)

_____

_____

Supervisor(s)

_____

_____

Chairman

_____

Date: _____

DEPARTMENT OF METALLURGICAL AND MATERIALS ENGINEERING

NATIONAL INSTITUE OF TECHNOLOGY

WARANGAL - 506 004 (T.S) INDIA

CERTIFICATE

This is to certify that the work presented in the thesis entitled "**Investigations on the Applicability of Pressure Slip Casting and 3D Printing for Alumina (Al_2O_3) and Aluminum Titanate (Al_2TiO_5) Systems**" which is being submitted by Mr. P. Raju (Roll No.718052) to the National Institute of Technology Warangal in partial fulfilment of the requirements for the award of the degree of Doctor of Philosophy in Metallurgical and Materials Engineering is a bonafide work carried out under my supervision. To the best of our knowledge, the work incorporated in this thesis has not been submitted to any other university or institute for the award of any other degree or diploma.

Dr. M. Buchi Suresh
Scientist "E"
Centre for Advanced Ceramic Materials
International Advanced Research Centre
for Powder Metallurgy and New
Materials, Hyderabad.

Dr. Asit Kumar Khanra
Professor
Department of Metallurgical and
Materials Engineering
National Institute of Technology
Warangal.

DECLARATION

This is to certify that the work presented in the thesis entitled "**Investigations on the Applicability of Pressure Slip Casting and 3D Printing for Alumina (Al_2O_3) and Aluminum Titanate (Al_2TiO_5) Systems**" is a bonafide work done by me under the supervision of Dr. Asit Kumar Khanra, NITW and Dr. M. Buchi Suresh, Scientist E, ARCI and was not submitted elsewhere for the award of any degree. I declare that this written submission represents my ideas in my own words and where others' ideas or words have been included, I have adequately cited and referenced the original sources. I also declare that I have adhered to all principles of academic honesty and integrity and have not misrepresented or fabricated or falsified any idea/data/fact/source in my submission. I understand that any violation of the above will be a cause for disciplinary action by the Institute and can also evoke penal action from the sources which have thus not been properly cited or from whom proper permission has not been taken when needed.

(P Raju)

Acknowledgements

I would like to take this opportunity to express my sincere gratitude and appreciation to my research supervisors, Dr. Asit Kumar Khanra, Professor, Department of Metallurgical and Materials Engineering, National Institute of Technology, Warangal, and Dr. M. Buchi Suresh, Scientist-E, ARCI Hyderabad for their unwavering support, inspiration, direction, and patience throughout the research process. This thesis would not have been feasible without his tireless mentoring, frequent inspiration, helpful talks, and ideas. Working under his direction was a true honour and privilege. I would like to take this opportunity to express my sincere appreciation and gratitude to Dr. Y. S Rao, Scientist G, B.P. Saha Scientist G, Head of the Centre for Advanced Ceramic Materials, and also Dr. Roy Johnson Scientist G and Associate Director, ARCI, Hyderabad for their support.

I am grateful to Prof. N.V. Ramana Rao, Director, NIT Warangal and Dr. Tata Narasinga Rao, Director, ARCI, Hyderabad for giving me an opportunity to carry out research work.

My sincere thanks to the Doctoral Scrutiny Committee members, Dr. T. Mahesh Kumar Talari (Chairman & Head of the Department), Dr. Brahma Raju Golla (Associate professor), Dr. V. Rangadhara Chary (Assistant professor), Department of Metallurgical and Materials Engineering, and Dr. T. Venkatappa Rao (Professor), Department of Physics, NIT Warangal for their helpful suggestions, during periodical review of my research progress. I am thankful to Dr. Papiya Biswas, Sc ‘E’, Dr. S. Kumar Sc-E, other scientists Dr. Pandu Ramavath, Dr Amith Das, Dr. Shiv Prakash singh, from ARCI.

I sincerely acknowledge the technical support provided by the organisation during the entire period of doctoral research study. I thank technical staff Mr. G. Anjababu, Rajeshekar Reddy, Yadagiri, Sushanth, for helping me to carry out Laboratory Experiments at ARCI Hyderabad.

I would like to extend my gratitude to my former and current lab colleagues and friends Dr. Vemoori Raju, Dr. Katti Bharath, Dr. Shaik Mubina Mr. V. Ganesh, Miss. S. Mamatha. for their assistance with tests.

Finally, I would like to express my sincere gratitude to my grandparents, father Sri. P. Ramulu, mother Smt. Prameela, wife Mrs. Pravallika, son Sreeman and daughter Sudheeksha, mother-in-law Mrs.Ch. Jaya, father-in-law Sri.Ch. Venkateshwarlu, as well as other family members for their patience, compassion, love, support, and motivation.

P RAJU

(MARCH-2023)

List of Abbreviations

AL-Alumina (Al_2O_3)

ALT-Aluminum Titanate ($Al_2 TiO_5$)

MR-01-Alumina particle size of 1 micron

HIM-10-Alumina particle size of 7 microns

HM-Mix of Alumina grades of 1 and 7 microns

MC-Methyl Cellulose

Wt.%-Weight Percent

CSC- Conventional Slip Casting

PSC- Pressure Slip Casting

SAMA-Scientific Apparatus Makers Association

PCS-Pressure Casting System

PCM-Pressure Cast Machine

CIP-Cold Iso-static Pressing

POP-Plaster of Paris

SS316-Stainless Steel 316 grade

AM-Additive Manufacturing

3DP-3Dimensional Printing

CAD-Computer Aided Design

STL- Standard Tessellation Language

FDM-Fused Deposition Modelling

FFF- Fused Filament Fabrication

DIW- Direct Ink Writing

CODE-Ceramic On-Demand Extrusion.

DMLS-Direct Metal Laser Sintering

SLM-Selective Laser Melting

EBM Electron Beam Melting

SHS-Selective Heat Sintering

MJF-Multi Jet Fusion

CAD- Computer Aided Design

CATIA-Computer Aided Three-Dimensional Interactive Application

PM-Powder metallurgy

XRD-X-ray diffraction

ICDD- International Centre for Diffraction Data

TG-DTA-Simultaneous Themo Gravimetric - Differential Thermal Analyser

FESEM-Field Emission Scanning Electron Microscope

SEM-Scanning Electron Microscopy

ASTM- American Society for Testing and Materials

UTM-Universal Testing Machine

SENB-Single Edge Notch Beam

CTE-Coefficient of Thermal Expansion

List of Symbols

D_{50}-Average of particle size

μm-Micro Meter

θ -Diffraction angle

d -Interplanar spacing

λ -Wave length

°C -Degree Celsius

ρ - Density

ϕ -Diameter

P -Load

N-Newton

MPa-Mega Pascal

Bar-10^5Pascal

Abstract

Since the previous few decades, researchers have tried to increase fracture toughness and microstructure modification in an effort to address the issue of ceramics intrinsic brittleness, which has limited its use in structural applications. Researchers have looked into how ceramic materials can be altered so that one or more mechanisms can be activated to improve the desired properties. Every facet of a ceramic component's material performance is governed by the processing history, the inherent material qualities, and other variables. Colloidal forming is a common technique for shaping ceramics because it has the advantages of increased uniformity, densification at lower temperatures, and flexibility in complex design. The goal of the current study was to create oxide-based ceramic products using various ceramic processing techniques in order to achieve the necessary complicated shapes and densification levels for best mechanical properties.

Pressure slip casting is a technique known in table ware industry for producing near net-shaped green bodies with shorter processing cycles and very good consistency. Of-late, the possibility of utilizing the pressure slip casting technique for making advanced ceramic components started being looked at to exploit the advantages associated with it such as the higher green densities, near net shaping, consistency and the productivity. The preparation and control of stable, well-dispersed ceramic slip is considered as key parameter to achieve the desired properties in the green bodies. An emerging preparation method for pressure-assisted casting of advanced ceramics allows for the use of colloidal slips during pressure-based shaping. In addition to good homogeneity, outstanding green density, strength, and high productivity, the application of pressure allows for flexibility in the formation of complex structures. The current study contrasts the methods used to prepare alumina green bodies, including conventional slip casting (CSC), pressure slip casting (PSC), and cold isostatic pressing (CIP). Additionally, the ceramic products were created using ceramic 3D printing and contrasted with colloidal techniques such as CSC, PSC, and CIP. Corresponding mechanical properties of the dense ceramics were also characterised, along with their microstructural characteristics. For this purpose, both the polymer based and Plaster of Paris moulds were fabricated by designing to cast objects in the standard shapes of a cylindrical disc ϕ 80 mm, square of 60 mm, and a spherical ball of ϕ 60 mm.

Present work has been undertaken with a focus on studying the shaping of Al_2O_3 and its combinations by pressure slip casting process and understanding the results in comparison

with that of the conventional slip casting method. Aluminum Titanate (Al_2TiO_5) and Alumina (Al_2O_3) products are prepared from powder state in a variety of proportions and to optimise slip preparation for appropriate rheological behaviour and colloidal ceramic processing processes (CSC, PSC). The same initial alumina powder produced by mixing powders with two different average particle sizes (7 μm and 1.43 μm) in the ratio of 65:35 was utilised in all three operations because to the fixed pore size of the mould. The average particle size (d_{50}) of the mixture HM-mix powder is 3.18 μm. The optimization of slip/slurry has been done with solid loadings varying from 65% to 80% along with rheological behaviour of shear thinning which is required in pressure slip casting for better consolidation. The shear thinning behaviour that is a necessary characteristic in the development of casts is demonstrated by the rheological data stress-exponent n=0.5. The plot unequivocally exhibits a pseudoplastic behaviour appropriate for CSC and PSC processes. Under conditions of atmospheric pressure by CSC and external pressures of up to 35 bar by PSC casts for cylindrical discs, square, and Spherical Alumina balls samples were made. According to the results of the TG-DTA experiments, the samples sintering schedules developed over time at a slow heating rate of 10°C per minute up to the final sintering temperature of 1600°C.The green densities of the discs were calculated after drying and before subjecting them for sintered schedule with the peak temperature of 1600^{o}C.It has been observed that green densities of 65%TD at 35 bar for PSC and 66%TD at 1200 bar following CIP were achieved which is attribute to interlocking nature. However, the density of the CSC samples was only 50%TD. Flexural strength and fractographic examinations were conducted and connected with the corresponding processes. Also, the samples were sintered at 1600 °C to test their sinterability.

The PSC products have a high density due to the compact packing made possible by applying pressure to the slip, which complements the enhancement of the hardness. The PSC processed samples with refined grain structure and minimal imperfections/pores is found to improve the mechanical properties such as hardness, flexural strength, and fracture toughness, which are measured to be 14.92±0.15 GPa, 294.40 ± 2.5 MPa, and 4.06 ± 0.25 MPa $m^{1/2}$ respectively in comparison of conventional cast sample's respective values of 3.73 ± 0.25 MPa $m^{1/2}$, 242.70 ± 2.5 MPa, and 11.77 ± 0.15 GPa, it is clear that the mechanical properties are improved. Alumina (Al_2O_3) is a favoured material for wear-resistant applications due to its high mechanical as well as chemical inertness. Owing to the mechanical properties, PSC alumina is shown to have a 56% lower wear rate than CSC alumina, with a wear rate as low as 2.35×10^{-18} m^3/Nm (with 0.5 m/sec at 5N load). Commercial repercussions in the ceramic sector

will result from PSC alumina's improved wear rate. Successfully demonstrated that the physic-thermal properties of Alumina and Aluminum Titanate were measured for a variety of geometrical shapes. Titania and Alumina MR-01 powders were combined dry in an equimolar ratio of 1 (TiO_2): 1.27 (Al_2O_3) and ball milled for four hours. After blending, the dry mixture was heated to between 1350 -1440 degrees Celsius for two hours soaking, in order to calcinate the powder to generate the aluminium titanate phase using the solid-state reaction pathway. The X-ray diffraction method along with line scanning of FESEM Microstructures, will be used to confirm the phase. According to the same predictions, XRD patterns and FESEM results show the confirmed phase of aluminium titanate. Alumina, titanium, and aluminium titanate all had particle size distributions of 1.43 mm, 0.5 mm, and 1.27 mm, respectively. The slips have been prepared for calcined powder of Aluminum Titanate in varying proportionate ranging from 30 - 45 wt. % Solid loadings and with additions of remaining water in order to get best way of cast in both the processes. For the 45 wt.% of solid loading its giving the better required rheological behaviours and measured shear rate exponent around 0.5. The observed green, sintered densities in the cases of 3D-printed AL and AT ceramics are in the ranges of 55-57% and 65-70% of theoretical density, respectively. It is reported that the Al_2TiO_5-containing sintered samples made by CSC and PSC have a low thermal expansion coefficient. PSC, with a value of $1.88 \times 10^{-6}\ K^{-1}$, and CSC, with a value of $2.20\times10^{-6}\ K^{-1}$, have the lowest thermal expansion coefficients at 1100 °C and also the samples of sintered materials by 3D printed with a value of CTE is $2.58 \times10^{-6}\ K^{-1}$.

Key Words: Pressure slip casting (PSC), Slip solid loading, Rheological behaviour, Interlocking, Microstructure, Mechanical properties, Ceramic 3D Printing, Coefficient of Thermal Expansion, Al_2O_3 and Al_2TiO_5.

Index

LIST OF FIGURES

LIST OF TABLES

CHAPTER 1

INTRODUCTION

1.1 Introduction to ceramics:

Ceramics are a material group that has a long history and was originally made from natural resources like clay and various alumina's. For thousands of years, humans have utilised ceramics to create tools and artwork. Ceramics are solid compounds created by applying heat, and occasionally pressure along with heat and consisting of with at least two elements, one of which must be a non-metal or non-metallic elemental solid. A non-metallic elemental solid or a metal could make up the second component. Kingery provided a clearer definition of ceramics by stating that it is "The art and science of manufacturing and using solid items, having their basic component and being primarily composed of inorganic non-metallic materials". A ceramic, then, is a substance that is neither a metal, a semiconductor, nor a polymer [1-2].

1.1.1 Classification of ceramics:

Traditional ceramics and advanced ceramics are the two types of ceramics available. Traditional ceramics have porous microstructures that are generally silicate-based, coarse, non-uniform and multiphase. They are normally made by mixing clays and feldspars, then moulding them on a potter's wheel or by slip casting, sintering them in a flame kiln, and finally glazing. Some ceramics that aren't made of clay or silicate relied on far more complex raw materials, like binary oxides, carbides, perovskites, and even completely synthesised substances for which there aren't any existing natural analogues. These contemporary ceramics contain microstructures that are at least one order of magnitude more uniform, less porous, and finer than their conventional parts [3].

Ceramics can be classed based on their chemical makeup [4].

1. Oxide Ceramics - constructed entirely of oxides such as Al_2O_3, MgO, ZrO_2, $MgO.SiO_2$, and so on
2. Non-oxide ceramics-no oxides are present, such as BC, SiC, Si_3N_4 and
3. Based on the number of compounds

a) Monolithic ceramics are made up of only one compound, such as clay, glass, SiC, AlN, or YAG
b) Composite ceramics: made up of several different materials, such as concrete

4. Based on atom arrangement -
    a) Crystallite Ceramics: Atoms in these materials have a specific periodicity and long-range order across the substance, such as pottery.
    b) Amorphous Ceramics: Atoms are randomly organised and there is no short-range order of atoms, as in glass.

Ceramics are normally made by combining constituent powders with water or a binder, pressing the powders into the desired shape, pre-firing to remove the binder, and sintering at a high temperature to accomplish full densification. Because, the brittleness of traditional ceramics is a major drawback, new novel ceramic materials have been investigated. Ceramics with outstanding hardness and thermal stability are employed in specialised applications across the industry [5].

1.2 Alumina Ceramics: Alumina, also known as aluminium oxide (Al_2O_3), has long been a preferred candidate material for the production of armour systems, abrasive materials, cutting tools, electronics, aero and automotive parts due to its superior properties, which include low density, high melting temperature, high hardness, chemical inertness, good wear resistance, corrosion resistance, and good thermal and electrical insulating properties. Nevertheless, alumina (Al_2O_3) brittleness and poor bending strength have restricted its use in structural applications and the industry for some innovative components, which has encouraged researchers to gradually increase alumina's fracture toughness. [6].

1.2.1 Alumina phases: Aluminum oxide, also known as corundum (Al_2O_3), diaspore or gibbsite, and bauxite, is the only oxide produced by the metal aluminium. Aluminum hydroxides, which are impure mixes of gibbsite, $Al(OH)_3$, boehmite, and diaspore, polymorphs are the most common type of alumina found in nature AlO(OH). After being mined, most raw bauxite ores must be processed using the Bayer process. This process removes the impurities after calcination at temperatures as high as 1600^{o}C, leaving a nominal 99.5% alumina. Around 100%-Alumina is produced by calcination at high temperatures, although finer powders may still contain some of the transitional alumina phases shown when calcination is done at lower temperatures. Because, transition alumina's, unlike the alumina phase, have somewhat disordered crystal structures, this may present some difficulty in subsequent processing of the

powder. Since the structural characteristics of transition Alumina's rely on the surface characteristics/morphology of the beginning material and its thermal calcination conditions, this transition sequence is idealised. Phase changes in alumina are accompanied by symmetry changes, which produce a variety of polymorphs and both. Transition alumina's (Table 1.1) are particularly difficult to study because of their similar diffraction patterns, low crystallinity, and smaller particle size [7-8].

Table 1.1: Thermal transition of alumina's derived from calcination of alumina [9].

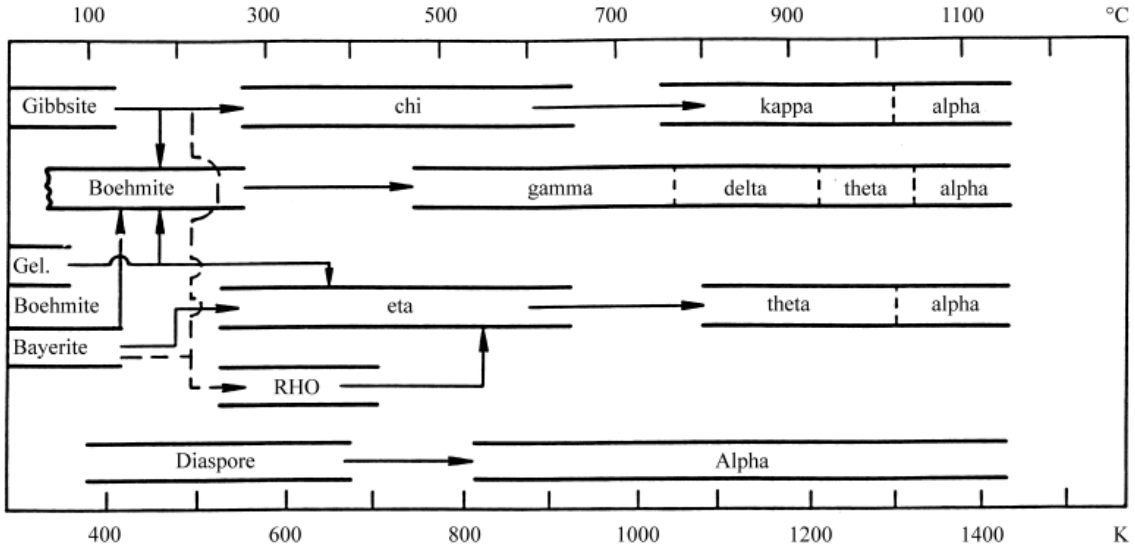

$$\text{Boehmite}\ (AlOOH) \xrightarrow{800K} \gamma\text{-Alumina}\ (Al_2O_3) \xrightarrow{1000K} \delta\text{-Alumina} \xrightarrow{1200K} \theta\text{-Alumina} \xrightarrow{1300K} \alpha\text{-Alumina}$$

1.2.2 Crystalline Structures of Alumina:

The basic unit cell structure of corundum is hexagonal. The atoms in aluminium oxide are stored in two types of sites: hexagonal and octahedral. Between two layers of vertical stacking, hexagonal sites are identified, and between two layers of vertical stacking, octahedral sites are found. Four octahedral sites share oxygen whereas four other octahedral sites are occupied by two-thirds aluminium cations and one-third oxygen anions. It has a hexagonal structure and each unit contains two alumina molecules. With aluminium, above and below the triangle's centre, three oxygen molecules create an equilateral triangle and formed different crystalline structures (Table 1.2). Each cube's corner is assigned to one of these classes, while the cube's centre is assigned to another [10].

1.2.3 Gibbsite: Gibbsite (Fig.1.1) has been the most fully defined of the trihydroxide phases due to the availability of well-crystallized coarse specimens. Gibbsite is classified as monoclinic and it is found in both natural and triclinic crystals, which dispersed throughout the monoclinic structure of the natural form [11].

Table 1.2: Crystalline Structures of Alumina's [12]

Phase	Formula	Crystal System	Unit Cell Parameters (Angstroms)			Angle
			A	B	c	
Hydrated Alumina's						
Gibbsite	α-$Al_2O_3.3H_2O$	Monoclinic	8.64	4.07	9.72	84°26′
Bayerite	β-$Al_2O_3.3H_2O$	Monoclinic	4.72	8.68	4.06	90°07′
Nordstrandite	$Al_2O_3.3H_2O$	Monoclinic	8.63	4.01	19.12	90°00′
Boehmite	α-$Al_2O_3.H_2O$	Orthorhombic	2.87	12.22	3.7	
Diaspore	β-$Al_2O_3.H_2O$	Orthorhombic	4.4	9.43	2.84	
Transition Alumina's						
Chi		Cubic	7.94			
Eta		Cubic(spinel)	7.9			
Gamma		Tetragonal	7.94	7.94	7.79	
Delta		Tetragonal	7.97	7.97	23.47	
Iota		Orthorhombic	7.73	7.78	2.92	
Theta		Monoclinic	4.63	2.94	11.86	103°42′
Kappa		Orthorhombic	8.49	12.73	13.39	
Corundum	α-Al_2O_3	Rhombohedral	4.76		12.99	
	Al_2O_3	Cubic	4.68			

1.2.4. Boehmite:

Boehmite (Fig.1.2) is made up of two layers, each of which has a cubic packing of oxygen ions. These layers are made up of chains that stretch in the direction of the a-axis and are made up of double AlOOH molecules. Between hydroxyl ions in adjacent planes, hydrogen bonds hold

the double layers together. Hydrogen bridges have a centre distance on average of 0.27 nm. If there is a significant amount of excess water (usually >14 wt. percent), the a, b, and c lengths in the three-dimensional directions of crystallographic dimension lengthen, resulting in pseudo-boehmite. The predecessor of -alumina is boehmite (AlOOH), a hydroxide with a sublattice of cubic close-packed (CCP) O^{2-} anions and Al^{3+} cations interstitially organised in octahedral positions. Because of heat treatment, boehmite loses water and degrades in the order shown below [13].

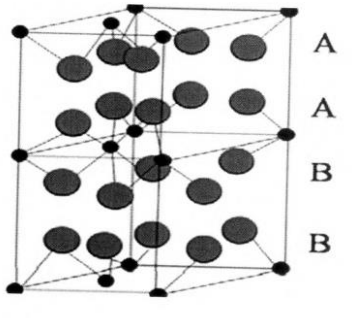

Fig.1.1: Structure of gibbsite [13].

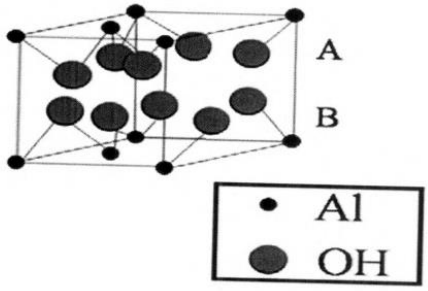

Fig.1.2: Structure of boehmite [13].

1.2.5. Diaspore: The structure of diaspore (Fig.1.3) was originally made up of double molecule chains. In an approximately hexagonal configuration, the chains are densely packed. The exact position of hydrogen using neutron diffraction. According to the researchers, the AlOO coordination octahedral is distorted, resulting in two Al-O atomic bond lengths of 0.184 and 0.198 nm, respectively. The presence of hydroxyl ions, but structural simulations suggested a more ionic proton [14-15].

1.2.6. Bayerite: Bayerite is a rare mineral that is synthesised commercially for catalysts and other high-quality applications. By hydrolyzing aluminium alcoholates at temperatures below 40°C, bayerite is produced, according to Fricke et al. Bayerite (Fig.1.4) has a structure similar to gibbsite, which is composed of basic Al-OH octahedral layers. The following is the order in which the layers are applied: A-B-A-B-A-B-A [16-17].

1.2.7. Structure of Transition Alumina: Transition Spinel or a comparable substance with a functional lattice is where Al_2O_3 crystallises. In the spinel structure, Al^{3+} ions occupy tetrahedral interstitial spaces whereas oxygen ions form a face-cantered cubic lattice. The FCC lattice is made up of close packed planes. However, the stacking order is A-B-C-A-B-C. Al^{3+} ions prefer octahedral coordination in most situations to occupy all octahedral sites, with cation vacancies confined to tetrahedral sites [18-19].

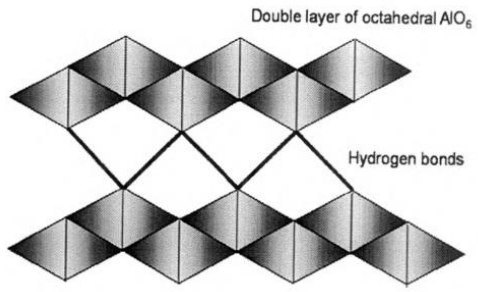

Fig.1. 3: Structure of Bayerite [12]

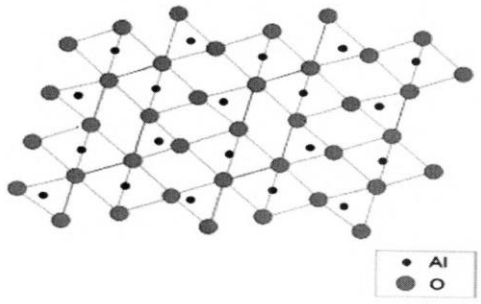

Fig.1. 4: Structure of Transition Alumina [12]

1.2.8. Alpha Alumina: Among all the crystalline polymorphic (δ, θ, β, η, γ, κ, and χ) phases, α - Al_2O_3 is the most thermodynamically stable phase which is rhombohedral alpha alumina at elevated temperatures and the close packing nature of aluminium and oxygen atoms which absolutely attributed as the main reason for its best thermo-mechanical properties. Alpha alumina, unlike transition alumina, has a well-known crystal structure. When alpha alumina crystallises in the corundum structure, sapphire mono crystals form (mineralogical term). At room temperature and Z=6, the corundum structure belongs to the rhombohedral system, with a =0.4749 nm and c =1.299 nm on hexagonal axes. The structure is a dense hexagonal stacking of O^{2-} anions, with Al^{3+} cations taking up two-thirds of the octahedral interstices. Anions and cations frequently mislead the bond's iconicity. For two-thirds of its length, the alumina bond is assumed to be ionic, and for the remaining third, it is thought to be covalent. The $Al^{3+}$and O^{2-} ions are easily sintered due to their great mobility at high temperatures. Refractory and other high-temperature applications, including as pump seals, semiconductor components, aviation components, and vehicle sensors, as well as electrical and electronic insulators, are among the most important uses of alumina in the ceramic industry [20-22].

1.3 Titania (TiO_2): Titania is found in three crystallographic structures. Brookite is orthorhombic, Rutile is tetragonal, and Anatase is tetragonal. Only rutile is the most thermodynamically stable of these three TiO_2 polymorphs, but anatase and brookite are metastable, changing to rutile when heated [23-25]. At very low temperatures, brookite turns into rutile. In industrial applications, only rutile and anatase play a significant role. Due to its rarity and difficult preparation, brookite's applications are limited. A schematic of a rutile TiO_2 unit cell is shown in Fig. 1.5. However, anatase is the predominant element of monocrystalline solids and is often the majority product of inorganic syntheses. At temperatures between 600 and 700°C, titania reportedly goes through a phase shift from rutile to anatase [26-28].

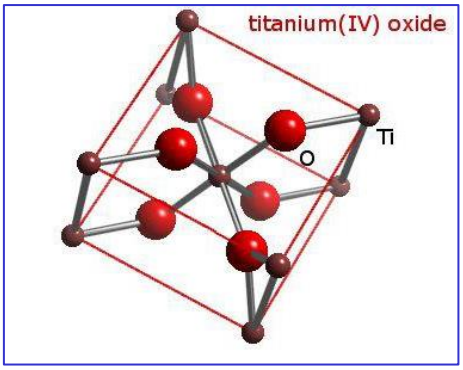

Fig.1.5: Unit cell of rutile (TiO_2) [28].

1.4 Aluminum Titanate (Al_2TiO_5): Aluminum Titanate (Al_2TiO_5) is an alumina and titania intermediate phase having a 1:1 stoichiometric composition of the components Al_2O_3:TiO_2. In an air atmosphere, a mixture of alumina and titania is heated to temperatures above 1350°C and best advantageous properties (Table 1.3) [29-31].

Table 1.3: Salient properties of Alumina (Al_2O_3), Titania (TiO_2), and Aluminum Titanate (Al_2TiO_5) [32-34].

Properties (Unit)	**Alumina (Al_2O_3)**	**Titania (TiO_2)**	**Aluminum Titanate (Al_2TiO_5)**
Melting Temperature (°C)	2400	1843	1860
Density (g/cc)	3.98	4.23	4.05
Thermal Expansion ($\times 10^{-6}/^{O}C$)	8.1	11.8	1.0
Young's Modulus (GPa)	375	288	30
Fracture Toughness ($MPa.m^{-1/2}$)	4	3.3	4
Hardness (GPa)	15	10.3	8.8
Flexural Strength (MPa)	300-700	367	60
Compression Strength (MPa)	2100	3675	157

Aluminum Titanate (Al_2TiO_5) is a potential material for a range of structural applications due to its high melting point, low thermal conductivity, almost nil thermal expansion, and strong thermal shock resistance. As a result, it is being considered as a material for insulating ports in combustion engines, piston heads, manifolds, turbocharger linings, swirl chamber insulation, and valve insulation. It is a kind of ceramic that resists thermal shock well and has a thermal expansion coefficient of zero [35-40]. After the sintering process, it develops minute cracks during the cooling process. These intergranular cracks reduce the material's strength, but they

also act as a useful mechanism for collecting strain energy during thermal shock and preventing catastrophic crack growth [41-43]. Also, it is a suitable replacement for machinable BN-ceramics, which are currently used as insulating substrates in the microelectronics industry but are quite expensive, requiring the development of new affordable machinable substrate ceramics [44]. Several research have demonstrated the potential of using this composite to produce machinable ceramics that are less expensive than BN ceramics. In the region of 20 to 1000^{o}C, it exhibits an almost zero thermal expansion coefficient ($0.810^{-8}/^{o}$ C). However, at 1280^{o}C, this substance is unstable, and it decomposes into Al_2O_3, - Titanium Oxide (rutile) via a eutectoid reaction (Fig. 1.6) [45-46].

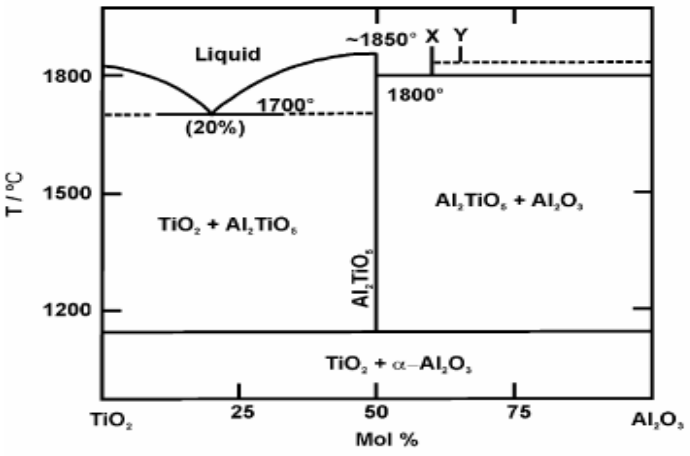

Fig.1.6: Aluminum Titanate phase diagram [47].

Alumina, in combination with Titania, has been utilised for high-temperature applications that demand mechanical qualities, and it is highly recommended for ceramic new-era generations. Some of the applications are listed below. In the glass industry, thermal insulation liners, filters for diesel engines and catalytic converters, foundry crucibles and nozzles, riser tubes, thermocouples, (Fig.1.7) and moulds are used [47].

Fig.1.7: Aluminum Titanate products [47].

1.5. Ceramic processing routes:

As the size and complexity of ceramic items grew, so did the demand for them. To solve this, large-scale manufacturing of ceramic materials has numerous challenges, such as heterogeneous densification throughout green components, which increases the likelihood of shrinkage allowances during drying and subsequent sintering. The needed qualities were not improved because of the non-uniformity in the materials, inappropriate deformation, and cracks. It is common knowledge that the final qualities of ceramics are inextricably linked to the processing routes and parameters [48-49]. However, because of inherent brittleness and relatively low bending strength, ceramic products has limited its wide use for structural applications. Therefore, there is a technological as well as scientific desire to overcome these constraints by sophisticated processing techniques that allow for the customization of microstructures [50-51]. The structural application often demands components in near-net shape with homogenous properties in larger sizes and complex features. Additionally, the process also should have a combination of high productivity and commercial viability [52-53]. The major criteria, especially for complex-shaped and high densification with homogenous microstructures, are easily achieved by adopting colloidal shaping procedures rather than traditional dry pressing. For ceramic processing, and notably for alumina and aluminum titanate products, several shaping techniques are available to manage interparticle forces with effective agglomeration breakdown in order to achieve full dense bodies with regular and intricate complex geometries [54-55].

As a result, the current research focuses on evaluating the attributes of ceramic products based on different advanced ceramic processing techniques and their connections with better microstructures. We are primarily interested in the impact of processing parameters on the evaluation of ceramic products, with a slight comparison of colloidal (Conventional Slip Casting (CSC), Pressure Slip Casting (PSC)), semi-colloidal (Extrusion Based Ceramic Paste 3D Printing), and non-colloidal (Cold-Isostatic Pressing (CIP)) processes.

1.6 Advanced Colloidal Ceramic processing techniques (Conventional Slip Casting, Pressure Slip Casting):

1.6.1. Conventional Slip casting: Traditionally slip casting is a widely used aqueous ceramic process that produces products with reasonably excellent and required qualities. In this traditional casting technique, the capillarity effect in the mould creates a pressure differential,

which causes water to be removed from the mould, particulate deposition on the mould walls, and finally the product's thickness to be built up [56].

Slip casting is the process of moulding ceramic granules floating in liquid into porous plaster moulds. Slip casting of alumina is extensively used for advanced ceramic formation because it can produce green body specimens in intricate shapes with a relatively high density and low cost. During consolidation procedures including the removal of water, particle segregation is common in the slip casting method. Controlling the viscosity of the slurry and ensuring homogenous solid material dispersion are essential for creating high-density green bodies. The needs of the application dictate the choice of starting powder. Fine powder is required in the vast majority of applications. Improved sintering of ceramic specimens necessitates a high temperature and a long soaking period [57-58].

1.6.1.1 POP Moulding for Conventional Slip Casting: In order for capillary action to extract the fluid from the slip, the mould for slip casting must have regulated porosity. Water and powdered plaster of paris are mixed together to make plaster moulds. After putting the plaster mixture into the pattern mould, let it cure. As a result, the mould has a smooth surface. The mould is separated into segments, each of which is sized so that it may be easily removed after casting without causing damage shown in figure 1.8 [59-60].

$$3CaSO_4.2H_2O\ (180^oC) \longrightarrow 2CaSO_4.\ O\ .5H_2O + 3H_2O$$

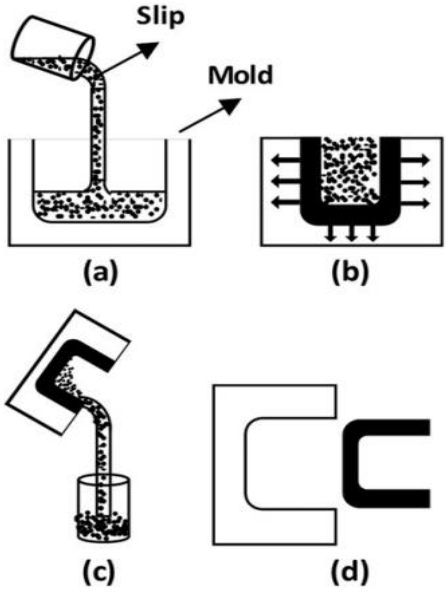

Fig. 1.8: Slip casting involves four basic steps: (a) filling the mould with slip (b) capillary action draws liquid away from the mould walls, forming a cast layer (c) draining the excess slip from the mould and (d) removing the green body after partial drying [59].

Although 18 percent water can chemically satisfy the reaction, substantially more water is required to make the liquid fluid enough for mould making. Thermocol was ingested in a solid state. A cubic structure was then built using hard thermocol. Then, using a beaker, a hollow cylindrical-shaped body is created. The hollow component's dimensions should be the same, with equal and appropriate spacing between them. This facilitates the casting process normal drying process. Plaster of Paris and water are combined at a ratio of 40 to 60 to create the slurry. Slurry is kept from spilling out of the holes or gaps between them by plastic tape. After that, the slurry is carefully poured into the hollow cubical box until it reaches the desired height. The body is allowed to air dry for about an hour. After 1 hour, the body was removed from the hard thermocol, and the inside and exterior surfaces of the mould were polished and allowed to air dry. After that, the mould is dried in a drier at 60 to 70^{o} Celsius to eliminate complete water. When the slip is poured into a permeable mould, filtration of the liquid from the suspending media creates a layer of tightly packed particles against the mould wall [61-62].

1.6.2. Pressure slip casting: Pressure slip casting, a shaping technique created for sanitary ware and white ware, has been thoroughly investigated for the influence of pressure on the slip, ranging from 5 to 40 bar. In order to improve product attributes and yields pressure slip casting is a more advanced technology that ensures a faster and complete consolidation of solid particles, resulting in products with the highest possible qualities [63-64]. Despite the fact that it has not previously been considered for advanced ceramic component manufacture, the pressure slip casting technology is currently being investigated to determine its appropriateness. The primary need in both the conventional and pressure slip cast processes is to generate a well-dispersed and stable slip that can yield a homogeneous green body with good surface finish [65-66]. Work has been done on the PCS 100N (SAMA GmbH) (Fig. 1.9) to produce Advanced Ceramics products like alumina and aluminium titanate.

1.6.2.1 PCM Features:

1. Extremely efficient, having a potential for approximately 30 cycles per hour depending on the slip and product.
2. Green density and consistency are guaranteed in yields of 58%-60%.
3. Simple to scale up to fulfil industrial/commercial needs.
4. Aqueous slips make it simple to pressure cast a variety of intricate shapes and structures.
5. Using polymer moulds, at least 15000-20000 cast cycles may be produced.

6. Eco-friendly with a maximum (3% of rejection).
7. PC technology may include the production of polymer moulds.
8. minimum manpower is needed
9. could be automated if necessary

1.6.2.2 Pressure slip casting steps:

Overall, the process will complete in 4 stages:

1. Two moulds come closure and slurry pumped to the moulds
2. Infiltration has done by means of compressed air pressure to filter to slip
3. Applying pressure make the layers as per the patterns in the moulds
4. By applying back pressure demoulding so as to get exact green compound

Two polymeric moulds (Male-Female), one is fixed to fixed plate and other is fixed to movable plate, which can able to sustain for pressure application that is connected to crank. As per programme given in the setup, crank rotates which is connected to connecting rods that makes reciprocating motion and rotary motion converts reciprocating made two moulds come closure. Slurry containers from which slip will send to the moulds through hosepipes. Infiltration process has done by applying the compressed air, which is also included in the setup here. Pressure developed by means of pneumatic system by hydraulic pump set up which can give max of 30 bar. Demoulding has done by back pressure where we can get exact green compound.

Fig.1.9: Pressure Slip Casting Machine (PCM) -100-N (SAMA GmbH) at ARCI

The particle packing in the slip cast body and the microstructure of the sintered body were both significantly influenced by the average particle size and distribution. In order to

obtain consistency, the initial powders must be consumed in a highly controlled manner with a range of particle sizes present. Hence, a mixed batch in which smaller powder particles are distributed among larger powder particles may successfully enhance performance and density uniformity [67-68]. The zeta potential of the stabilised slip is determined by various elements, including the deflocculants used in mixing, the homogenization time, and the pH of the slurry, among others. Solid loading and slip stabilisation are critical for producing the correct rheological behaviour with shear thinning property, which is critical in any casting process [69-70]. However, it is thought that interlocking the particles to keep their shape while ejecting under pressure will have a greater impact on the green compacts than obtaining a stable slurry using non-plastic advanced ceramics. Overall, the shaping process is important in creating a green body with improved qualities in achieving the desirable mechanical and microstructural behaviour of the final sintered product [71-72]. In this context, the current study aimed to optimise the solid loading and slip rheology of powder fractions suitable for pressure slip casting, as well as fine-tuning of operating parameters such as feed rate, slip pressure, and pressure holding time, to achieve high green densities and, as a result, sintered alumina bodies with improved mechanical properties [73-75].

1.7. Cold Isostatic Pressing: The method of compacting powders in an elastomer mould is known as CIP (cold isostatic pressing). The mould is fixed inside a pressure chamber, into which a liquid medium is pumped before high pressure is uniformly applied from all sides. It is based on a theory put out by French scientist Blaise Pascal, according to which "a change in the pressure of a contained incompressible fluid is transferred undiminished to every component of the fluid and to the surface of its container" [76-77].

1.7.1. Types of Cold Isostatic Pressing:

Wet bag and dry bag are two different types of CIP moulding procedures that depend on the interplay of a forming mould for filling powder and a pressure medium for conveying pressure [78-79].

1.7.1.1. Wet bag Process:

The wet bag method involves filling powder into a forming mould, sealing it airtight outside the high-pressure vessel, and then submerging it directly into a pressure medium, as illustrated in the diagram (Fig.1.10a). The powder is then compressed into a shape by applying isostatic pressure to the moulds outside surfaces. This method is appropriate for a variety of low quality, complicated-shapes or large-scale products, as well as trial production research. External

pressurises the pressure medium from the outside into the pressure vessel, and replacing the top closure with a piston for direct pressurisation of the enclosed area inside the high-pressure vessel [80-81]. The resulting compact has a homogeneous density and low entrapped stress, making it possible to machine it while it is still green (unfired). When burned, there is almost little deformation, minimising or eliminating the need for laborious and expensive machining that requires the use of diamond tools. The method of evacuating and sealing the tool before pressing is occasionally used to lessen the cracking effect of entrapped air. Another benefit stated for this method is that it enhances potential density, though this has not been demonstrated at the pressures employed in ceramics [82] as like shown in Fig.1.10b.

1.7.1.2. Dry bag process:

The dry bag method, as depicted in the diagram below (Fig. 1.11), involves applying pressure to a pressing rubber mould in a high-pressure vessel to mould powder that has been packed in a forming rubber mould. With its labour-saving automatic operation, this approach is appropriate for mass manufacturing of simple and limited variety products.

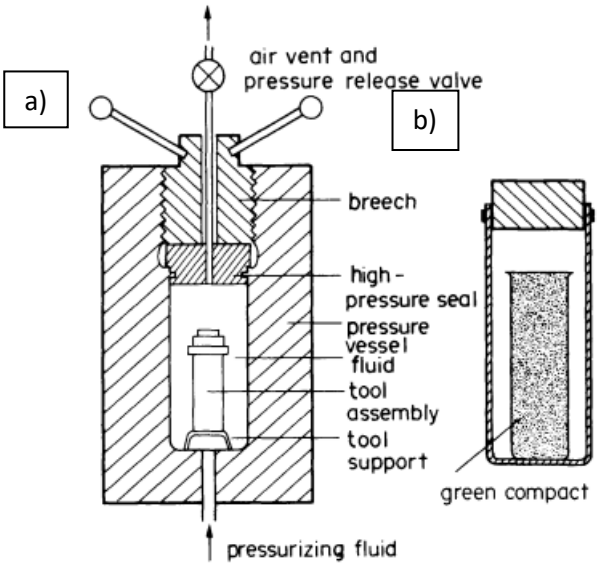

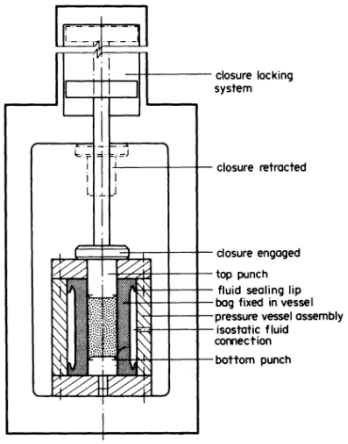

Fig. 1.10: Simple wet bag pressing system
a) Press loading and pressurization, and
b) Section through bag pressed Compact before removal from tool.

Fig. 1.11: Simple Dry bag pressing system

Two systems make up the dry bag process: the circumferential + axial pressurisation system and the circumferential pressurisation system. The cap-shaped pressing rubber mould's top

surface and outside mould surfaces are both under pressure from the circumferential + axial pressurisation system. Through a cylindrical pressing rub

ber mould, the circumferential pressurisation system only applies pressure from the exterior surfaces of the forming rubber moulds. The pressure exerted on the green compact, however, is nearly equal to isostatic pressure due to the powder's fluid-like characteristics [83-85].

1.8. 3D-Printing (3DP):

In contrast to traditional subtractive manufacturing, the AM technique allows for the progressive creation of a three-dimensional object from a pre-designed 3D model by layering raw materials. Traditional subtractive manufacturing employs a top-down process that involves removing material from a bulk solid sample until the required geometry or shape is achieved, which takes longer. Unlike traditional fabrication methods, the AM process has advantages in terms of reducing the time it takes to arrive at an optimal prototype design, as well as cost savings and waste reduction [86-88]. The basic premise of three-dimensional printing is extensively documented, and it entails creating a 3D model using Computer Aided Design (CAD), following which it is formatted in Standard Tessellation Language (STL). The thickness of the layer printed throughout the production process might vary from a few microns to a millimetre, depending on the technique used. The layer thickness and speed affect the printed object's surface quality and resolution. Because of the fine layer thickness and optimal speed for each material, good resolution and surface quality are achieved [89-90].

By using this technique, any solid form or detailed, complex shaped components or items can be produced. Despite the fact that they overlap in many phases as shown in the following manner, the AM process is specific to materials [91-93]:

1.Material extrusion, 2. Powder bed fusion, 3. Vat photopolymerization, 4. Material jetting, 5. Direct energy deposition 6. Sheet lamination, and 7. Jetting of binder sheets.

1. Material Extrusion: Material extrusion is an additive manufacturing technique that uses a heated nozzle to feed a continuous strand of thermoplastic material. To build the real 3D item, the molten feed filament is extruded through the nozzle layer by layer according to the virtual 3D CAD model. Thermoplastics, ceramics, and composites can all benefit from this approach. Fused Deposition Modelling (FDM), Fused Filament Fabrication (FFF), Direct Ink Writing (DIW) or Robocasting, Freeze Form Extrusion (FEF), and Ceramic on-demand Extrusion are the different types of material extrusion (CODE). Thermoplastic

filament is fed through a heated nozzle and deposited onto the printer platform, where it solidifies according to the 3D model.

2. Powder Bed Fusion: In powder bed fusion, powder particles are fused together using a laser, heat, or electron beam to produce an object based on a 3D CAD model. The powder particles are fused using three different energy sources: laser light, electron beam energy, and heat energy. Powder bed fusion is divided into Direct Metal Laser Sintering (DMLS), Selective Laser Melting (SLM), Electron Beam Melting (EBM), Selective Heat Sintering (SHS), and Multi Jet Fusion, depending on the type of energy utilised to fuse the powder particles (MJF). Despite the fact that the methods discussed above use different energy sources, they all follow the same procedure. Powder bed fusion printers typically feature two chambers, one for the powder and one for the build. Powder rollers are used to disperse powder on the platform for each layer in the powder chamber. The build chamber uses energy to fuse powder particles according to a virtual 3D CAD model that is imported into the machine software, and to construct the object under vacuum, which is filled with inert gases to avoid molten metal corrosion. This technology can be used to prepare 3D items out of metals and polymers.
3. Vat photo polymerization: Photo polymerization is a well-known additive manufacturing technique in which ultraviolet (UV) light is used to cure liquid resins and generate a hard body through polymerization. The feedstock (liquid photo-polymer resin) flows through the nozzle according to the required 3D model, and the liquid resin is UV light cured by conducting the polymerization reaction. Photo-polymers are light-activated resins that change their characteristics when exposed to light, resulting in a hard substance. Stereolithography (SL), Digital Light Processing (DLP), Lithography-based Ceramic Manufacturing (LCM), and Direct Light Processing are some of the other techniques that fall under this category (DLP). This technology enables the use of high concentrations (about 25%) of photo polymers in the preparation of resins from raw materials.
4. Material Jetting: The material Jetting printing method entails the dropwise or continuous deposition of feedstock (liquid) layer by layer on the surface of the printer platform, as per the 3D model, and then allowing it to cool and solidify. UV light exposure is also used in some settings to harden the printed layers. Nano Particle Jetting (NPJ) and Drop-on-Demand Ink Jetting are two types of material jetting.
5. Direct Energy Deposition: By melting the material, as it is deposited using focused thermal energy such as a laser, electron beam, or plasma arc, direct energy deposition creates 3D objects. A gantry system or a robotic arm is used to manipulate both the energy source and

the material feed nozzle. In hybrid production, where the bed may also be manipulated to form complicated geometries, direct energy deposition is becoming more popular. Metals, ceramics, and polymers are all employed in this approach to create 3D complicated shapes. This technology is further categorised into Laser Metal Deposition (LMD) and Electron Beam Additive Manufacturing, depending on the energy source used to melt the feedstock (EBAM).

6. Sheet Lamination: In the additive manufacturing method of sheet lamination, 3D objects are built by stacking thin layer sheets on a printing platform. These thin laminated sheets are fused together using ultrasonic welding or brazing, and then laser cutting or CNC machining is used to obtain the final shape. Parts made with the sheet lamination process have a low additive layer resolution. Depending on the type of bonding source used to join the sheets, such as adhesive bonding, thermal bonding, and ultrasonic welding, it has been further divided into laminating, laminating objects (LO) and computer-aided manufacturing of laminated engineering materials (CAM-LEM). CAM-LEM allows you to create layers and then bind them together. Other approaches, like as UAM, use heat to fuse the laminar layers together and generate the desired structures.
7. Binder Jetting: Binder jetting, as the name implies, is a technique for creating 3D objects by spraying a binding liquid on a distributed layer of powder in accordance with a 3D CAD model. This binding liquid, which is sprayed on the powder layer, aids in the bonding of powder particles. Binder jetting is unique among additive manufacturing processes in which the process does not use heat or other energy sources to fuse powder particles into a dense mass. This approach can be used with a variety of materials, including polymers, metals, and ceramics.

1.8.1. Steps in an Additive Manufacturing Process :

The manufacturing process, entails designing the CAD model, converting the CAD model to a STL file, slicing the 3D model into layers, and printing the model, as explained below [94-99].

1. Create a CAD model: The first stage in employing Additive Manufacturing (AM) processes to make 3-Dimensional objects is to design a 3D model with exact dimensions. By providing the exact measurements of the model and simulating the object under various conditions, a 3D object can be designed using Computer Aided Design (CAD) or Computer Aided Three-Dimensional Interactive Application (CATIA).

2. Conversion of CAD model to .STL file: CAD and CATIA design tools can store files in a number of formats, including IGES (Initial Graphics Exchange Specification), STEP (Standard for the Exchange of Product Data), VRML (Virtual Reality Modelling Language), and 3DS (3D System), among others. The default format for a designed CAD model is IGES. In addition, the developed model must be translated to Standard Tessellation Language (.STL), which is the most common file format for 3D printing. In addition to the STL file format, most 3D printers will accept the 3DS, amf, and obj 3D file formats.
3. Slicing of 3D model into layers and printing process: Import the designed CAD model to the PC that is linked to the 3D printer. The thickness of the layer, the number of perimeters, the number of solid layers required, the percentage of infill, the fill pattern, the direction of filling-in of the imported model, the diameter of the nozzle, the printing speed, the temperature, and the X-Y-Z offset positions from the home position will all be applied to the imported 3D model. Furthermore, using Slicing (slice3r, Cura engine, matter control, simplify 3D, etc.) software, the imported 3D model will slice into layers with the set printing circumstances and generate Geometrical codes (G-Code) of X, Y, Z, and extruder location in a layer pattern. G-Codes can be kept in a microprocessor, or the model can be printed straight from a computer connected to a 3D printer.

1.9. Organisation of thesis:

The thesis is divided into the following chapters

1. Chapter 1: Introduction.
2. Chapter 2: Literature Review.
3. Chapter 3: Experimental Methods.
4. Chapters 4: Results and Discussions.
5. Chapter 5: Summary's, Conclusions and Future Scope.

A brief discussion of these chapters is given below:

Chapter 1: Introduction presents the background of ceramics, classification of ceramics and oxide-based ceramics fields, Alumina and Aluminum-Titanate ceramics used to fabricate densified ceramic products through different ceramic processing routes.

Chapter 2: Literature Presents Literature survey of Alumina and Aluminum Titanate materials work background through different processing routes including colloidal processes, non-colloidal processing is of Cold Isostatic Pressing and 3D Printing.

Chapter 3: Experimental Methods describes that the materials used along with ceramic processing techniques (CSC, PSC, CIP &3D Printing) to enhance the mechanical & microstructural properties.

Chapter 4: Results and Discussions describes those results obtained through the processing routes PSC and CSC comparison on Mechanical & Microstructural properties comparison of processing routes of colloidal (PSC, CSC) and dry Cold Iso Static Pressing on green samples Mechanical & Microstructural properties. Also Results and Discussions describes those results obtained for PSC influence on wear properties. Results and Discussions describes those results obtained through the processing routes PSC and CSC influence on Aluminum Titanate Results and Discussions describes those results obtained through 3D Printing of Alumina and Aluminum Titanate properties

Chapter 5: Summary, conclusions and future scope describes about practical applications.

CHAPTER 2

Literature Review

From the previous few decade's researchers have been attempting to increase fracture toughness and microstructure tailoring to tackle the problem of ceramics intrinsic brittleness, which has limited its use in structural applications. Despite tremendous gain in material characteristics, ceramics remain below their expected locations on the materials map (Fig. 2.1). Researchers have looked into ways to modify ceramic materials such that they can trigger one or more mechanisms that will improve the desired properties. All the material properties and performances of a ceramic component are controlled by the processing history as well as the intrinsic attributes of the materials. Differences in the processing environment and raw material sources have also played a key role in the discrepancies in findings achieved from similar trials. Ceramic matrices have been used in composite formulations with metallic, intermetallic, and ceramic phases as well as microstructural alterations. Key factors affecting the evolution of desired qualities, such as the method used to process the powder, the sintering temperature, the rate and duration of the sintering, the formation of the grain and grain boundaries, and others, must be understood and controllable [100-105].

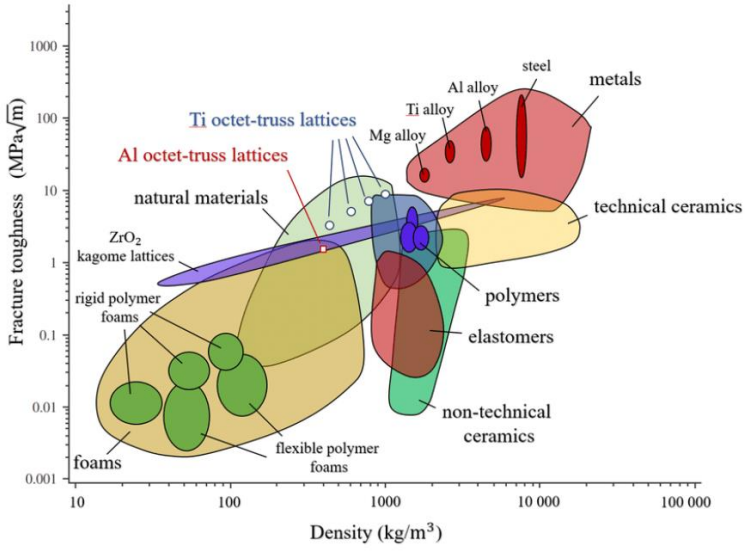

Fig.2. 1: A graph showing the relationship between density and fracture toughness for engineering materials and the low fracture toughness of technical ceramics is demonstrated [106].

2.1 Ceramic Processing Techniques:

For ceramic products, several shaping procedures were developed in order to obtain fully densified bodies with regular and intricate complex geometries. Colloidal forming is a frequently used ceramic shaping process due to its shown benefits of better uniformity, densification at lower temperatures, and flexibility in complex shape. A Prior to colloidal processing, compacts were dried out and pressed to prepare ceramic materials. Due to faults caused by the method inhomogeneous green density, the compounds tensile strength and dependability were reduced. Dry pressing is sufficient for making low-tech components, but it is insufficient for high-reliability advanced applications because: 1) it cannot be used to de-agglomerate dry powder or remove flaws from the powder that may be present in the raw material as received and 2) it is uneconomical to produce due to shape restrictions and extensive machining required to achieve the final shape. Colloidal methods were later used to manufacture increasingly complicated shapes for a broad and developing variety of applications for both dense and porous ceramics, replacing dry processing methods [107-110].

2.2 Colloidal Shaping Technique:

According to reports, the first attempts to make colloidal process gels from silicate esters were made in Germany in 1946. After that, investigations of alumina-based gels were conducted, and in the 1950s, these gels were used for the first time in the production of catalysts. The potential of the colloidal technique was generally acknowledged following the confirmation of the low-temperature synthesis of barium titanate and multicomponent glasses from alkoxides. Since the late 1970s, when advanced ceramics first gained traction, there has been a considerable rise in interest in the method among the world's ceramic community. The market size of the goods is sometimes underestimated because the colloidal method is applied in so many different industrial domains. The strength and dependability of materials are increased by colloidal processing methods capacity to disintegrate agglomerates and eliminate defects by managing interparticle forces. The development of the near-net-shaping notion as a result of colloidal processing led to the invention of ceramic processing methods such as slip casting, gel casting, and freeze casting. Even though these ideas have been in use for years, new trends and combinations of these techniques have been reviving processing methodologies recently and are still being developed [111-116].

The colloidal process will open up a new path to advanced ceramics, according to Sugita et al. [117] (Fig. 2.2). Interdisciplinary approaches are thought to be essential in the research and development of the process because it is based on several different scientific and technological fields. The study's methodology should advance, including an analysis of the material's atomic structures, in order to strengthen the theoretical foundation. To make the process industrially reliable and affordable, novel processing methods are also required. Possibilities for the process in terms of advantages are higher in purity, increased homogeneity in multi-component systems, a variety of product shapes, and suitability for mass production with having little disadvantages such as the price of raw materials is higher, there is more shrinkage during drying and sintering, there are still small pores and impurities, and the processing time is longer.

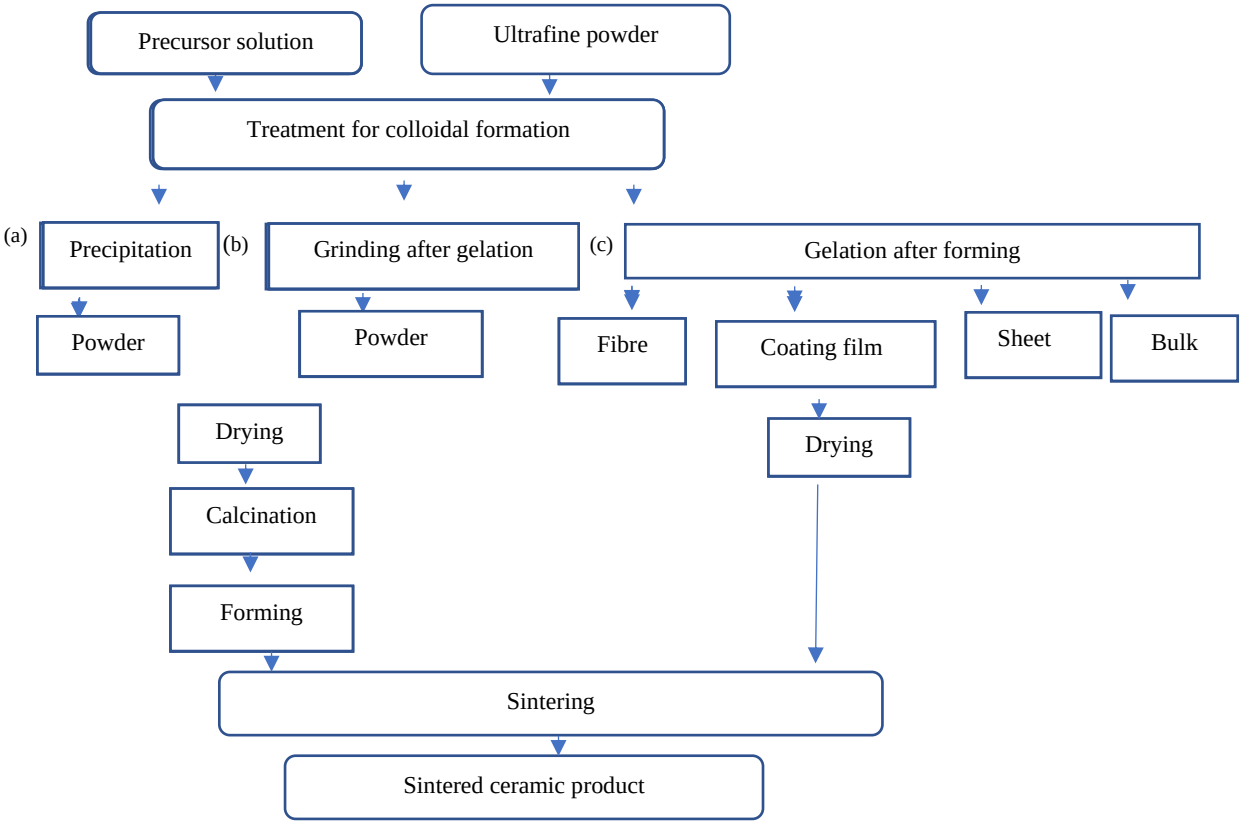

Fig. 2.2: Schematic Representation of Colloidal processing [118].

According to Lewis et al. [118], a crucial aspect of colloidal processing is the consolidation of colloidal suspension into dense, uniform green solids. Bodies should be created straight from the slurry condition in order to benefit from this technique. The rheological characteristics of the body as-formed must be drastically changed after shaping in order to permit demoulding (if required) and subsequent handling without shape deformation. To achieve control over structural evolution and hence minimise undesirable heterogeneities,

a colloidal-based approach is used to fabricate ceramics. Customizing interparticle forces, suspension rheology, consolidation, and drying behaviour will result in the optimal microstructure for a particular application. There are a number of colloidal processes (Table 2.1) that can be used to make ceramic parts with different geometrical shapes, levels of complexity, and levels of microstructural control.

Table 2.1: Representative colloidal routes [118]

Forming Method	Consolidation mechanism	Component shape
	A. Fluid Removal	
Slip casting	Fluid flow into porous mold drive Fluid flow into	Complex, 3D, thin walled
Pressure filtration	porous. Through capillary forces by pressure being	Simple, 3D
Osmotic consolidation	exerted.	
	Driven by the differential in osmotic pressure, fluid	Simple, 3D
Robocasting	flows across a semipermeable membrane.	
	Fluid evacuation due to evaporation.	Simple, 2D, thin layers
	B. Particle flow	Complex, 3D
Centrifugal consolidation	Gravitational force-induced particle flow.	
Electrophoretic deposition	Flow of particles induced by an electric field.	Complex, 3D
	C. Gelation	
Aqueous Injection	A temperature shift causes a physical organic gel to	Simple, 2D or 3D
molding	develop.	
Gel casting	Because of chemical reactions, a cross-linked organic	Complex,3D
	network develops.	
Direct coagulation casting	Flocculation causes the formation of colloidal gel.	Complex,3D
Robocasting	The process of flocculation results in the formation of	Complex,3D
	colloidal gel.	

Near-ideal green microstructures can be created through colloidal processing, which regulates ceramic particle packing on the scale of particle size rather than granule size. It is possible to approach particle coordination numbers to create dense, homogenous burned microstructures with little grain. Two of the primary characteristics of colloidal processing are the high degree of particle dispersion that leads to microstructures without textures and the high level of homogeneity and reproducibility connected with cavity filling. In order to improve sintering ability at lower temperatures by preventing coarsening of the sintered microstructure and thereby increasing performance reliability, colloidal processing routes enable effective particle agglomeration breakdown, control of interaction forces between dispersed particles, and good packing ability [119-124].

By carefully regulating the formation of the initial suspension structure and its evolution during fabrication, colloidal processing has the potential to manufacture ceramic films and bulk forms with great reliability. The five fundamental steps of this process are: (1) powder synthesis (2) suspension preparation (3) component shape consolidation (4) solvent phase removal and (5) densification to provide the final microstructure necessary for optimal performance. Unintentional heterogeneities (or flaws) introduced at any stage of production remain or deteriorate with densification. To obtain the required spatial distribution of phases (including porosity) in as-consolidated materials, there is a persistent drive for a deeper comprehension of colloidal stability and assembly. Strongly attractive interactions produce a particle network that is resistant to consolidation and compressible over a wide stress range. After consolidation at various centrifugal speeds, the weakest flocculated suspension showed an essentially incompressible and homogeneous density profile [125-128].

Bell et al. [129] state in their study that the use of colloidal processing principles in the creation of ceramic materials is widely acknowledged for achieving homogeneous material properties in sintered products, enabling novel ceramics or 3D printing forming techniques, and controlling microstructure to achieve optimised material properties. Due of the close connection between a ceramics microstructure and its macroscopic electrical properties, it is crucial to manage the variables that affect the microstructure, such as grain size distribution, grain boundary features, porosity, and other elements. Optimized conditions, starting particle sizes, customised sintering schedules, and particular chemical compositions must be developed according on the macroscopic property requirements for a particular application or use.

Advanced ceramics with more intricate shapes are becoming more and more popular. Manufacturers have been forced to seek improvements in their current processing procedures as well as to embrace new processes that may be more suited to fulfil market demand as a result of this as well as the requirement for more dependable components. Contrarily, because the interparticle forces may be varied, shape approaches that employ colloidal suspensions have a major benefit in minimising inhomogeneities in particle packing. These forces can aid in the reduction of inhomogeneities in the green microstructure by dispersing agglomerates, improving packing density uniformity, reducing average pore size, and lowering the scale of mixing homogeneity [130-134].

Franks et al. [135] claim that colloidal processing of fine ceramic powders enables the manufacture of complex-shaped ceramics with distinctive micro and macro structures, which

is not attainable using conventional dry processing procedures. Because to their enhanced structural control and shaping powers, colloidal processing has been employed to create ceramic components with ever-increasing complexity and functionality. Also shown as examples of multiscale designs that can be produced utilising cutting-edge colloidal processing are hierarchical porous structures with great mechanical efficiency. The effects of material characteristics, sintering temperature, casting method, and pressure all have an impact on the size and porosity of ceramic grains, which directly affects the mechanical strength, corrosion resistance, and optical properties of ceramic components. Compacts that were nearly mono-sized and treated colloidally reached full density at substantially lower temperatures than those that were dry-pressed. A fine starting particle size encourages the sinterability of powder compacts, other things being equal. There is an ideal particle-size distribution beyond which the sinterability of the powder compacts substantially declines, even while increasing the particle-size distribution enhances sinterability. The importance of suspension rheology control in these approaches is then highlighted by the primary colloidal shape forming and additive manufacturing procedures that use colloidal pastes and inks. Because the demands and potential for ceramics are already diversified and developing quickly, the industry is in a particularly active stage of development. This puts various demands on ceramic processing, such as better characteristics, more homogeneity and reproducibility (and consequently reliability), and larger-scale, more effective production [136-139].

The current state of knowledge about colloidal processing is reviewed for large-scale and long-term applications. It is to encourage more research into low-cost and energy-efficient methods of producing ceramics with dynamic properties that can be used in a variety of fields with outstanding performance. The researcher's focus has also been expanded to include knowledge gaps in these areas, giving us a better understanding of how the field might benefit ceramics future advancements. With this process, high green and sintered densities were generated, demonstrating the concept's promise for the near-net shaping of a variety of high-performance ceramics. The most common colloidal forming methods that are given high emphasis and are on the rise are conventional slip casting and pressure slip casting.

2.2.1. Conventional Slip Casting:

The well-known traditional technique of conventional slip casting (CSC), which generates products with mainly desirable properties, is used to shape ceramics. Due to the fact that this method relies on the capillary effect in the Plaster of Paris mould under atmospheric pressure

to create a pressure gradient that causes water to be removed and particulates to deposit on the mould walls, ultimately resulting in the thickness of the finished product being built up. It is necessary to first prepare high volume fraction, well-dispersed suspensions with low viscosity values so that the suspensions can be moulded into a range of finely formed components. Even while very small particles have the huge specific surface area needed to promote proper densification, the high suspension viscosity they produce prevents them from packing into a green body efficiently. Unless special densification techniques are used, it is typically challenging to sinter the lower green density bodies [140-142].

Many researchers have been drawn to the hypothesis that colloidal properties may be related to the casting behaviour of clays. Physical chemists who saw the potential for a beautiful application of theoretical concepts and those workers whose approach to clay technology was heavily influenced by attitudes passed down from the past were both drawn to a theory that clay had some special quality. Slip casting has received more attention, and many studies have been published. Many of these have discussed how clays behave when alkaline dispersants are present, as well as the various elements that affect the stability and casting qualities of deflocculated slips. CSC, a colloidal processing method, provides improved cast part homogeneity. High green and sintered densities were generated with this technique, illustrating the concept's promise for nearly net-shaping a variety of high-performance ceramics. Processing colloidally CSC is based on the capillary effect in the PoP mould at atmospheric pressure that generates a pressure gradient that causes water to be removed, particle deposition to occur on the mould walls, and ultimately causes the product to thick [143-144].

Murfin et al. [145] explained that the ceramic powders are consolidated into complex shapes with high green densities using the slip casting process. Because the expenses involved prevent using alternative techniques like die pressing or isostatic pressing, it is typically employed to make large components, those with thin walls, or shells with delicate contours. Due to the relatively high cost of the mould material, it is also employed for prototype manufacturing runs and small-scale product testing.

The sintering behaviour and final material properties of green compacts depend on the homogeneity of the particle packing. The rheological characteristics of the slurry created from them are directly related to the product properties created by slip casting. By regulating the slurry rheology, the ideal circumstances for slurry control and, consequently, the final products, are attained (solid particle behaviour in liquid medium, particles stability, etc.). The most

important factors to control and optimise for homogeneity and high density of manufactured green bodies include pH values, slurry stabilisation using the proper kind and amount of dispersant, particle size, particle size distribution, particle shape and morphology, volumetric solids content, and inter-particle force. The dispersions boost the electrostatic, steric, or electro-steric stability of the ceramic particles in suspension [146-151].

Tallon et al. [152] investigated how particle size affects the viscosity of suspensions used to form ceramic bodies. It has been discovered that particles smaller than 50 to 100 nm cannot produce the high-volume fraction, low viscosity solutions required for colloidal processing to make complicated shapes, and the resulting green density is also insufficient to fully densify. The production of high green density bodies and low viscosity suspensions by particles larger than roughly 300–500 nm is also possible; however, in this instance, the absence of sufficient surface area prevents the densification process from being successful. It has been shown, however, that particles with sizes ranging from 100 to 300 nm can be prepared as low viscosity, high volume fraction suspensions to produce green bodies with sufficiently high green densities to fully densify (99 percent theoretical value), resulting in homogeneous microstructures.

The effective volume of one particle (interaction size), which is unrelated to the stabilising mechanism provided by the dispersant, is established by its own volume (hard size) plus the range of the interparticle forces. The product size is a function of the solid loading of a solution. The stabilising mechanism that produces the repellent forces between the suspended particles determines how well the stabilisation works. These repelling forces typically result from interactions between electrical double layers (electrostatic stabilisation) or layers of non-charged polymers (steric stabilisation). The two mechanisms may be combined in some systems, such as those that use dispersants of the polyelectrolyte type (electrostatic stabilisation). However, the effective volume fraction of a dispersed suspension is determined by the interaction size, or the size at which the particles may begin to feel one another's presence. It is well known that the range of electrostatic forces exceeds that of steric forces. Since the effective volume fraction of the suspended particles is higher than that indicated by the hard size as a result, it may be connected to the stabilising process [152-160].

Tari et al. [161] cleared that the Brownian motion, the interaction of interparticle forces, and whether or not these collisions result in aggregation all affect the stability and other characteristics of colloidal dispersions. As two particles come together, various interactions

could happen. The origins and causes of different surface forces, as well as how these forces depend on factors like the medium between the surfaces, have been documented in the literature on colloid science direct measurement of certain types of surface forces as well as ceramic processing.

According to Tiller et al. [162], the notion of colloidal filtration in ceramic slip casting developed by Aksay and Schilling for incompressible cakes has been expanded to compressible materials. Gypsum is used to create a mould (plaster of Paris) for slip casting that will be used repeatedly. Suction pressure in the molds porous structure ranges from 0.1 to 0.2 MPa (1 to 2 atm.). Water is sucked out of the slip by the capillarity as it is poured into the mould, the cake layering the slip-mold interface. The finished product is produced after drying and sintering. The capillary pressure and permeability of the mould both affect how quickly the cake deposits itself in the mould. The capillary suction-induced pressure drop, P_C, is applied to both the cake and the mould. As shown, the liquid's pressure P_L, decreases. The pressure on the solids, PQ, rises in tandem as a result of accumulative drag and reaches its maximum at the intersection of the consolidated layer and the mould. Given that the permeability is directly proportional to the square of the diameter and the capillary pressure is inversely proportional to an average diameter typical of the mould, there is an ideal dimension for generating the highest pressure drop throughout the cake and the maximum rate of deposition. It requires a pressure gradient for flow to happen. The pressure gradient increases as the cake gets closer to the mould because cake porosity decreases in the direction of flow. Different pressure distribution curve shapes can be obtained depending on the cake's compressibility (Fig. 2.3).

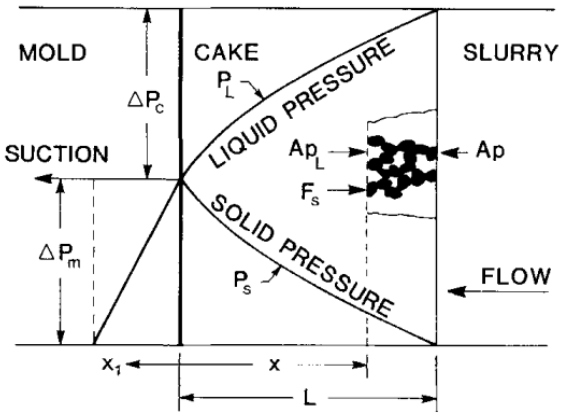

Fig.2.3: Schematic diagram of filter cake and accumulative drag [163]

Fig. 2.4 displays experimental data demonstrating the pressure drops across the cake and medium for kaolin filtration. The medium initially accounts for the entire pressure drop.

As cake accumulates, P_c rises and typically quickly approaches the applied pressure (P). Tiller and Hysing [164] demonstrated that ΔP_C was constant for a slip-casting-involved incompressible cake.

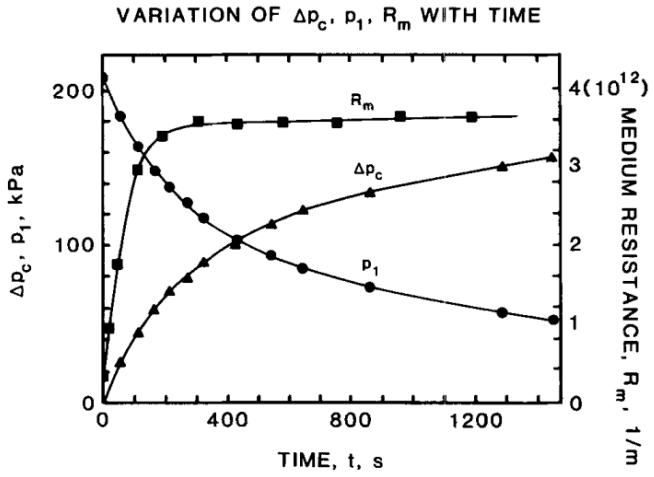

Fig.2.4: Variation of Pressures at mould and cake with time [164].

Numerous researchers [165-167] have looked for ways to speed up the colloidal filtration process, and many of them have done so with a high degree of success. The majority of methods are based on changing the parameters that govern casting, which are generally expressed by the equation: $L^2 \alpha P. t / \eta$, where L is the body thickness, P is the systems differential pressure, t represents the casting time, and η represents the slip viscosity. In other words, since the rate of creation of the cast body is proportional to the differential pressure and inversely related to the slip viscosity, a change in either of these factors will alter casting rate. According to studies by various authors [168-172], the main variables that affect the casting rate are the application of pressure to the slip (or vacuum to the mould), the slips solid content, the resistance of the cast and mould to moulding (which is primarily determined by the porosity of the cast layer and mould), and the slips viscosity.

However, applications are limited, especially for advanced ceramics demanding high productivity, because of the poor green density of the cast components, prolonged cast forming and drying durations, and greater rejection rates. Advanced processing methods that allow for the customization of microstructures are being sought after as a result of these limitations for both technological and scientific reasons. Recent years have seen a rise in the use of pressure-aided slip casting, which combines the advantages of dry processing and colloidal forming while applying pressure throughout the cast formation process. Unlike traditional ceramics, a cast created of advanced ceramics has an irregular shape that prevents it from strengthening

itself under pressure and disintegrates during demoulding. This limits the extensive application of pressure casting for technical ceramics, and little study has been done in this field.

2.2.2. Pressure slip casting:

Pressure slip casting is a popular method of shaping ceramics, especially for tableware and sanitary equipment. It is suitable for producing technical ceramics as well. By using this forming technique, parts with complex shapes can be created in manageable processing times. Costly additional machining is no longer necessary. Organic additives like binders and dispersants are only needed in trace amounts. Although slip casing has been utilised for many years, its quantitative mechanics are not yet completely understood. This is most likely due to (1) the historical association of this approach with intricate slip systems and (2) the use of low-durability porous moulds for filtering and suction, which makes process management extremely difficult. If the role of the mould is restricted to filtering and the driving force is altered and regulated by pressure supplied to the slip, i.e. pressure slip casting, the development of durability gives the opportunity to considerably expand the process mechanisation. Improved instrumentation for characterising slips is now available. In slips with relatively high electrophoretic mobilities, the casting rate was decreased, and the resulting cakes had small pores, a wide range of pore sizes, drying shrinkages, and dimensional distortions. The effects of improved deflocculation were augmented by higher pressures, which accelerated casting, decreased its coefficient of variation, and generally increased its rate. High pressures and appropriately deflocculated slips allowed for the rapid and repeatable formation of cakes with porosities as low as 28 percent, no coarse pores, a narrow pore size distribution, and almost no drying shrinkage [173-174].

Moreno et al. [175] use of a standard pressure slip casting (Fig. 2.5) on a large scale allowed for the manufacture of complicated and thicker pieces. The study described how the magnitude of the applied pressure affected the kinetics and green microstructure of silicon nitride compositions. The rate at which wall thickness forms increases with applied pressure. This statement is true during the whole casting procedure, even if the first cake forms before the final pressure is attained. It was observed that the initial layer formed for all pressures, and that it took less time to reach the final pressure when the applied pressure was higher. successfully demonstrated that pressure casting's kinetics is 20 times faster than slip casting's, allowing the technology to be scaled up for industrial manufacturing. The drop in green density can be ignored when considering the technological developments of the method for continuous

manufacturing. Additionally, using pressure cast prevents contamination from plaster moulds and the resulting surface oxidation degree. The controlled order of processing stages detailed in this work enables us to create and prepare any composition of this system with the purpose of increasing a certain property, despite the fact that the original compositions were plainly not picked with the goal of improving any specific attribute.

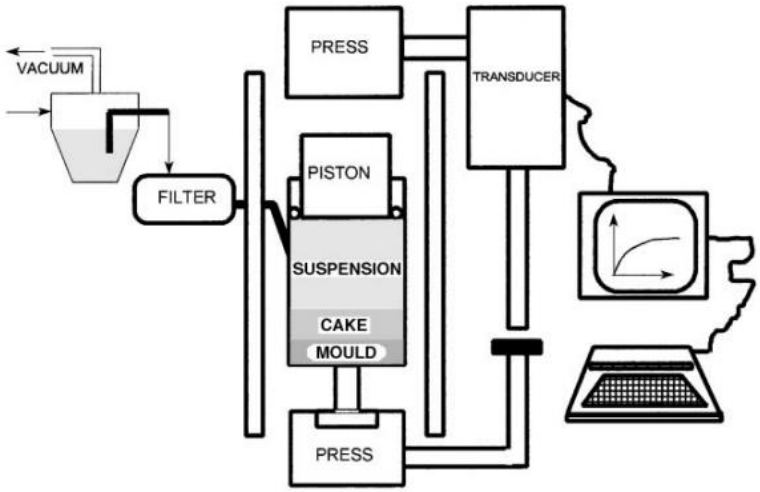

Fig.2.5: Schematic representation of pressure slip casting equipment [175]

Additional study has been done on pressure slip casting since it can generate almost net-shaped green bodies with shorter processing cycles, as shown by Moreno et al. [176]. The creation and management of stable, evenly dispersed ceramic slips is regarded as a crucial parameter, just like with the other colloidal forming techniques. In this study, a variety of alumina slips containing different types of dispersants, such as potential determining ions, counterions, or electro steric forms, were created in accordance with the shear stress/shear rate relationships.

Darcy's differential equation is obeyed by fluid flow through a porous medium with connected pores under pressure: $S^2 = ((2\Delta P/ \eta P_\rho . R_S) \times (\phi_c / \phi_c - \phi_s))$ t. where, S is the cake's thickness, P is the slurry's pressure, V is its viscosity, and P is its particle density. Rs stands for the cake's permeability, ϕ_c stands for the cake's solid volume fraction, ϕ_s for the slurry's solid volume fraction, and t for the casting time. In actuality, the resistance of the cast layer and the thickness of the mould regulate casting rate. Furthermore, the cake is predicted to increase more quickly until it reaches a peak value, then decrease with a parabolic behaviour with respect to other variables. Pressure casting relies not on capillary forces but rather on external pressure applied to slurry isostatically up to 6 MPa and sturdy polymer moulds with

average pore diameters of 10 μm in order to considerably increase the isotropy of characteristics and productivity. This ground-breaking tool also enables the process mechanisation, resulting in high efficiency. Regarding hollow and solid shapes, pressure casting is now firmly established in traditional ceramic processing. It is shown that pressure-cast components also benefit from lower cast-water content, better handling, and green strength [177-185].

Determine, in addition to Tsetsekou et al. [186], the conditions necessary to produce stable, high-solids-content alumina slurries that will lead to slip-cast objects of superior quality. Also, establish a connection between the properties of the slurry and the properties of the final product. Slurry stabilisation was examined for three commercial dispersants. Low viscosity for a slurry with a high solids content can be accomplished by varying the concentration of each dispersant within a specific range that has been determined to be appropriate. In addition to the slurry solids concentration, the dispersant used affects the casting rate because it increases the viscosity of the slurry. Higher densities are produced in both the green and fired states of the objects when a high slurry solids content and a slower casting rate are combined.

Olhero et al. [187] showed the effects of particle size, particle size distribution, and milling time on the rheological behaviour and particle packing of silica suspensions using slurries with a total solid loading of 46 vol. percent. Three silica powders with different average particle sizes (2.2, 6.5, and 19 μm), as well as a colloidal fumed silica powder with a 0.07 μm, were created by wet milling sand. Each of the coarser silica powders received varying amounts of colloidal fumed silica powder, and the mixtures underwent varying lengths of ball milling. The impact of these factors as well as the particle size ratio was examined on the rheological behaviour of suspensions and densities of green slip cast bodies.

Bouncier et al. [188] investigated how the particle shape and particle size distribution affected the cakes filterability and compressibility (PSD). The classic industrial types (sphere, cube, needle, and platelet) of calcium carbonate and uranium oxalate particles were precipitated into a variety of shapes and PSD. An image analysis method was used to evaluate the size and form factor distributions on SEM pictures. The cake filtration properties were determined under optimal monitored operation circumstances using a micro filtration cell configuration. Both the PSD 2 effect and its shape were quantitatively evaluated. Cake resistance and compressibility are influenced by these two solid characteristics, but not in the same way. When it comes to cake resistance and compressibility, the PSD has the biggest impact. When the shape is far

from the sphere, the particle shape is a crucial factor in cake compressibility. When putting the finishing touches on the creation of a filtration operation, both factors must be taken into account. Here, a useful model based on the Darcy law and a fresh correlation for calculating compressibility factor are suggested. For the four shapes under consideration, it provided acceptable estimates of cake filterability and compressibility.

The uniformity of particle packing in the green bodies of a ceramic body is a crucial factor in enhancing the sintering behaviour and ultimate characteristics of the material. This objective is more successfully realised when colloidal shaping techniques are employed to solidify the bodies. In order to produce uniform and dependable ceramic bodies, colloidal methods allow for the modification and control of the forces that interact between particles, the elimination or destruction of particle agglomerates, and the intimate mixing of two or more different powders. Two more important characteristics that have an impact on the rheology, processing ability, and packing of the suspensions are particle size and particle size distribution. The results show that the particle size distribution significantly affects the slips flow properties. The volume fraction of fines that can be added is practically constrained by the increased viscosity of suspensions caused by the addition of fine particles. On the other hand, modifying the size ratio enhanced the shear thinning properties of the suspensions while emphasising the shear thickening behaviour. Due to the size decrease of the silica powder and more efficient deagglomeration of fumed silica, green densities for all mixed solutions increased with milling time. As fumed silica concentrations reached their peak, particle packing initially increased. however, as more fumed silica was added, it started to decrease [189-194].

Raha et al. [195] claim that high pressure batch filtration of fine and colloidal suspensions performed to equilibrium under a variety of physical and chemical process conditions has resulted in a number of intriguing and potentially practical regularities. Two such patterns are detailed in this article. The first regular behaviour, which is displayed by a large number of colloidal suspensions, can be represented by the Pareto profile, which connects filtering rate with solid content of filter cake at equilibrium. The profile is discovered to be a strong function of material fineness even though it initially seems to be independent of the physical and chemical process conditions. Because it can be used as a restricted performance benchmark for the filtration of a suspension, it is relevant for evaluating the filtration process in terms of two of its most crucial process measures, namely kinetics and maximum amount of dewatering that is feasible.

In batch filtering, which is driven to equilibrium, it is often not possible to improve both measures at once, and any process alteration may improve one measure but always at the expense of the other. This is reflected in the Pareto regularity. The self-similarity in pressure filtration, the second regular behaviour, is shown for the filtration of a wide range of different materials and process conditions. By simply transforming and scaling the slurry filtration data with key solid volume percent and critical time during the transition from cake creation stage to cake consolidation stage, the filtration curves are converted into a form that is remarkably self-similar. In a wide range of experimental data for different colloidal systems under different physical and chemical process conditions, this self-preserving behaviour is demonstrated. It is addressed how regularities might affect things [196-200].

Alumina-rich magnesium aluminate spinel with particles no larger than 3 μm and an alumina-zirconia-silica mixture with particles no larger than 1 μm were the two types of coarse-grained oxide refractory materials Klippel et al. [201] investigated utilising this shaping approach on. The authors emphasised the significance of a plug flow in the tubes during mould filling in order to prevent segregation or blocking. They asserted that the slips yield stress must be just right-neither too high nor too low-in order to prevent both segregation in the tubes and settling of the coarse grains in the mould. The plugging problem could be remedied by reducing the percentage of the coarsest particle fraction and employing an acceptable inner tube diameter.

Gerlach et al. [202] used pressure slip casting to create coarse-grained ceramic heat shields from an alumina-mullite mixture. With the aid of this shaping technique, created composites made of coarse-grained alumina and steel, zirconia, and steel.

We discovered that the slips behaved in a variety of ways, including Newtonian, plastic, pseudoplastic, and thixotropic ways. The slips were cast at 3.4 MPa pressure, and the Newtonian slips without thixotropy or with very little thixotropy had the highest densities. The cast bodies constructed with plastic slips and/or significantly thixotropic behaviour failed to reach the specified density and wet cast consistency. Less dispersed slips (if not partially flocculated) display greater viscosities and higher casting speeds because their cast bodies do not have an intensively packed structure and consequently a high density. Low viscosity and low yield point slippage are important for efficient casting rate management and the ensuing high relative density of the cast bodies [203-204].

According to study by Moritz et al. [205], pressure slip casting can be used to shape alumina carbon refractories with coarse grains. Slurries including modified coal tar pitch, graphite, and carbon black, as well as 3 microns alumina particle size fractions, were created in a lab setting and tested utilising pressure filtering tests and rheological studies. The large grains were evenly scattered. A carbon-bonded alumina material with good thermal shock resistance was made by pyrolyzing carbon. The outcomes show that pressure slip casting can be used to shape coarse-grained, carbon-containing materials. When it comes to carbon-bonded refractory materials, this technique may be useful. The goal of upcoming research is to lessen the apparent porosity of cast Al_2O_3-C composites.

According to a study by Schaffner et al. [206], pressure slip casting was used to create graded functional composites for refractory applications. In a pressure filtration cell, two layers of filter cakes constructed of slips with maximum grain sizes of 1 mm and 3 mm and a thickness of 20 mm were progressively filtered. Using a full factorial experimental design, the graded filter cakes performance was maximised. It was discovered that by employing a lower filtering pressure for the first, coarser slip and a higher filtration pressure for the second, finer slip, the bonding between the two filter cake layers may be improved. In order to manufacture filter cakes without cracks and to make it simpler to extract the filter cakes from the PMMA filter medium, the same xanthan/guar gum solution that was used to stabilise the slips was also applied as a thin prefiltered layer. In order to improve the connection between the filter cakes, the initial filter cake layer should only be filtrated up until a soft layer is still visible on top. The pressure slip casting of graded refractories can be advantageous for each layer of the filter cake.

2.3. Cold Isostatic Pressing (CIP):

On the other hand, dry processing techniques like pressure assisted compaction create high green density values with noticeably higher green strength. Cold isostatic pressing is one of the most popular forming techniques for producing ceramic objects with significant length-to-diameter ratios or complex geometries. In comparison to uniaxial pressing, cold isostatic pressing has a number of benefits, including much reduced density gradients and improved mechanical reliability of the resulting ceramic products [207-210].

Many writers have studied the compaction of ceramic, metal, and composite powders under cyclic uniaxial and cyclic isostatic conditions [211 -213]. Smaller density gradients and a stronger densification were produced, especially by cycling at maximum pressure. As a result

of the breaking up of agglomerates and enhanced particle packing with a higher particle coordination number, cyclic pressing resulted in considerably increased densification of single-phase powders.

Schaffonera et al. [214] researched the effects of cycling at maximum pressure or applying a cyclic pressure increase on the cold isostatic pressing of coarse-grained alumina refractories. It was also looked at how the maximum pressure and particle size distribution affected the physical, mechanical, and thermomechanical properties. The apparent density and apparent porosity were marginally higher and lower as a result of the cyclic pressure increase. The median pore size decreased to some extent after cycling at maximum pressure. Unexpectedly, an optimised particle size distribution resulted in reduced apparent porosity, a smaller median pore size, a higher Youngs modulus prior to and following thermal shock, as well as a slightly slower rate of relative Youngs modulus decline. A higher pressing pressure that decreased the perceived porosity had no effect on the Young's modulus.

According to an experiment by Yan et al. [215], the shrinkage, bulk density, Weibull modulus, and dependability of the specimens during the succeeding CIP process depend on the dry pressing pressure and sintering temperature being appropriate. The dry pressing pressure has a considerable impact on the microstructures and depend abilities of ceramics that are made of 99 percent alumina and reshaped using CIP. A suitable dry pressing pressure (75 MPa) and an appropriate sintering temperature help the specimen's densification and grain growth (1580^{o}C). A appropriate dry pressing pressure and sintering temperature are crucial for the specimens reliability, bulk density, and Weibull modulus during the succeeding CIP process. This opens the door to customising compositions, microstructures, and thermomechanical characteristics. Future study will therefore focus on scaling up trials with the goal of increasing the functionality of the created refractory components. Recently, pressure-aided slip casting has become more well-liked as a technique for applying pressure during cast formation while combining the advantages of dry processing and colloidal forming.

2.4. 3D Printing:

Numerous studies have been conducted on three-dimensional (3D) printing of polymers and metals, but the most recent development to receive attention is 3D printing of ceramics. In contrast to traditional subtractive manufacturing, additive manufacturing (AM) enables the gradual creation of three-dimensional objects from pre-designed 3D models by layering on raw materials. In traditional subtractive manufacturing, material is removed top-down from the bulk

solid sample until the desired geometry or shape is obtained, which takes more time. In contrast to traditional fabrication methods, additive manufacturing (AM) offers benefits in speeding up the process of developing the best prototype design while also generating the least amount of waste. Chuck Hull first created and patented the 3DP procedure for plastic materials in 1984 under the name stereolithography. Three-dimensional printing (3DP), rapid prototyping (RP), fast manufacturing, layer manufacturing (LM), additive fabrication, and others are general terminology for additive manufacturing (AM) [216-218].

Three-dimensional (3D) printing technologies, often known as additive manufacturing, are regarded to have started a manufacturing revolution (AM). By digitally sectioning 3D CAD models into 2D cross sections, a variety of cutting-edge manufacturing processes collectively referred to as 3D printing are utilised to produce physical items in a discrete, line-by-line, layer-by-layer, or additive way. A revolutionary manufacturing philosophy called 3D printing allows for the flexible preparation of exceedingly complex and accurate structures that are difficult to realise using standard fabrication techniques like casting and machining. Using CAD software to create a 3D model and then exporting it in the Standard Tessellation Language (STL) format is the basic concept underlying three-dimensional printing. After conversion, the printing device employs the STL file to build 3D structures layer by layer [219-221].

The manufacture of ceramic components via 3D printing gives up entirely new possibilities for resolving the aforementioned problems and challenges. In the 1990s, ceramics were first reported to be printed in three dimensions by Marcus et al. [222] and Sachs et al. [223]. With the most current advancements in computer and materials science, a variety of 3D printing technologies have been developed to date, specifically for the production of ceramics. According to the shape of the pre-processed feedstock before printing, these technologies may generally be split into slurry-based, powder-based, and bulk solid-based approaches, as summarised in the following Table 2.2 [224-225].

Table 2. 2: 3D printing techniques for ceramic [224-225].

Feedstock in	Technology for Ceramic 3D Printing	Abbreviations
Slurry-based	Stereolithography	SL
	Digital light processing	DLP
	Polymerization with two photons	TPP
	An inkjet printer	IJP
	Writing in direct ink	DIW

Powder-based	Three-dimensional printing	3DP
	Selective laser sintering	SLS
	Selective laser melting	SLM
Bulk solid-based	Laminated object manufacturing	LOM
	Fused deposition modelling	FDM

Traditional ceramic shaping methods require making dies and moulds in multiple iterations during the expensive and time-consuming fabrication of prototypes. Although it is well established for plastics and metals, additive manufacturing technology has recently gained popularity in the field of ceramic materials. Because of the processing requirements (feedstock preparation, sintering), ceramics are difficult to fabricate using additive manufacturing. But a plethora of additive manufacturing techniques have been created to process ceramic materials for a range of applications. Because ceramic 3D printing is still a new field, there are a growing number of publications in this field, but the total number of publications is still quite small.

Alumina and zirconia were used to create dense ceramic parts using thermoplastic 3D printing, according to research by Scheithauer et al. [226]. According to the study, alumina and zirconia were prepared into a homogeneous suspension with optimised rheological parameters and printed. 99 percent density and homogeneous layer bonding are visible in the microstructure of printed samples, which have undergone characterisation.

Digital light processing and stereolithography were used to create a complex shaped Zirconia triangle cutting tool with a withdrawal tool, according to Hea et al. [227]. The shrinkage, phases, hardness, fracture toughness, and density of sintered samples were examined. According to the study, all measured values of the specified properties are relatively close to the structural characteristics of commonly processed zirconia ceramics.

Wu et al. [228] reported on the creation of a quick prototyping procedure to create the alumina-based complex ceramic core by combining stereo-lithography and gel casting. Gel casting was used to create an integral sacrificial resin mould from a stereolithography-prepared integral sacrificial resin mould and a ceramic body with a green core. In place of traditional drying, freeze drying was used because it causes less shrinkage and preserves the structural integrity of complexly shaped ceramic cores. The addition of the mineral magnesium oxide improved the sintering conditions.

A solid body was printed using the freeze-form extrusion method using a triple extruder to print various ceramic materials (aluminium, zirconia) that were made into paste. This research was conducted by Leu et al. [229], According to the study, additives give ceramic particles enough adhesion, and their optimal concentration changes the pastes rheological behaviour into pseudoplastic behaviour with a high yield stress that is suitable for printing.

Griffith et al. [230] described how ceramic parts were made using a Freeform fabrication method that is based on the stereolithography method. The viscosity and cure depth of ceramic suspensions made with the acrylamide photo polymer in both aqueous and non-aqueous media were examined. Non-aqueous di-acrylamide suspensions, which have higher viscosity than aqueous acrylamide suspensions, showed a higher cure depth during printing. The Beer-Lambert law was also used in the study to analyse the impact of layer curing depth, and it was found that both curing depth and the percentage of ceramic powder and the difference in refractive indices between the ceramic powder and liquid media are inversely connected.

The photopolymerization behaviour of ceramic suspension, which is a fundamental step in shaping the ceramic component, was investigated by Halloran et al. [231]. The behaviour of photopolymerization is determined by the characteristics of the monomer and photo initiator. Photopolymers were used to create the rheology and curing characteristics of ceramic suspension. Bae et al. [232] investigated a technique for estimating the amount of sedimentation that takes place as layers in ceramic additive manufacturing. According to the study, using Fast Fourier Transforms (FFTs) makes it easier to spot flaws that develop as a result of the ceramic fabrication process sedimentation from layer to layer.

Zirconia ceramic parts created using laser scanning stereolithography were evaluated for their physical and mechanical characteristics by Xing et al. [233]. Along with studies on the impact of microstructure on mechanical properties, physical properties such as surface roughness of the printed body and warpage were measured with respect to printing sizes of Zirconia bars. As an alternative to the lost wax process for creating small and complex designs and patterns, Bae and Zhou et al. [234,235] proposed the direct fabrication of ceramic shell moulds and the steps involved in the process by the ceramic stereolithography method. The rheology of the ceramic suspensions and other photosensitive characteristics of the photopolymer-assisted preparation of ceramic suspensions should be assessed.

Chen et al. [236] investigated that the focused on the optimization of printing parameters for stereolithography-based ceramic part production. The effect of stereolithography-based printing parameters, such as layer thickness, laser energy beam scanning speed, etc., as well as sintering conditions, such as temperature, soaking time, and heating rate, were studied using the Taguchi method. Alumina-based ceramic antennas were created using the stereolithography technique by Nguyen et al. and Leigh et al. [237, 238] research on polymeric resin and magnetite nanoparticles allows for the fabrication of three-dimensional micro sensors using the micro-stereolithography technique.

Stereolithography was used to create zirconia ceramic bridges, according to research by Lian et al. [239]. Vacuum freeze drying was done after stereolithography on a suspension of light-curable zirconia. The sintering conditions and scanning speed were crucial variables that could affect the mechanical and microstructural properties. The stereolithography method was used by Bae et al. [240] to analyse the photopolymers present in the formed ceramic body's curing behaviour. The photopolymer resins were not completely cured and some areas still contained uncured resin, which caused microcracks to start and spread during the heat treatment. To prevent the initiation of cracks, photopolymer resins must be completely removed.

The ceramic structures were created using a freeze-form extrusion-based 3D printing technique, according to Huang et al. [241]. In the study, ceramic parts were printed using an optimally rheological alumina paste, which was applied in layers in an aqueous medium. The study also looked at how process variables affected the printed geometry. Leu et al. [242] investigated the printing of functionally graded composite structures utilising the freeze-form extrusion process. The colloidal sol was created by the authors using a composite of tungsten and zirconium carbide and was then printed into intricate structures. The mechanical and microstructural characteristics of the sintered samples were also examined.

Alumina, bioactive glass, and tricalcium phosphate were used to create cellular structures using lithography-based stereolithography. To produce dense ceramic components, the rheological parameters for ceramic suspensions should be optimised and According to Gmeiner et al. [243], stereolithography can be used to print ceramic bio devices for cell culture, and proper surface topography control produces surfaces with controlled microstructure. Schwentenwein and colleagues [244-245] investigated the production of dense ceramic parts using a ceramic manufacturing process based on lithography that was highly effective in terms

of the physical and mechanical properties (LOM). LOM involves printing ceramic suspension that, when exposed to light, hardens, resulting in the production of highly dense ceramic.

2.5: Identification of problem of statements

Based on the above literatures the gaps we found that in the research and investigation on the applicability of the following statements:

- So-far advanced ceramic products developed are still having issue of less densification and green strength
- Restricted consistency in the processing of the complex shaped products
- Achieving High productivity in ceramic processing with accurate dimensions
- Less time consumption for fabrication of higher green strength ceramic products
- Limited literature of Pressure Slip Casting and ceramic 3D Printing for advanced oxide-based ceramics
- Limited use of either of finer or coarser grain size particle for the processing of colloidal
- The 3D printing process is currently primarily focused on shaping conventional ceramics using UV curable monomer resins. The process for advanced ceramic materials like Alumina and Aluminum Titanate studies.

2.6: Objectives of the research work: The present research was focusing on the following contents.

- The objective of present research was to develop oxide-based ceramic products through different ceramic processing routes in order to develop required complex shaped way along with densified manner.
- To prepare Alumina (Al_2O_3) and Aluminum Titanate (Al_2O_3–TiO_2) products from powder state in various proportionate and to optimise preparation of slip for suitable rheological behaviour and colloidal ceramic processing techniques (CSC, PSC).
- To design and fabricate polymeric resin-based mould to cast a typical shape of a cylindrical disc (~ ϕ 80mm)., Square of 60mm, Spherical crucible (~ ϕ 60mm).

- Optimise the processing parameters like applied pressure, rheology, solid loading and study the effect on thickness built up as a function of time. To be validated on the Pressure Slip Casting.
- To compare the Pressure Slip Casting, Conventional Slip Casting Process with respect to their performance and parameters effect in obtaining ceramic bodies with dimensional accuracies in required complex manner.
- To correlate green and sintered densities of the densified ceramic products along with the Mechanical and microstructural properties.
- To compare colloidal techniques (PSC, CSC) and dry stage Cold Isostatic Pressing techniques with respect to processing parameters effect on the evaluation of mechanical &microstructural properties and it' s attributed correlations among all the process.
- To study the wear properties of Alumina Cast samples prepared through PSC & CSC with corresponding microstructural evaluations.
- To prepare the ceramic products by using Ceramic 3D printing and comparing with colloidal techniques of CSC, PSC & Dry cold isostatic pressing with correlate mechanical properties characterisation along with the microstructural properties of the obtained dense composite ceramics.

2.7: Scope of the work: Following are the scopes listed after evaluating the above body of literature to investigating the applicability of colloidal and non-colloidal processing shape techniques for further research.

1. Because of its intrinsic brittleness and low mechanical properties, advanced ceramic products usage in structural applications has been limited. As a result, there is not only a scientific but also a technological desire to overcome these restrictions using modern processing techniques that allow microstructures to be tailored.
2. Components in near-net shape with homogeneous qualities in bigger sizes and complicated characteristics are frequently required for structural applications, requiring a fair balance of high productivity and commercial feasibility. Several processes, including as uni-axial compaction and isostatic pressing, are commonly used for basic and sophisticated shaping, however they suffer from the constraints listed above. Colloidal processing techniques are the suitable to above requirements.

3. Slip casting is a well-known traditional method for moulding ceramics that produces products with acceptable and desirable qualities. However, this method is very versatile in terms of output, homogeneity in delicate designs and rejection losses are key bottlenecks, particularly in traditional and advanced ceramics. Pressure casting with polymer moulds is currently gaining popularity in this area.
4. Despite the fact that pressure slip casting has not been considered for advanced ceramic component production, thorough research on the process has recently been limited for oxide-based ceramics.
5. Unlike traditional slip casting, slip characteristics for casting under pressure should fulfil the basic requirements of a well-dispersed and stable slip while also keeping shape during the election cycle through interparticle locking. Research is been into improve particle interlocking by mixing alumina with varied particle sizes and then analysing the effect on physico-chemical and mechanical properties after sintering.
6. The goal of whole work is to complete the investigations on the applicability of oxide based ceramic products colloidal under pressure / pressure less conditions and or non-colloidal cold iso-static dry pressing in order to improve the properties.
7. Developing good mechanical and sliding wear property enhancement for high temperature applications by these above colloidal processes.
8. Creation of intricate ceramic components of Alumina and Aluminum Titanate using 3D printed polymer replicas.
9. Characterization of physical, thermo-microstructural characteristics of printed and sintered components.

CHAPTER 3

Experimental Procedures: Materials & Methods

The experimental techniques use the powder metallurgy route to manufacture ceramic products in innovative and creative ways to further develop new materials required in application-oriented industries. Basically, powder metallurgy is the use of various powders as raw materials in processing technology to create new materials and products, followed by sintering and / or other secondary processes if required. Powder metallurgy (PM) is a powder-product forming technology that uses powders (Metals or ceramics) as raw material, which are formed into a specific shape and size and then sintered at high temperature, which can able to have high performance properties depending on the processing route and amount of porosity control. The PM techniques for manufacturing ceramics or metals products involves the following steps 1. Making or selecting the required powder, 2. Mixing or blending 3. Shaping or product making 4. Sintering or firing 5. Secondary processes if required [246-252]. This chapter describes the raw materials utilised in this research to fabricate Alumina (Al_2O_3) (AL) and Aluminum Titanate (Al_2TiO_5) (AT) using various ceramic manufacturing methods, as well as the equipment & techniques used for physico-mechanical along with microstructural characterisation.

Overall processing work flow chart

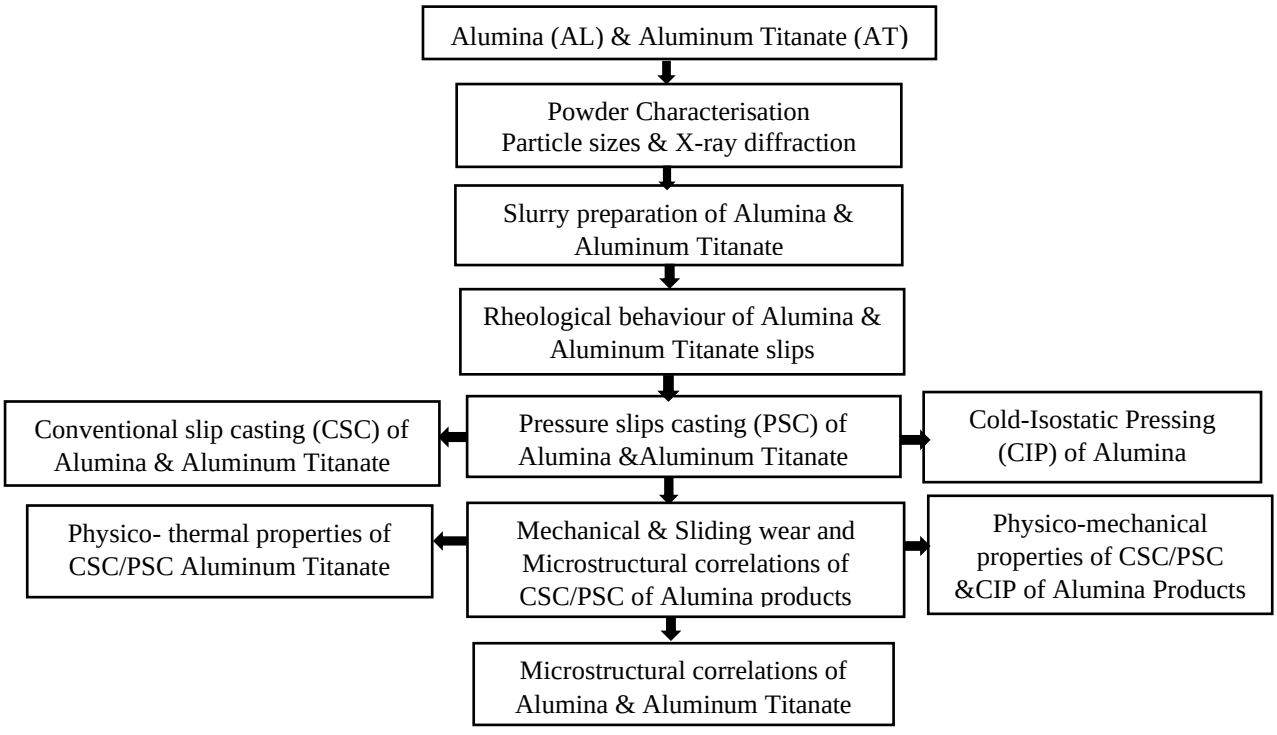

3.1 Powder characterisation:

The starting powder is used as the foundation for creating or processing ceramic components, and its properties are crucial for the final product's physical (density, porosity, and pore size), mechanical (hardness, compressive strength, flexural strength, and fracture toughness), and microstructural (microstructure) characteristics (grain size and their distribution). Because of this, the choice of raw material and its characteristics, such as particle size and distribution, morphology (Particle shape and shape distribution), are crucial for adaptability to attain better packing densities with different ceramic processing procedures.

3.1.1. Raw materials for fabrication of AL and AT ceramic products:

Raw materials used for ceramic products were Alumina, Titania and Aluminum Titanate were fabricated in different required proportionate quantities (Table.3.1) were measured with the Mettler electronic micro-balance with a precision of 4 decimal places.

Table: 3.1 The Raw materials used for the processing of ceramic products

Material	Chemical Formulae	Purity	Source
Alumina	Al_2O_3	99.99%	Hindalco, India
Titania	TiO_2	99.99%	Loba chemicals, India
Darvan 821A	$[C_2H_4COO^-]_n [NH_4]_n^+$	99.99%	RT Vanderbilt Inc, CT, USA

3.1.2. Particle size and its distribution: Advanced ceramic powders are generally characterized by laser diffraction or dynamic light scattering techniques for particle size and its distribution, and the basic principles & procedures are described [253-254]. The most popular method for determining particle sizes, which range from hundreds of nanometers to several millimeters, is laser diffraction. It establishes particle size by angularly varying the intensity of light scattered from the distributed sample. The wave phenomenon known as diffraction occurs when incoming light is bent because of obstructions in its path of travel. It is a method of analysis to determine how finely the powder in the solvent is dispersed. The inverse relationship between angular variation and particle size serves as the fundamental guiding principle of the laser diffraction technique. The diffracted light shows a smaller angular variation when the particle size is large, and a larger angular variation when the particle size is small. In actuality, the particles measured size should fall within the laser light's wavelength range in order to measure particle size. The diffracted beam is found and studied using the

Fraunhofer and Mie theories. While Mie theory accounts for both optical and scattering properties of particles, Fraunhofer theory is straightforward, effective for opaque particles, and only takes into account optical properties [255-259]. One or more particle sizes are indicated by D_{mode} in the particle size distribution. D_{mode}, the magnitude of the cumulative distribution curve, represents a range from 0% to 100%. The D_{50} reference point, which is the most common in laser diffraction, denotes the region where 50% of the particles are smaller and 50% are larger than a particular diameter. Particle size can be measured using the dry method with laser diffraction, which calls for 3-5g of powder in the chamber. According to the particle size, the incident laser beam is diffracted during the process at various angles, and each diffraction angle is recorded and displayed on the screen as a diffraction pattern. A sophisticated algorithm analyses the diffraction pattern and calculates the particle size and distribution values [260-261].

Dynamic light scattering, also known as quasi-elastic scattering or photon correlation spectroscopy, is another popular technique for estimating particle size. The analysis of particle size involves measuring the velocity of particles dispersed in liquid media as a result of a particles random motion. Brownian motion is the name of this motion. When the particle is exposed to monochromatic light, it scatters in all directions. The fluctuation of local particles suspended in the liquid as a result of random particle motion causes inhomogeneity in the materials refractive indexIn addition, it generates a Rayleigh scattering spectrum whose line width is proportional to the diffusion coefficient and has the form (half width at half maximum) (D). By using the formula R=(KT/6D), where K is the Boltzmann constant, T is the absolute temperature, is the medium's coefficient of viscosity, and D is the diffusion coefficient, the Stokes-Einstein equation can be used to calculate the mean radius of a particle under the assumption that the particles are spherical and not interacting [262-264]. During the current research project, a typical particle size analyzer, Nano-SZ, from Malvern Instruments Limited, UK (Fig.3.1), is used.

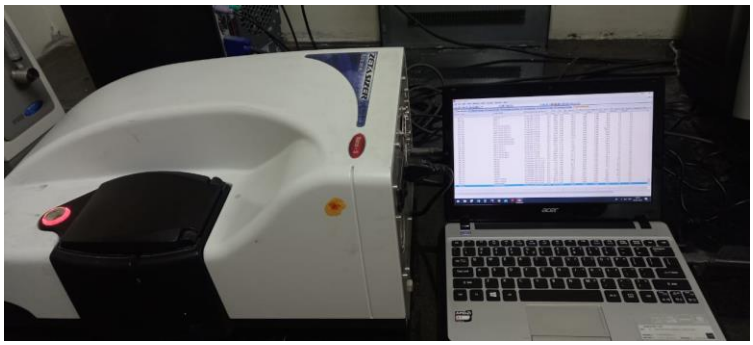

Fig .3.1: Particle size analyzer (Nano-SZ, Malvern Instruments Limited, UK).

3.1.3. X-Ray diffraction: The family of non-destructive analytical methods known as X-ray scattering techniques provides insight into the chemical make-up, physical characteristics, and crystal structure of materials and thin films. These methods rely on observing how an X-ray beams scattered intensity changes in relation to incident and scattered angles, polarisation, and wavelength or energy. X-ray diffraction is one of the most efficient techniques for identifying crystalline substances, such as metals, intermetallic compounds, ceramics, minerals, polymers, plastics, or other inorganic or organic substances (XRD). Similar to how crystals are ordered arrangements of atoms, X-rays are electromagnetic radiation waves. X-ray waves are primarily reflected off of atoms by their electrons. Secondary spherical wave fronts emerge from an electron when an X-ray hits it. The electron is referred to as the scatterer in this phenomenon and is known as elastic scattering. A regular array of spherical waves results from a regular array of scatterers. Even though these waves interfere destructively in most directions, Braggs law states that they add constructively in the following few directions: $n\lambda = 2d\sin\theta$. Here, n is any integer, d stands for the separation between diffracting planes, for the incident angle, and for the wavelength of the beam. Reflections are spots on the diffraction pattern that represent these particular directions. As a result, X-ray diffraction happens when an electromagnetic wave (the X-ray) strikes a predictable arrangement of scatterers (the repeating arrangement of atoms within the crystal). The diffraction pattern is produced by X-rays with a wavelength that is typically in the same range (1-100 angstroms) as the separation between the crystal's planes. To cause significant diffraction, the distance between the scatterers and the wavelength of the incoming wave must be equivalent in size [265-266]. Current research uses the X-ray diffracted approach (Fig. 3.2) for the diffraction analysis.

Fig.3.2: X-ray diffraction (D8-Bruker, Germany).

3.1.4. Characterization of AL & AT powders and preparation of slips for PSC / CSC / CIP:

Alumina powders of grade MR-01 and HIM-10 (with different average particle sizes of 1.43 and 7 µm, purchased from HINDALCO, India) were used in the present work, together with their mixture in the ratio of 65:35 (HIM-10: MR-01) denoted as HM-mix. Dynamic light scattering (Nano-SZ, Malvern Instruments Limited, UK) was used to examine the particle size distributions of all three powders and X-ray diffraction (D8-Bruker, Germany) to identify the associated phase composition. Darvan 821A (R. T. Vanderbilt Co. Inc, Norwalk, CT, USA), a dispersant, and octanol, an antifoaming agent, were used to disperse the mixed alumina powder (HM-mix) in distilled water.

Fig.3.3. Pot jar mill.

Following that, the suspension was ground for two hours in a pot jar mill (Fig. 3.3) using alumina balls with a 2 mm diameter and a 1:1 charge to ball ratio. For the suspensions used in pressure slip casting (PSC) and traditional slip casting, solid loading of 73-75 wt.% (42.3 - 42.9 vol.%) was attained (CSC). Similarly, three aqueous slips were prepared using the MR-01, HIM-10 and HM-mix powders with solid loading of 35-40 wt.% (12.76-14.32 vol.%), from which granules for cold isostatic pressing (CIP) were obtained. Throughout the procedure, spray granulation was done using a spray dryer (B290/295, BUCHI Switzerland) with optimal settings of let temperature of 200°C and atomization pressure of 6 bars.

Aluminum Titanate, AT (Al_2TiO_5), from raw materials-Alumina (Al_2O_3) and Rutile-Titania (TiO_2) were taken in equimolar proportions and considered without/with minor additions of Magnesium-di-oxide or Zirconia for stabilisation purposes, and then dry mixed with ball milling for 3 hours. A TG-DTA analysis was performed to determine the thermal behaviour of the softening temperature range in relation to heat treatment. Calcination was performed at temperatures ranging from 1350 to 1400^{o}C before being crushed and sieved for

micron level particle size, which can be measured using a particle size analyser in the DLS technique. The phase formation of AT was confirmed using X-ray diffraction analysis.

To prepare the slurry for CSC & PSC, the composition was optimised with various solid loadings ranging from 50-60 wt.% and were mixed with an optimised concentration of distilled water with the 1 wt.% dispersant (Darvan 821A, ammonium polyacrylate, RT Vanderbilt Inc, CT, USA). In a pot jar mill, above- mentioned suspensions were wet-mixed for four hours at a rate of 20 rpm to obtain the requisite homogeneity and slip stability, and afterwards, Aluminum Titanate slurry was created.

3.1.5. Rheological behaviour of ceramic slips and flowability of granules:

Fundamentally, the interactions between thermodynamic and fluid mechanical forces determine the rheological characteristics of concentrated colloidal suspensions. This shows that the particle interactions, including Brownian motion, and the suspension structure (i.e., the spatial distribution of the particles in the liquid), are closely related to the rheological response. When particles are in the colloidal size range (at least one dimension is 1 μm), the magnitude and range of the interparticle forces will significantly affect the suspension structure and, consequently, the rheological behaviour. Both the fluid mechanical interactions and the interparticle forces are significantly influenced by the average separation distance between the suspended particles. Consequently, the range and amplitude of the interparticle interactions, particle size and shape, and solid concentration all affect the rheological behaviour of concentrated suspensions. Rheology and flow behaviour play a significant role in shaping ceramics [267-270]. The current work uses an Austrian rheometer, model MCR 51 by Anton Paar, to characterise and analyse the rheological behaviour of ceramic slips.

Fig.3.4. Rheometer

3.1.6. Rheological behaviour of AL &AT ceramic slips:

The prepared slips of different solid loadings of AL and AT were examined for their rheological characteristics using a rheometer (MCR 51, Anton Paar, Austria) (Fig. 3.4) at various shear rates by concentric co-axial cylindrical plates setup with 1.75 mm centre distance between them while maintaining constant temperature at 25^{o}C. Rheological behaviour of the slip was measured using rheometer with a configuration of two parallel plates at room temperature at various shear rates. The viscosity is estimated and recorded as a function of shear rate. Granules subjected to granule flow measurement using a powder flow analyzer (Stable Micro System, UK), that uses a rotating helical blade moving through the granules under controlled speed as per the standard operating procedures. In the typical measuring process, 50 gm of the granules will be taken in a programmed blade motion inside the cylinder containing the granules, which validates the flow modes of compression while travelling downhill and clockwise and slicing while moving oppositely. At the same time, the blade moves up in the clockwise direction and lifts the powder granules. The comprehensive measurement technique is reported.

3.2 Pressure Slip Cast (PSC) / Conventional Slip Cast (CSC) Processing:

The Pressure slip cast / Conventional slip cast processing will follow the following schematic procedure.

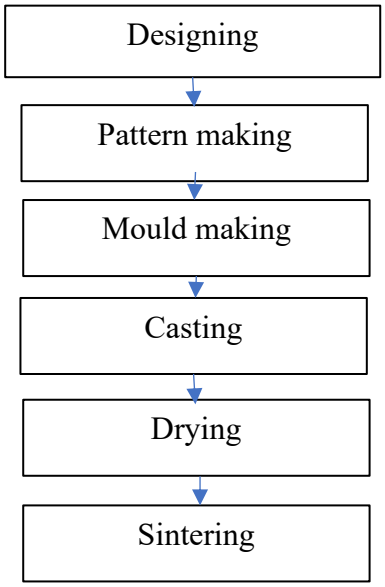

3.2.1. Designing and pattern making:

For the required the product to be fabricate designing is to do by using CAD software with correct dimensions including shrinkage allowances for both the above process. After designing the pattern which replica of the required product to be made is to be fabricated with stainless steel material. Following are the required patterns (Fig.3.5) for fabricating all the models of Alumina and Aluminum Titanate products.

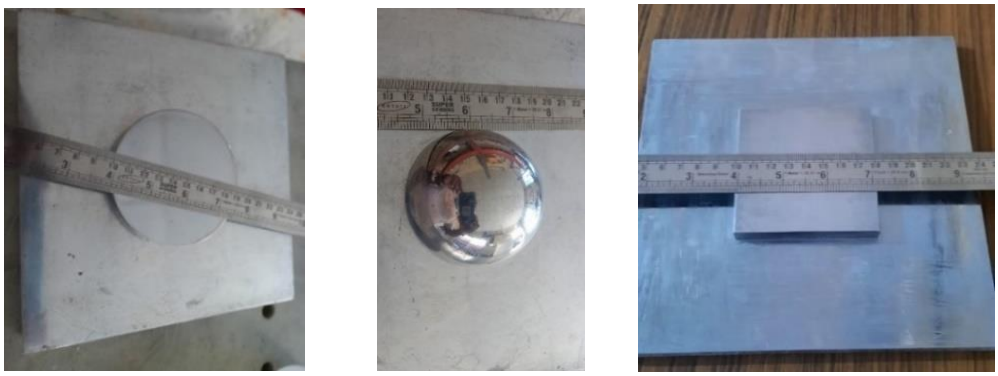

Fig. 3.5: Patterns made for cast of a) Cylindrical disc b) Spherical ball c) Square patterns

3.2.1. Fabrication of moulds for CSC, PSC and CIP:

The first step in sample preparation was the preparation of suitable moulds for pressure slip casting (PSC), conventional slip casting (CSC), and cold isostatic pressing (CIP). The porosity of the mould is critical for PSC and CSC processes to ensure the flow of liquid medium into the mould while the cast is formed. The fabrication of a CSC Plaster of Paris (PoP) mould is relatively simple. PoP powder was mixed with water in the appropriate proportion before being poured into a prefabricated SS316 (stainless steel) patterns of square of 60x60x10 mm, and disc of ϕ80mm with thickness of 10 mm shown in fig.3.6 a) and b). When the pattern was finished, it was removed from the mould. Because the PoP moulds are weak, the processing pressure is limited to atmospheric pressure.

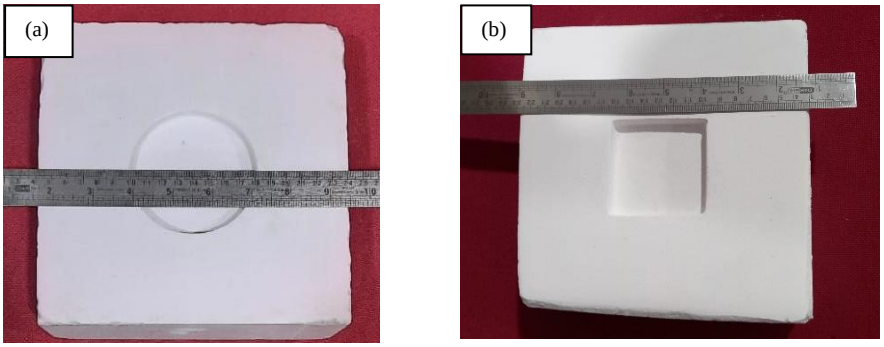

Fig. 3.6 : Plaster of paris moulds for conventional slip casting (a) cylindrical disc and (b) Square.

3.2.2. Fabrication of moulds for PSC:

On an industrial model PCM (PCS-100N, SAMA GmbH, Germany) (Fig. 3.7), PSC experiments were performed with a variety of processing control parameters, including slip feed rate, slip pressures ranging from 1 to 40 bars, pressure dwell time, and cast de-molding in accordance with the PSC Cycle (Fig.3.8). Stainless Steel (SS) patterns and shrinkage tolerances were used to manufacture polymer moulds for PSC, resulting in final dimensions of about 80

x 7 mm thickness and 60 x 60 x 10 mm. To prepare specimens for mechanical characterization in line with ASTM standards, these specimens are utilised to optimise sintering conditions. PSC fabricates resin-based polymer moulds using proprietary polymer materials supplied by M/s. SAMA Maschinenbau GmbH, Germany. The fabrication process entails mixing polystyrene granules and additives and casting on a prefabricated pattern of SS-316 with dimensions of 100 mm x T: 8 mm and a 20% allowance for shrinkage in the cast part. Furthermore, optimised releasing angles were used to create polymer-based (SAMA pore, SAMA Maschinenbau GmbH, Germany) macro porous moulds. Scanning Electron Microscopy (SEM) was used to further characterise these moulds, and micrographs were taken.

The mould has a square block profile with dimensions of 60x60x10 mm^3 and outer dimensions of 200 x 200 x 150 mm^3. The mould also has 5mm diameter holes with a 20 mm pitch in the 140 mm^2 area for air and water circulation on the opposite side to facilitate a faster casting process under pressure on the slip loaded in the cavity. These holes serve as channels for removing water from the slip during cast formation under pressure, as well as for pressurizing with air during demoulding. Polymer moulds have a longer life and can withstand pressures of up to 40 bar while casting. The moulds SEM micrograph revealed highly porous features with inter-connected pores, which facilitates filtration and cast formation.

In order to prepare the two-part polymer mould set for pressure casting alumina solid spheres of about 60 mm, SS patterns were also made based on the data base created by these samples. Figures 3.9 and 3.10 show cross-sectional views of the polymer casting moulds and the moulds used for casting. It is clear that, in contrast to CSC, PSC comprises four key processes: feeding the slide, pressurisation, cast development, and cast release. In theory, the PCM will have static and mobile plates, each with a polymer mould part fixed to ensure proper surface contact when brought forward. During the casting cycle, the mobile part will move forward to ensure that the two parts make perfect contact. When pressure is applied to the slip in the cavity, a pressing load of up to 250 bars can be applied to the two polymer mould parts through the mobile plate to make the contact point leak proof. The typical pressing pressure used in this study was 80 bar. Once the mould parts are held together, the casting process follows the following steps: slip feeding, pressurising the slip in the cavity, holding the pressure, de-pressurization, and finally de-molding of the cast piece using air / water back pressure.

Fig.3.7: PCM -100-N (SAMA GmbH)

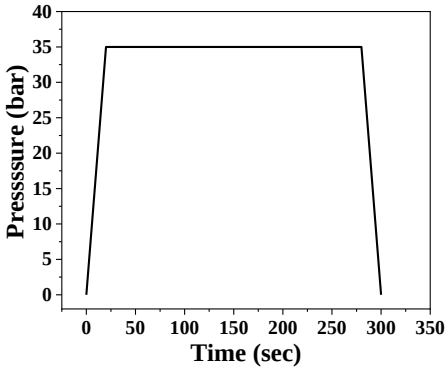

Fig. 3.8: Pressure cast cycle

To find the perfect conditions that would result in the cast forming with greater green density values of > 60% of theoretical densities, numerous experiments were conducted in our lab. To produce densities that were similar to the theoretical value, CSC and PSC samples were sintered under the same conditions at 1600^0C for 1-2 hours.

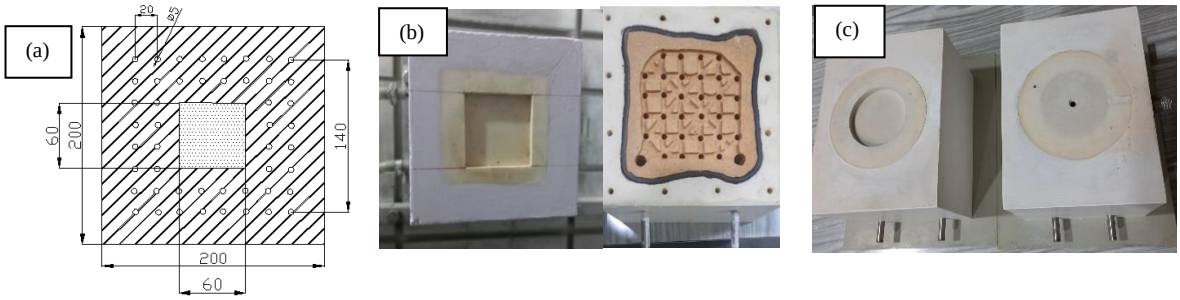

Fig.3.9. (a) Cross section of polymer mould and (b) square (c) Cylindrical disc moulds

Fig. 3.10. Polymer moulds of (a) Square, (b) Cylindrical disc and (c) Spherical shape mould.

3.2.3. Fabrication of moulds for CIP:

For Cold Iso-static Pressing designed and fabricated a non-permeable elastic mould for CIP using flexible latex rubber (Dhas Rubbers, Kanyakumari, Tamil Nadu, India) for the prerequired size of 55 x 60 x 10 mm^3 shown in Fig.3.11.

Fig.3.11: Non-Permeable rubber- mould used for cold iso-static pressing

3.2.4 Cast formation through CSC, PSC and CIP

Porosity of the mould is very important to ensure flow of liquid medium into the mould while casting formations. The previously obtained homogeneous slip with 75 wt. percent solid loading was poured into the porous PoP mould in conventional slip casting (CSC). Water was absorbed via the capillary process, which was followed by the formation of a layer along the walls of the PoP. To make up for the slip level, a small amount of slip was put into the cavity of the mould. The cast was not released from the mould until the mould had dried after casting.

A pressure casting machine (PCM-100, SAMA Maschinenbau GmbH, Germany) with a closure force of 1000 N and a maximum working pressure of 40 bar was used to perform pressure slip casting (PSC)(Fig.3.12). The slip was poured into the porous polymer mould for 15 seconds at a feed pressure of up to 5 bar. After filling, a slip pressure of 35 bar was applied with a 5-bar increasing step and held for 60 seconds to control the pressure effect on cast build-up. Finally, using air pressure, the cast was extracted from the polymer mould.

Fig.3.12: Pressure Slip Casting Machine in operating condition (PCM-100, SAMA, GmbH, Germany).

The prepared spray dried granules were vacuum sealed in a rubber bag, placed in a 55x60x10 mm SS vessel, and cold isostatically pressed at 1200 MPa using a CIP equipment (10027, Avure Technologies AB, Sweden). Casting of the slip was performed using a pressure

casting equipment of model PCM-100 (SAMA GmbH) using 1000 N of closing force and a maximum operating pressure up to 40 bar. The slip was injected with a feed pressure of up to 5 bar and a filling time of 15 seconds into the porous polymer mould (as constructed above). To control the pressure effect on the build-up of the cast, a slip pressure of 35 bar was given after filling with an increase of 5 bar, and this pressure was held for 60 seconds. Slip was also casted through conventional slip casting generally used in ceramic processing. For CIP processing granules were vacuum sealed in rubber bags and cold isostatically pressed at a pressure of 140 MPa using a CIP equipment (10027, Avure Technologies AB, Sweden).

3.3. Drying, sintering and characterization of samples:

All the samples were allowed to dry at 110°C and the green densities are determined by dimensional method. All the Alumina samples were further sintered at 1600°C for 2 hr and sintered densities were determined by Archimedes principle.

3.4. Mechanical characterisation of Alumina sintered samples from PSC / CSC:

According to ASTM D792, 2013, hardness values were obtained by ASTM C1327, and the density of the samples (PSC and CSC) was assessed using the Archimedes principle utilising a density measuring kit (LA 120S, Sartorius AG, Germany) (Fig. 3.13). Vickers Macro Hardness Tester was used to determine the samples micro hardness (ASTMC1327) (Fig. 3.14).

Fig. 3.13. Archimedes principle kit

Fig.3.14. Microhardness tester

Three-point bend tests (ASTM C1161) were used on sintered samples with dimensions of 45 x 4 x 3 (L x W x d) mm^3 to estimate the flexural strength values. Moreover, fracture toughness (KIC) was assessed using ASTM-C1421, (SENB), using the Universal Testing Machine (UTM-Instron-model 5584, UK) (Fig. 3.15). For each of the aforementioned test circumstances, five samples were tested to obtain the average values, and for this 50–80 N range testing with a ramp rate of 0.5 mm/min were employed. Also, the samples were compressed, and the compression strength was calculated as the load per unit area.

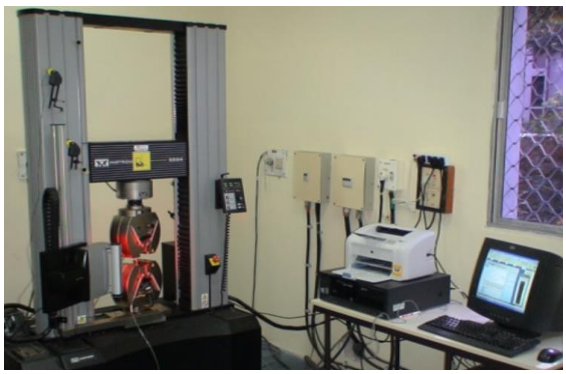

Fig.3.15. Universal Testing Machine

Fig. 3.16. DUCOM Pin-on-Disk Tester.

3.5. Sliding wear characterisation of Alumina sintered samples from PSC / CSC:

According to ASTMG99 requirements, a sliding wear test was performed using a DUCOM pin-on-disk tester (TR-20LE-PHM400-CHM600, DUCOM Instruments (Asia), Bangalore, India) (Fig. 3.16) To fit inside a square pin slot, specimens were prepared into 10 × 10 × 7 mm^3 sizes. The material employed was a round WC-Co disc with a hardness of 21±0.15 GPa, a 160 mm diameter, a 5 mm thickness, and a roughness of 0.25±0.01 m. The sliding velocities ranged from 0.5 m/s to 2.5 m/s, while the weights ranged from 5 N to 25 N. The worn samples microstructural characteristics were documented using a FESEM (S-4300SE/N, Hitachi, Japan).

3.6. Comparative analysis of colloidal (PSC / CSC) and non-colloidal (or) dry (CIPing) of Alumina products:

The green CSC, PSC, and CIP samples (an average of 5 samples each) were machined to 45 x 4 x 3 mm^3 size for flexural strength measurement using a 3-point bend test as per (ASTM-C1161) and measured with a Universal Testing Machine (4483, Instron, UK). A diametral-compression test was also used to determine the materials' green strength, and the failure stresses within the samples were compared to the shaping environment. High green strength is indicated by superior mechanical qualities, strong fracture resistance, smooth surfaces, sharp corners, and fine details. This test is carried out using a UTM (Model No. 5584, Instron, USA) and a technique known as diametral compression between two flat plates, which is frequently used to evaluate the crushing strength of compacts. Green CSC, PSC, and CIP blanks were cut into 20 mm diameter and 5 mm thick samples for testing. The samples were sintered again for 2 hours at 1600°C, and sintered density (average of 5 samples) was determined using the Archimedes principle (ASTM C373) and a high precision digital electronic balance (Secura 225D-10IN, Sartorius, Germany). FESEM was used to record the

microstructural properties of the green and sintered samples (Gemini 500, Carl Zeiss, Germany).

3.7. Physico-thermal properties of Aluminum Titanate products of PSC / CSC:

Fabrication of AT products done for casting in both cases of PSC/CSC on the moulds of previously fabricated with dimensions of ϕ 60 mm with thickness of around 10 mm having 20% allowance in shrinkage in the cast part. The physical properties such as density, thermal properties of Thermogravimetric-differential scanning calorimetry (TG-DTA) measurements, and coefficient of thermal expansion along with microstructural analysis done. With the help of a horizontal dilatometer, dilatometric measurements were made (DIL 402 PC, Netzsch Company). The 5×5 ×25 mm^3 rectangle bar sample was tested in air that was heated and cooled at a rate of 5°C/min from ambient temperature to 1400°C.

3.8. 3D Printing of Alumina and Aluminum Titanate:

An FDM-based 3D printing process is chosen to establish the AM process based on the ceramic extrusion processing expertise available at ARCI for the fabrication of ceramic honeycombs, concentric tubes, etc. As a result, the specifications were created, and a 3D printer was built by an Indian manufacturer (3D Cerami, Trivandrum), which depicts the machine that was created and constructed in accordance with the specifications and the overall schematic process schematic representation (Fig.3.17) is shown.

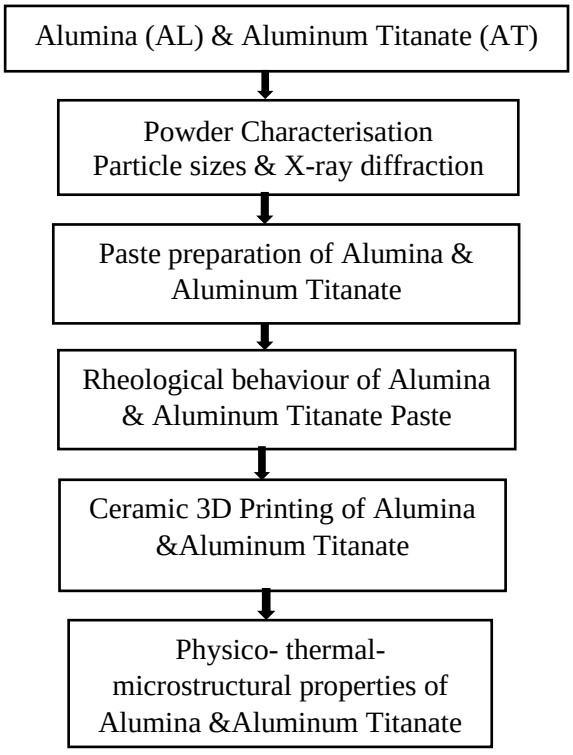

Fig.3.17: Schematic Representation of 3DPrinting of Alumina and Aluminum Titanate

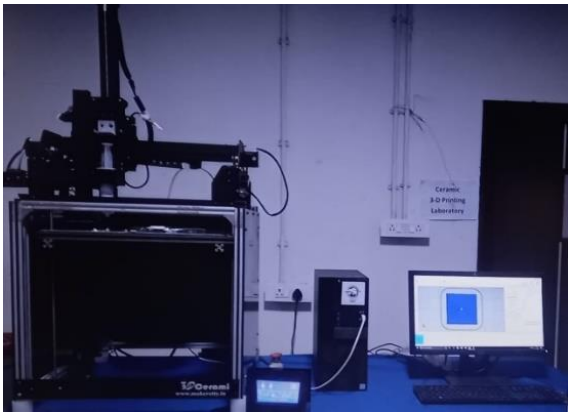

Fig.3.18: 3D Printing system

The 3D printer system, which can be seen in Fig. 3.18, is made up of a stepper motor, transmission screw, plunger, barrel, barrel holder, and platform that serves as the base support for printing the object. Stepper motors are responsible for all axis movement and transmission screw rotation. Electric motors that use direct current (DC) and move in discrete steps by dividing the number of rotations into an equal number of points are called stepper motors. The coils in a stepper motor are organised into phases, which are groups of coils. Additionally, with the aid of the electrical connections, each stepper motor phase will energise in turn, causing the motor to rotate one step at a time. Since the stepper motor is computer-controlled, the motor speed can be set with extreme precision.

The 3D printing system has a stepper motor combined with a driver motor for the X-axis and two stepper motors for each axis responsible for the movement of Y and Z. The machine's driver motor is located at the top and rotates precisely under computer control. The stepper motor transforms electrical energy into rotational energy and transfers the necessary power to the transmission rod, which causes the plunger head to translate. The plunger is forced into the barrel to extrude the interior feedstock material through the attached nozzle on the platform as a result of the rotation of the transmission screw applying pressure to the plunger's top surface. The 3D printing systems barrel was fixed in the extruder holder. Two extra stepper motors are used to anchor the bottom of the printer and control the layer-dependent translational movement of the Z axis. To control the Y axis, two stepper motors were mounted on the side of the printer, and one stepper motor was mounted on the back of the extruder holder to translate the X axis.

The printing parts were created using a CAD model created with the CATIA software. The Repetier Host software, which is user-friendly and compatible with all 3D printers, was

installed on the computer. By importing the CAD design into the software, slicing with predesigned printing parameters, and sending print commands to the 3D printer from the computer, this software enables users to operate 3D printers directly from computers. Also connected to the 3D printer is a microcontroller unit, which performs the following tasks (a) importing the CAD model into the repeater host software (b) performing a slice with the specified printing parameters (c) generating the G-codes (d) saving the G-codes on a data card; (e) supplying the microcontroller unit and (f) issuing the print command from the microcontroller. the order of events shown in the flow chart in the following section.

3.8.1. Design of pneumatic screw type extruder assembly compatible to 3D Printer:

A screw type extruder has also been designed and constructed in addition to the ram type extruder. Earlier 3D printer with a ram-type extruder that is fixed to the axis frame (described in the preceding section). Ram type extruders can only feed a certain amount (batch type) of paste into the barrel, which results in print components with lower heights. As a result, a screw type extruder is created and manufactured to the specifications needed for the existing 3D printer to operate semi-continuously.

The paste is continuously fed through the hopper during the screw type extrusion process. The paste is fed into a horizontal twin screw type of mixer. The paste is thoroughly mixed before being fed into the extruder. As opposed to the ram type extruder mentioned above, the ram type barrel and piston assembly, which is operated with a screw type extruder and has a higher capacity, is depicted in Fig. 3.18, engineering drawing and schematic assembly (a) and (b) respectively. A barrel with a plunger and an extruder assembly makes up a 3D printer. The extruder assembly also includes a stepper motor that is screwed to a coupler motor, a casing cover, a material inlet, and a nozzle. Ceramic paste is forced into the barrel by the plunger with the assistance of compressed air. air compressor-supplied compressed air. The filled stock material is pushed into the screw chamber by compressed air. Through a coupler, the screw is connected to the stepper motor. The screw is rotated precisely by a stepper motor. The direction of paste flow is determined by screw rotation, for example, clockwise screw rotation causes upward flow and anticlockwise screw rotation causes downward flow of material through the nozzle (Fig.3.19).

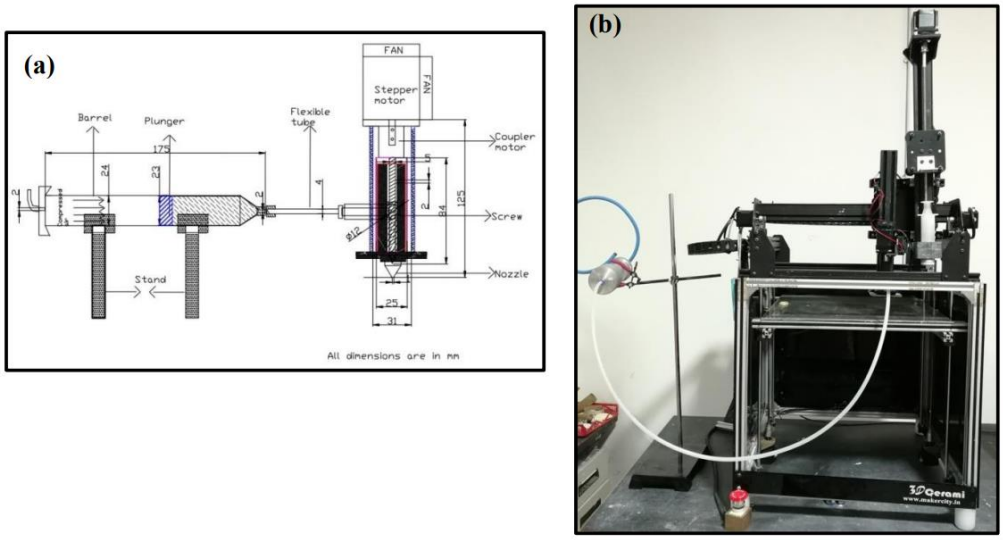

Fig.3.19: (a) Cross-sectional view and (b) Pneumatic screw type extruder assembly of 3D Printer.

The steps required in the whole printing process is shown below:

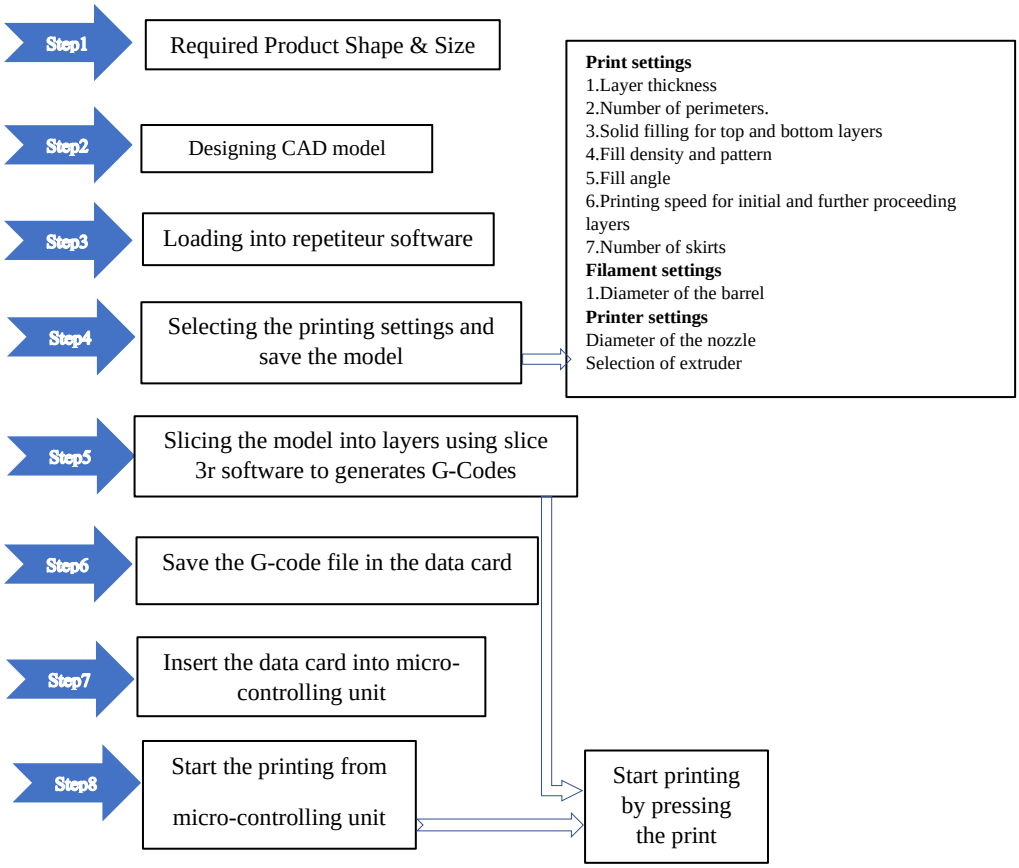

3.8.2. 3D printing of ceramic parts:

The block diagram of the 3D printer used in this investigation is shown in Fig. 3.20. The printer comes with a ram-type extruder that has a cylinder and piston coupled with an interchangeable nozzle. During the 3D printing process, a cone at the end of the barrel directs

the paste flow into a nozzle that normally has a diameter that is 22 times smaller than the diameter of the barrel. The paste is compressed within the barrel during this process, peaking up a load to overcome the initial resistance and starting to flow as extrudate through the nozzle, and printing takes place at the predetermined control printing parameters.

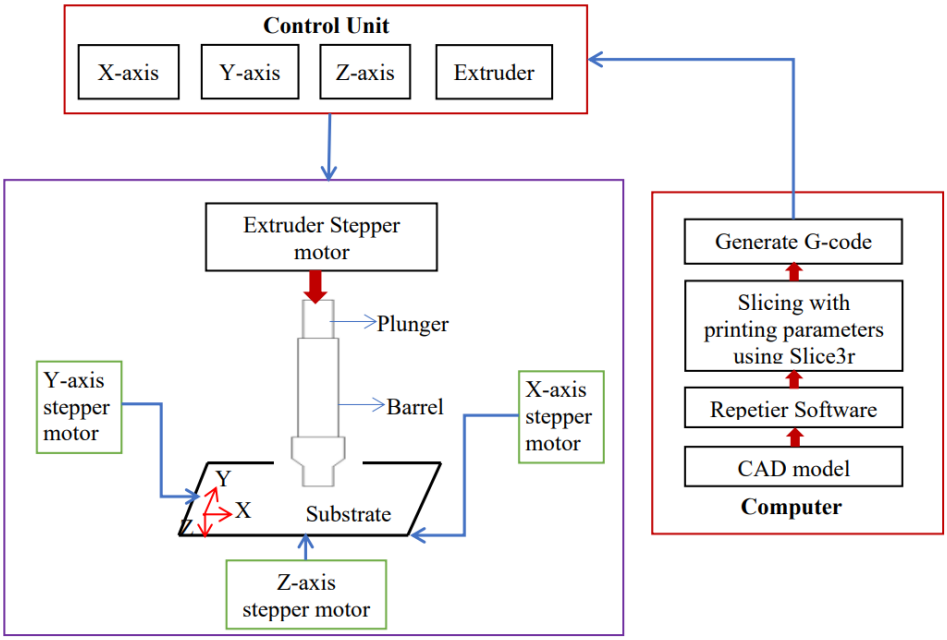

Fig. 3.20: Ram extrusion-based 3D printing process.

3.8.3. Enhancing printing parameters

The quality and characteristics of printed parts are greatly influenced by the printing parameters. The following is a list of printing parameters that were optimised for the study.

1. Self-standing distance
2. Length to diameter (L/D) ratio of the nozzle
3. Printing speed
4. Filling pattern
5. Filling angle

3.8.4. Self-standing distances impact on paste flow

According to Fig. 3.21, the self-standing distance is the vertical separation between the nozzle and substrate. The self-standing distance was adjusted from 0.5 to 1.5mm to examine how it was affected the quality of the samples and the printing process.

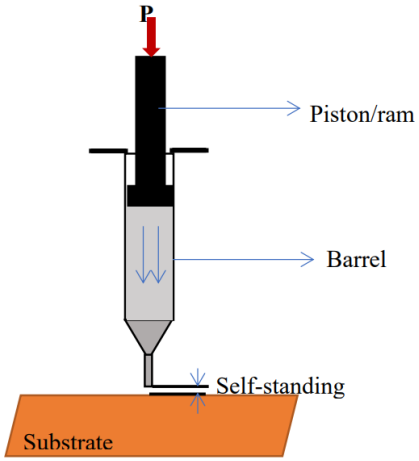

Fig. 3.21: Diagrammatic representation of the extrudates self-standing distance.

The following printing conditions were kept constant to study how self-standing distance affects printed part quality:

1. A 1 mm thick layer
2. The first layer prints at a speed of 4 mm/s, and the last layer prints at 6 mm/s
3. The first layer flows at 4 mm/s, and the last layer flows at 6 mm/s
4. Concentric filling pattern
5. Fill angle = 90^{o}
6. We choose nozzles with a 1 mm diameter

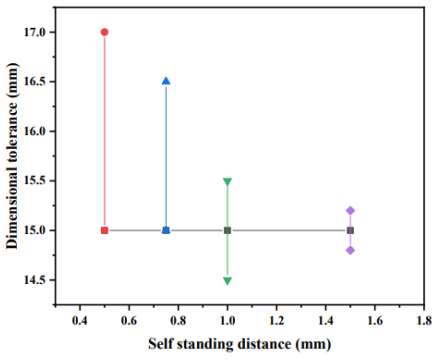

Fig. 3.22: Dimensional tolerances on effect of self-standing distance.

Fig. 3.22 illustrates how self-standing distance affects the printing of extrudate. Between 0.5 and 0.75 mm, or less than the nozzle diameter, the extrudate layers surface was smeared, and the item was produced outside of tolerance. When the self-standing distances were raised to 1

mm and 1.5 mm printed, extrudate was found to preserve the desired layer thickness and the printed parts were well within the tolerance limit. Moreover, there were discontinuities across the printed pieces at a self-standing distance greater than 1.5 mm due to the extrudate's overhanging and deviation from the intended print route. Though the self-standing distance is a function of the material chemistry and the rheology of the paste the present study provides an outline of the 3D printing process.

3.8.5. The nozzle's L/D ratio and the printed samples:

Nozzles with a fixed diameter of 1 mm and varying lengths of 10, 15, and 25 mm were made in order to examine how the L/D ratio of the nozzle affected the printed samples. The printed samples with equal rheology and L/D ratios of 10, 15, and 25 are associated with the green density. In Fig. 3.23, the relationship between green density and the nozzle's L/D ratio is plotted. The green density was identical at 2.10 g/cc for length to diameter ratios of 10 and 15, but it increased slightly to 2.14 g/cc for L/D ratios of 25. The longer nozzle's increased wall shear and paste intermixing, which enhance paste homogeneity, are responsible for the unusually high-density values.

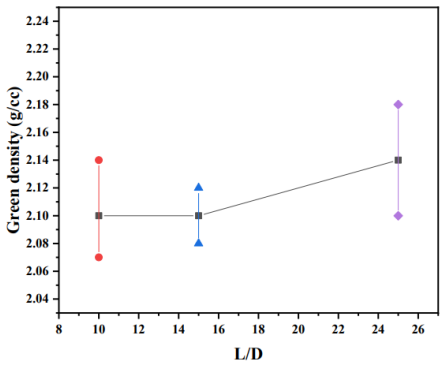

Fig. 3.23: Alumina sample plot of green density versus L/D ratio.

3.8.6. Printing speed and flow rate effects:

The X, Y, and Z axes speed can be used to define printing speed. The amount of material delivered through the nozzle in relation to time is called the flow rate. The flow rate and printing speed are interdependent. The flow rate will also increase as printing speed does. A good control of printing speed will therefore improve material flow, which in turn results in a printed part that is free of defects and within dimensional tolerances. Therefore, in order to maximise printing speed, the first and subsequent printing layer by layer thickness is kept constant, and the fill pattern and infill density are set to 100% and the perimeter, respectively. Printing takes

longer when the speed is less than 4mm/s, which further causes moisture to escape from the layers and causes inhomogeneity. When printing at a speed greater than 6 mm/s, the paste overflowed, causing deformations outside of the acceptable tolerance. Based on the observations we optimised that printing speed is 4-6 mm/s.

3.8.7. Filling pattern and filling angle effects:

Based on the optimal printing parameters discovered through previous experiments, the layer thickness of 1mm, printing speed of 4-6mm/s, and self-standing distance of 1mm were chosen to print cylindrical samples with concentric, rectilinear, and aligned rectilinear patterns. Additionally, studies were done to determine how the filling angle, which ranged from 30 to 90 degrees, affected the rectilinear filling pattern.

Base on the above experimental observations, we optimised the following parameters as layer thickness of 1mm, printing speed of 4-6 mm/s, and self-standing distance of 1mm, filling angle 90 degrees and filling pattern is rectilinear.

3.8.8. Paste preparation of Alumina / Aluminum Titanate for Ceramic 3D printing

In order to create a cohesive dough, alumina/calcined aluminium titanate powder was combined with 0.25 wt.%/ 0.45 wt.% of methyl cellulose (MC) (Loba Chemie, Mumbai, India) as a binder and 37% / 42 wt.% of water by weight of the powder. This mixture was then kneaded in a high shear blender for 30 minutes. In order to evaluate the paste's flow characteristics using a rheometer, the rheological behaviour of each paste was evaluated with regard to shear rate (MCR 51, Anton Paar, and Austria). For the printing of the specimens, a ram 3D printer was utilised. In order to print specimens at a speed of 6 mm/s with a self-standing distance of 0.5 to 2 mm, SS 316 nozzles with a diameter of 1 mm and a length of 10 mm were manufactured. After drying, the green density is associated with all the parameters.

3.8.9. Alumina / Aluminum Titanate products prepared from Ceramic 3D printing

The two pastes of MR-01 alumina powder and calcined aluminium titanate phase formed powder were made using 35 weight percent (wt.%) and 42 weight percent (wt.%) of water, 0.25 weight percent (wt.%) of methyl cellulose, and 30 minutes of kneading time, respectively. Rheological experiments were conducted on the resulting homogenous Alumina and Aluminum Titanate pastes at various shear rates (MCR 51, Anton Paar, Austria). A ram-type 3D printer with a 1.0 mm diameter nozzle and an L/D ratio of 10 to 25, with L/D 25 being the best, was used to manufacture the paste. With the current nozzle sizes, a self-standing distance

of between 0.25 and 1.25 mm was found to be ideal. Alumina and Aluminum Titanate green bodies with rectangular, hollow shapes have been produced via ceramic 3D printing.

CHAPTER 4

Results and Discussions

Based on the overall work of Ph. D, all the results and discussions is divided into the following sections:

1. Investigations of the comparative properties of colloidal-dry produced Alumina components under pressure- and pressure-free conditions.
2. Superior sliding wear characterisation of Pressure Slip Casting / Conventional Slip Cast Alumina.
3. Physico-thermal property evaluation of Aluminum Titanate by Pressure Slip Cast & Conventional Slip Cast.
4. Physico-mechanical & thermal property evaluation of Alumina & Aluminum Titanate by ceramic 3D Printing.

4.1. Results and Discussions on investigations of the comparative properties of colloidal-dry produced Alumina components under pressure and pressure-free conditions.

This chapter describes the results for development of Alumina and Aluminum Titanate products through the emerging techniques mentioned in chapter 3 above. It examines the relative effects of the properties that were specifically evaluated on the mechanical and microstructural correlations.

4.1.1. Raw Material's Characterization:

4.1.1.1 Particle Size and X-ray Diffraction Analysis: The powders MR-01, HIM-10, and HM-particle mix's size analyses are displayed in Fig.4.1. The average particle size (d_{50}) of the mixture HM-mix powder is 3.18 µm, which is larger than that of the MR-01 and smaller than that of HIM-10 powders narrow size distributions of 1.43 and 7 µm, respectively. Fig.4.2 displays the alumina powders (MR-01, HIM-10, and mixture HM-mix) X-ray diffraction patterns. The peak indexing data of the International Centre for Diffraction Data match the recorded diffraction pattern in terms of intensities and diffraction angle (2θ) (JCPDS-ICDD

File No 46-1212). The obtained diffraction pattern demonstrates that alumina powder exhibits pure α-phase.

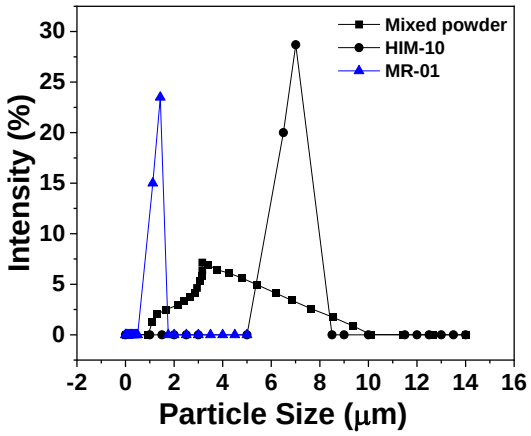

Fig. 4.1. Particle size distribution of alumina powders

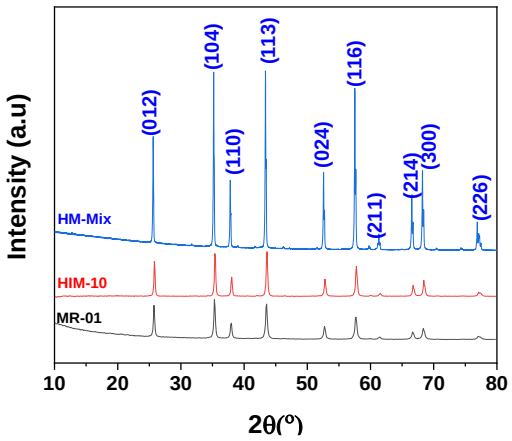

Fig.4.2. XRD pattern of alumina powders

4.1.1.2. SEM characterisation for flow behaviour of powders and polymeric mould: Fig.4.3. displays SEM micrographs of the spray-dried flowable spherical granules. The cohesion index calculated from the powder flow analysis was approximately 12.21, indicating free flow behaviour, due to the spherical morphology obtained through optimised spray drying parameters.

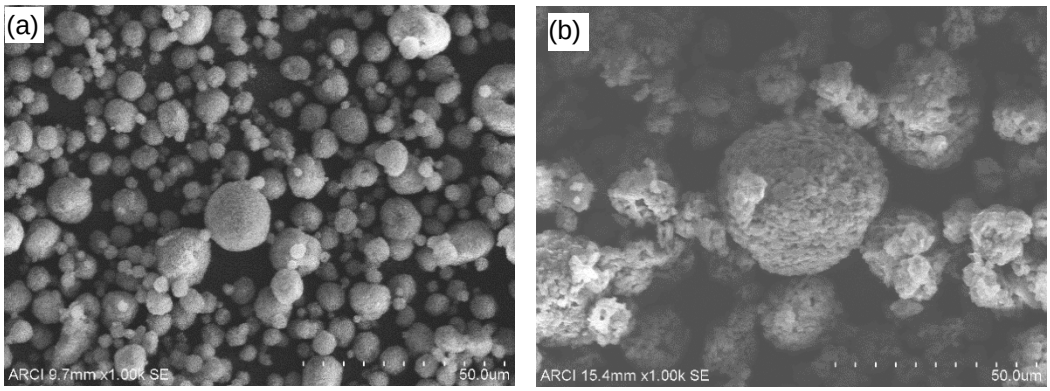

Fig. 4.3.: (a) MR-01 and (b) HIM-10 powders of SEM images that have been spray-dried.

The fabricated polymeric resin mould has a longer useful life and greater strength, which enables casting under pressure of up to 40 bar. The moulds SEM micrograph (Fig.4.4) reveals highly porous characteristics with interconnected pores, which aid in filtration and cast formation.

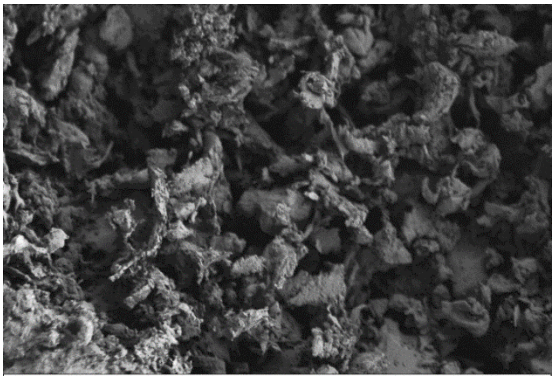

Fig. 4.4. SEM image of the polymer moulds.

4.1.1.3. Simultaneous Themo Gravimetric - Differential Thermal Analysis (STG-DTA):

To record the thermal events occurring during sintering, the green densities of the cast samples were estimated after drying and then subjected to thermal analysis subjecting to heating rate of 10^{o}C per minute using a simultaneous thermal analyzer (Netzsch STA 449 F3, Jupiter). Fig.4.5. shows the STG-DTA analysis of Mixed alumina powders showing exothermic reactions and mass change accordingly. Using data, the DTA peaks at 100-120^{o}C can be attributed to residual water dehydration of the sample after drying. Exothermic peak at 400-500^{o}C indicates the oxidation of organic dispersants added for the stabilisation of the slurry. Exothermic peak at high temperature above 1300^{o}C is probably due to the polymorphic transition to α-Al_2O_3. The TG curve shows prominent weight changes at 100 -120^{o}C and at 400-500^{o}C indicates complementing of the thermal events in DTA. However, weight change is negligible at high temperature. Based on the TG-DTA studies that the samples sintering schedules evolved at a slow heating rate of 10^{o}C per minute up to the ultimate sintering temperature of 1600^{o}C.

4.1.1.4. Rheological behaviour of alumina slips:

In order to make cast bodies with the necessary slip qualities, it is important to consider rheological examination of the suspensions. Darvan 821A (ammonium polycarbonate) is used as dispersant in the present study. This dispersant provides the charge to the particle and remains suspended through the electrostatic forces to avoid settling. In case of foaming, I used iso-octanol to prevent the foaming. It was found that only the slips with a solid loading of 75% (a powder mix ratio of 30:70) were stable and consistent. Following a rheological study of these slips, Fig. 4.6 displays the viscosity vs. shear rate plot. When a shear force (pressure) is applied, the slip must flow and fill every cavity of the mould, which requires a shear thinning behaviour. The current slips rheological behaviour supports the lowering of viscosity that is necessary to maintain the shape of the cast after pressure is released. From rheological data

stress-exponent n=0.5 which showing shear thinning behaviour required property in cast formation. The plot clearly demonstrates a pseudoplastic behaviour appropriate for CSC and PSC processes.

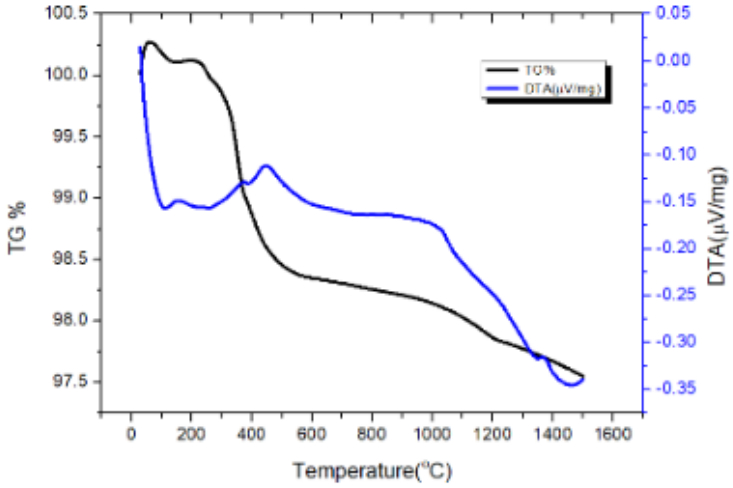

Fig.4.5: TG-DTA scan of the Al_2O_3 green cast parts.

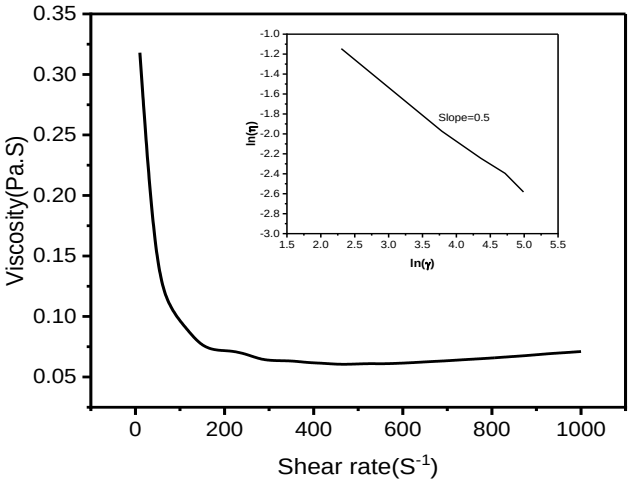

Fig. 4.6: Rheology of slips made for Al_2O_3.

4.1.2 Shaping through casting process: a) CSC and b) PSC:

In the standard slip casting procedure for CSC, plaster of Paris (POP) moulds is utilised. Under atmospheric pressure condition, Cast was performed for cylindrical disc, square dimensional products through infiltration process due to capillarity action of slips and samples were prepared. Fig. 4.7(a) and 4(b) displays the cast cylindrical disc and square dimensions products that CSC processed for alumina and Fig. 4.8 is Aluminium Titanate cylindrical disc samples.

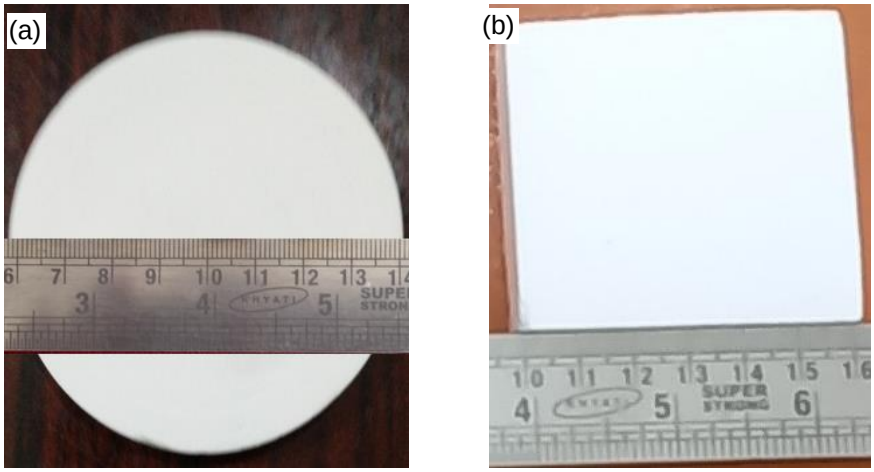

Fig.4.7.: Shows CSC processed Alumina (a)Cylindrical Disc (b) Square Samples

Fig.4.8.: Shows CSC processed Aluminum Titanate Cylindrical Disc Samples.

For cast by using PSC, processed as per the pressure cast cycle (Fig.4.9) that initially, pressure gradually increases to a peak of 35 bar and remains there for 250 secs before rapidly decreasing in accordance with the PLC programme and all the processed samples were shown in Fig.4.10.

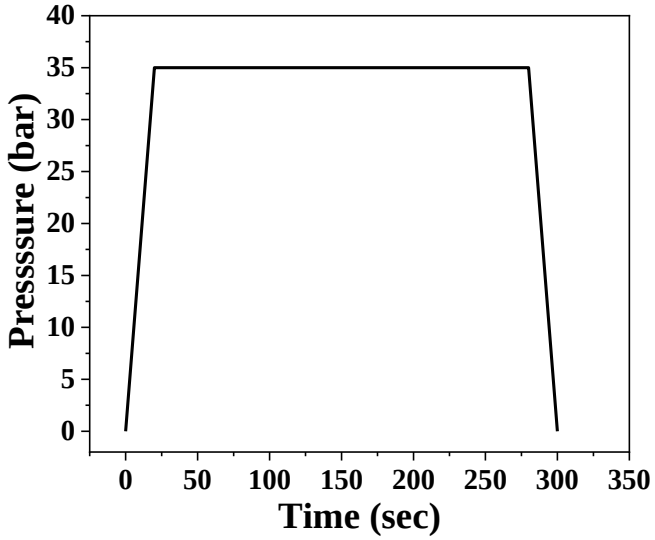

Fig.4.9: Pressure cast cycle for Alumina products

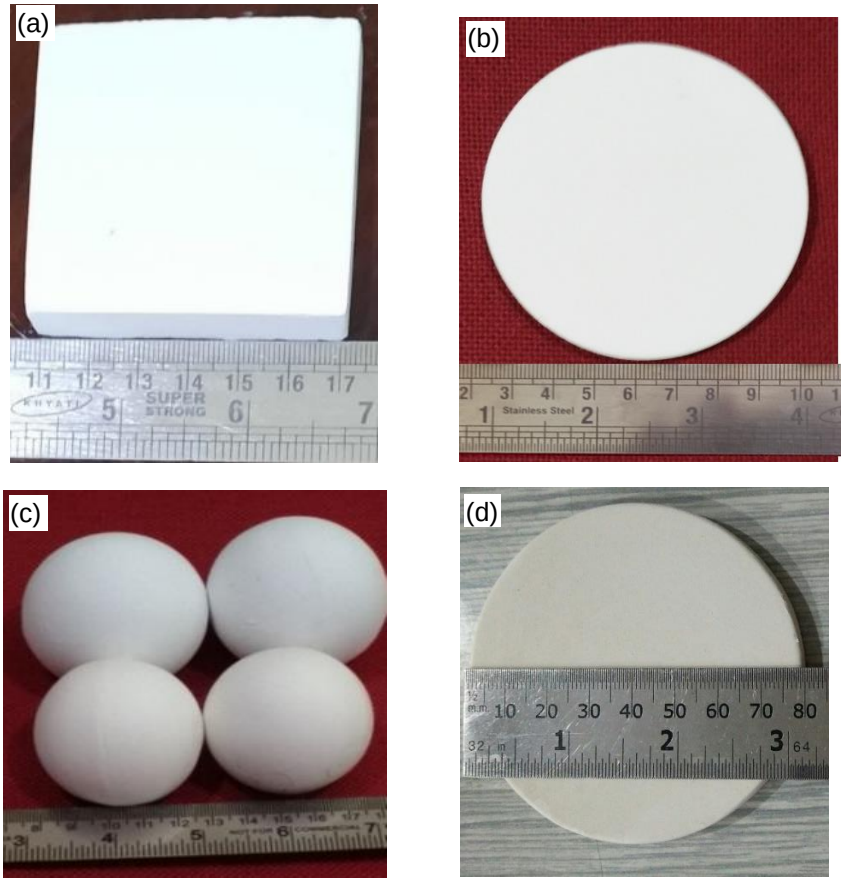

Fig. 4.10: Shows PSC ed Alumina (a) Square, (b) Cylindrical disc and (c) Spherical ball and (d) Cylindrical disc of Aluminium Titanate sample.

Although the molds average pore size was only about 10 microns, when put under pressure, alumina particles clump together and deposit as a cake, acting as a filter to remove water and create monolithic cast parts. Under low shear rates, the slip showed pseudoplastic behaviour

and was also pumpable, but as the shear rate increases beyond 100 S^{-1} because of the higher-pressure ranges encountered during pressure casting, the slip's behaviour shifts to shear thickening. This is also caused by the removal of water and by compressive forces that are significantly greater than the dispersant's repulsive forces, which keep the particles apart and cause consolidation that results in the formation of casts. Existing literatures reported that pressure casting used to make alumina refractories by using 3 microns particle size powders.
In the present study, I used 1, 7micron particle and their bimodal distribution to see the effect of particle size. Advanced ceramic products currently in development still struggle with issues like low densification and low green strength. Limited consistency in processing products with complex shapes. obtaining high productivity while processing ceramics with precise dimensions. The goal of the current study was to create oxide-based ceramic products using various ceramic processing techniques in order to achieve the necessary complex shapes and densification levels. To compare colloidal techniques (PSC, CSC) and dry stage Cold Isostatic Pressing techniques with respect to processing parameters effect on the evaluation
of mechanical &microstructural properties and it' s attributed correlations among all the process.
In pressure casting the average pore size 10 microns and I tried for a possible combination of coarser and finer particle sizes in the range of 65:35 for a solid loading of 65-75 wt.% in order to get better packing along with interlocking nature for full consolidation of the green samples under pressure without any dimensional damages.

4.1.3: Drying characterisation and thickness built up effect of PSC samples:

All the samples of PSC and CSC (Fig. 4.11), was precisely weighed (0.01 g) and exposed to outside environmental condition at a temperature of 25^{o}C to evaluate dryness condition. By comparing the weights of the wet and dried bodies, the water content was calculated.

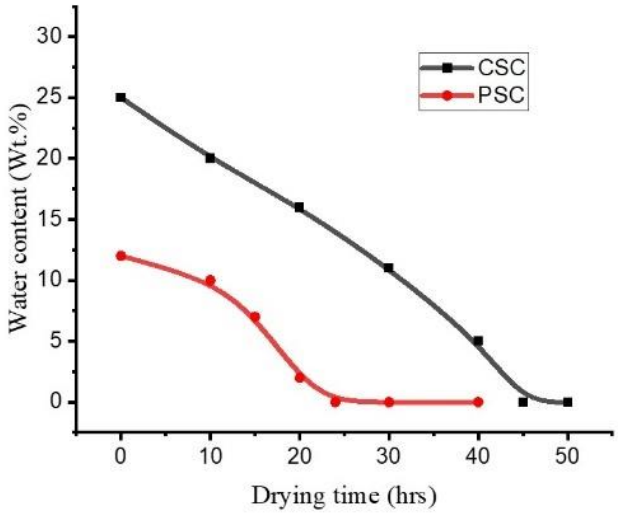

Fig.4.11: PSC and CSC Alumina cast samples drying behaviour.

The outcomes are shown in Fig. 4.11, where it is evident that the maximum moisture content for CSC and PSC samples is 25% and 12%, respectively, and that these samples can have their moisture entirely eliminated by open room drying in 24 and 45 hours, respectively. Because PSC bodies have a low moisture content, drying time can be cut during large-scale production, improving productivity and lowering the rejection rate. The PCS parameters, including feed rate, slip pressure, and pressure holding duration, were meticulously monitored for each slip in order to produce the highest green strength. The thickness of the Alumina disc cast samples steadily increases in accordance with holding time and various applied pressure levels, as illustrated in Fig. 4.12.

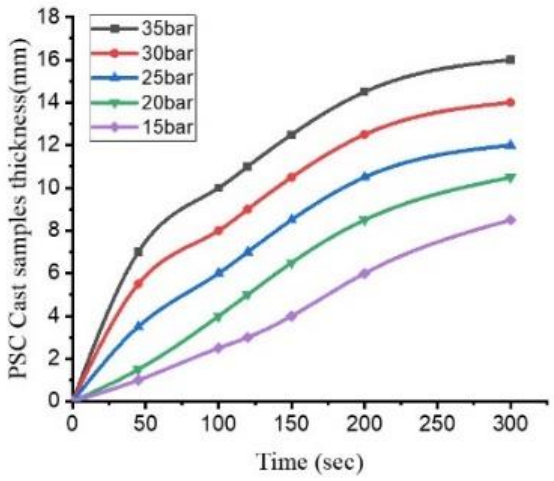

Fig.4.12: Impact of PSC on thickness built up of the Alumina samples

Up to 200 seconds of holding time, the sample's thickness developed much more quickly under the pressure that was applied to the slip. Then, the thickness-building process slowed down considerably, which is plainly caused by the fact that water finds it difficult to get through since the thick sample layer that had developed on the inside walls of the polymer mould is blocking the direct path to the pores. In order to discover the highest thickness built up that may be accomplished using the pressure slip casting technique, five different pressures and (pressure) holding periods of up to 300 seconds were investigated. Using polymer split moulds, a flat Alumina block with a thickness of more than 30 mm may be pressure slip cast in 5 minutes at a pressure of 35 bar. By fine-tuning the machine and slip settings, it is therefore simple to pressure cast green bodies up to 60 mm (30 mm thick on each part of the split mould). Pressure-cast solid Alumina spheres with a diameter of up to 60 mm were sintered in the current investigation to a density of at least 98.5%

4.1.4: Solid loading effect of CSC and PSC:

From Fig. 4.13, it can be seen how solid loading affects the green densities of samples that were pressure cast and samples that were traditionally cast as a function of the pressure that was applied to the slip. According to this graph, solid loading should be between 75 and 80 weight percent and pressure should be 35 bar in order to get the highest green density. This can be understood by the fact that, unlike dry pressing, slip occurs under pressurisation and holding conditions, with an ideal solid loading of 75 to 80 percent, and allows for the reorganisation of particles in the aqueous medium through rolling, twisting, and interlocking, ultimately leading to higher densities.

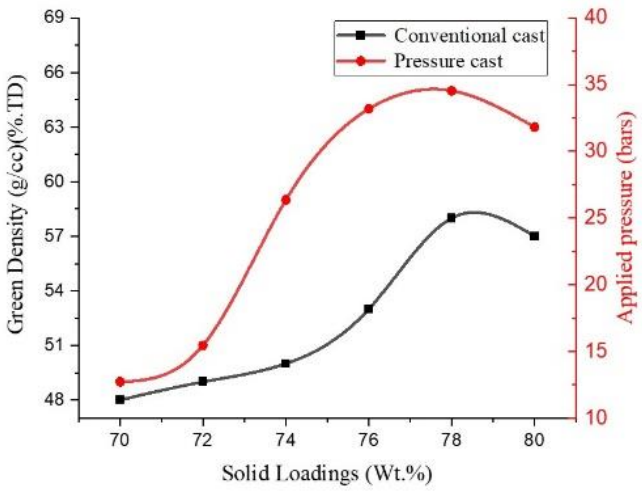

Fig.4.13: Solid loading effect on green densities through PSC & CSC.

Achieving the high packing factor will depend significantly on the average alumina particle sizes of 1.43 m and 7 microns. It is clear that solid loading above the optimum reduces green density due to movement restrictions brought on by higher particle densities during pressure-induced particle rearrangements and beyond 78% it shows slight decrease which is attributed to coarsening of the particles during sintering. A similar pattern is also observed with conventional slip casting due to the gravity-driven settling of the particles rather than cast formation under high solid loading circumstances. It should be obvious that removing extra moisture under pressure through the porous mould speeds up drying and reduces the possibility that a ceramic product will be rejected due to warpage and cracks caused by the differential drying stresses induced during the drying process as in conventional method.

4.1.5: Shaping through CIP:

Granules free-flowing behaviour made it simple to fill the mould and apply isostatic pressing to them. The manufactured granules had a free-flowing behaviour that made it simple to fill the mould before isostatic pressing. Fig.4.14 depicts the pressure cycle that was used along with a typical compacted sample in CIP. In this method, the pressure is progressively increased and applied up to a level of 1200 bar with brief holding times, then the pressure is gradually decreased. This method ensured that uniform compaction was finished in all directions, leading to the development of a well-dimensionally good product.Fig.4.15. displays the Alumina green CIP sample.

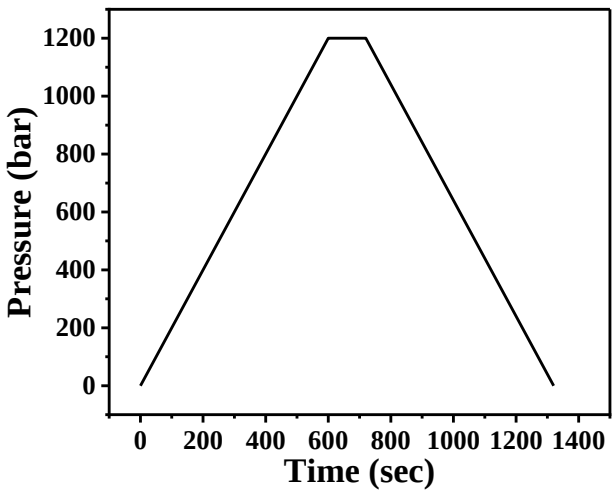

Fig.4.14.: Cold Isostatic Pressing Cycle.

Fig.4.15.: CIP ed Alumina Sample.

4.1.6: Characterisation of green and sintered samples:

The samples created by CSC using the MR-01, HIM-10, and HM-mix powders are listed in Table 4.1 below along with their green and sintered densities. The finer alumina powder was used to make the MR-01 sample, which has the maximum density.

Table 4.1: Green and Sintered Density of Samples of MR-01, HIM-10 and mix of both.

Property	MR-01	HIM-10	Mix powder
Green Density (g/cm^3) (% TD)	2.114 (53.05 %TD)	1.927 (48.36 %TD)	1.992 (49.99 %TD)

Green density for alumina samples prepared from CSC and PSC were 49.99% and 64.89 % theoretical density and its reflections almost in similar variation around 96.06% and 98.59%. However, warpages are negligible. Green densities of 66.0%TD at 1200 bar during CIP and 64.9%TD at 35 bars for PSC were both attained. The CSC samples density, however, was only 49.9%TD because of no pressure apply. Table 4.2, lists the green and sintered densities of the samples made by CSC, PSC, and CIP.

Table 4.2: Green and sintered density of CSC, PSC and CIP samples.

Property	Ceramic Processing techniques		
	Conventional Slip Casting	Pressure Slip Casting	Cold Isostatic Pressing
Green Density (g/cm^3) (% TD)	1.990 (49.92 %TD)	2.583 (64.89 %TD)	2.632 (66.03 %TD)
Sintered Density (g/cm^3) (% TD)	3.829 (96.06 %TD)	3.930 (98.59 %TD)	3.924 (98.45 %TD)

For the green CSC, PCS, and CIP samples conditions, multiple fractography at various magnifications are captured by using FESEM. Fig.4.16 shows a representative fractography for each condition. In contrast to CSC, it is clear from the green microstructure that in PCS/CIP, the two different sized alumina particles interlocked, resulting in small agglomerates dispersed throughout the microstructure with occasional pull outs.

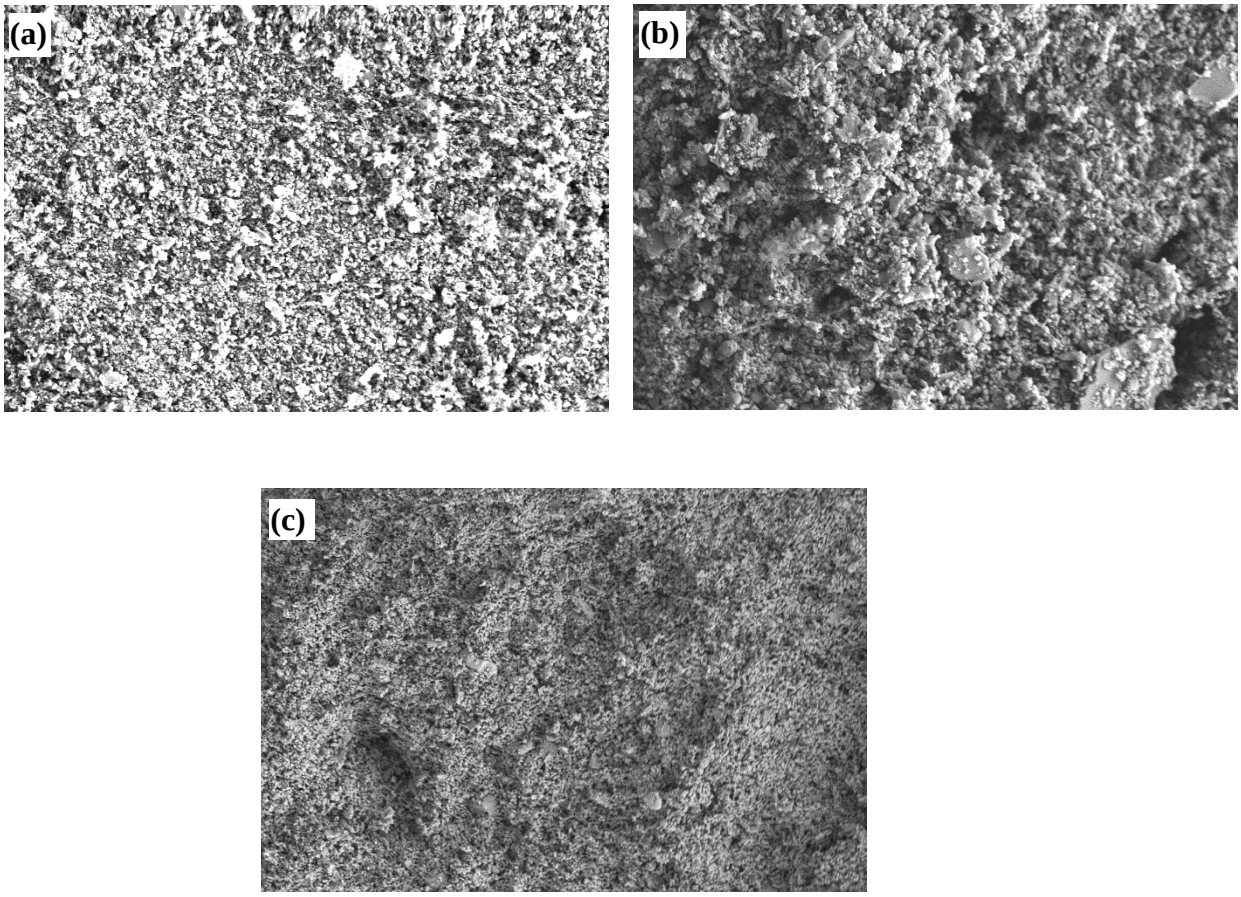

Fig. 4.16.: Green microstructure of (a) CSC, (b) PSC and (c) CIP samples.

For all the green samples of CSC, PSC and CIP, mechanical strength was measured and tabulated in the following table 4.3. As there are no binders added and mechanical interlocking under pressure in a water medium drives consolidation, pull outs are higher with PSC, which has a higher green strength of 6.02 MPa compared to 4.3 MPa (Table 4.3) observed with CIP. In the case of CIP, the binder uses van der Waals forces to hold the particle together, and further mechanical interlocking was found to be limited even when 342 times more pressure was applied than in the case of PCS. With a lowest flexural strength of 3.62 MPa, the CSC microstructure exhibits loosely packed particles that are gravitationally consolidated at energetically viable locations. Mechanically interlocking under pressure in water medium drives full consolidation and close packing in PSC comparatively gravitational consolidation occurs CSC accordingly effecting in the strengths.

Table 4.3: Flexural and Diametral Compressive Strength of green CSC, PSC and CIP Samples.

Property	Ceramic Processing Techniques		
	Conventional Slip Casting	**Pressure Slip Casting**	**Cold Isostatic Pressing**
Flexural strength (MPa)	3.62	6.02	4.30
Compression strength (MPa) (Diametral testing)	0.13	0.43	0.31

The failure stress of the samples under diametral compression tests for the same compression distance. Failure stress also exhibited a similar pattern, with the highest failure stress for PSC being 0.43 MPa, compared to 0.31 MPa for CIP, and the lowest failure stress for CSC being 0.13 MPa under radial compression. The related stress-strain curves are shown in Fig. 4.17, and these results can be attributed to the previously described explanations.

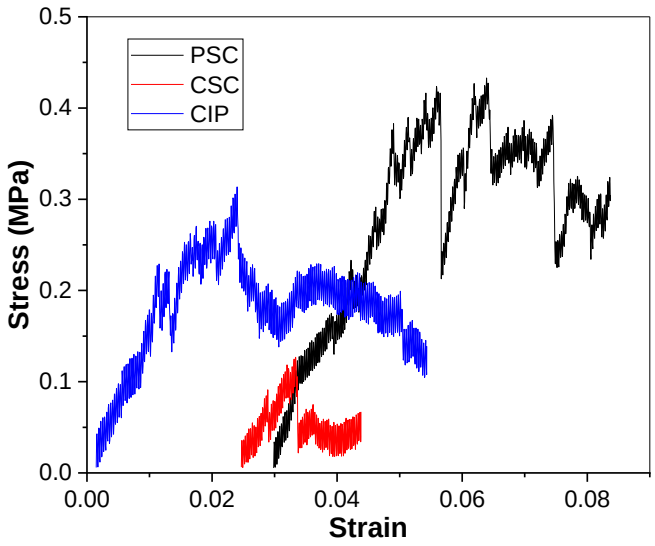

Fig.4.17: Stress vs strain curves of PSC, CSC and CIP green samples.

The sintered density and percentage theoretical values of the samples were processed through different route are shown in Table 4.4 and the representative microstructures of sintered CSC, PSC and CIP samples are also shown in Fig.4.18.

Table 4.4: Sintered density of CSC, PSC and CIP samples

Property	Ceramic Processing techniques		
	Conventional Slip Casting	**Pressure Slip Casting**	**Cold Isostatic Pressing**
Sintered Density (g/cm^3) (% TD)	3.829 (96.06 %TD)	3.930 (98.59 %TD)	3.924 (98.45 %TD)

4.1.7: PSC influence on Microstructural properties:

Comparative mechanical properties was measured in the following table 4.5 to evaluate the influence of mechanical properties by the PSC. The Vickers hardness of PSC samples is found to have risen by 22% when compared to CSC samples (11.77±0.15 GPa, 14.92±0.15 GPa). This is explained by the increased density, which is shown by the tightly packed grains in the microstructure. Flexural strength measured for CSC and PSC is showing around 242.70 to 294.40 MPa which is around 17.55% which is nearby equivalent to 20% variation. Whereas the fracture toughness of 3.73 to 4.06 $MPa.m^{1/2}$ which is around 8% variation. Table 4.5 lists for both the conventional and pressure cast samples as well as the samples flexural and fracture toughness's.

Table 4.5:Mechanical properties of CSC &PSC samples

Process	Mechanical Properties		
	Flexural Strength (MPa)	Fracture Toughness ($MPa\ m^{1/2}$)	Hardness (GPa)
Conventional Slip Casting	242.70 ± 2.5	3.73 ± 0.25	11.77 ± 0.15
Pressure Slip Casting	294.40 ± 2.5	4.06 ± 0.25	14.92±0.15

The samples were tested by three-point bend test method for flexural strengths. we have used 5 samples in each condition. It is evident that the application of PSC samples increased the flexural strength from 242.70 to 294.40 MPa and the fracture toughness from 3.73 to 4.06 $MPa.m^{1/2}$, which can be attributed to the interlocking of elongated grains with a major axis of 3.786 microns and a minor axis of 1.452 microns with smaller grains with an average size of 0.514 microns.

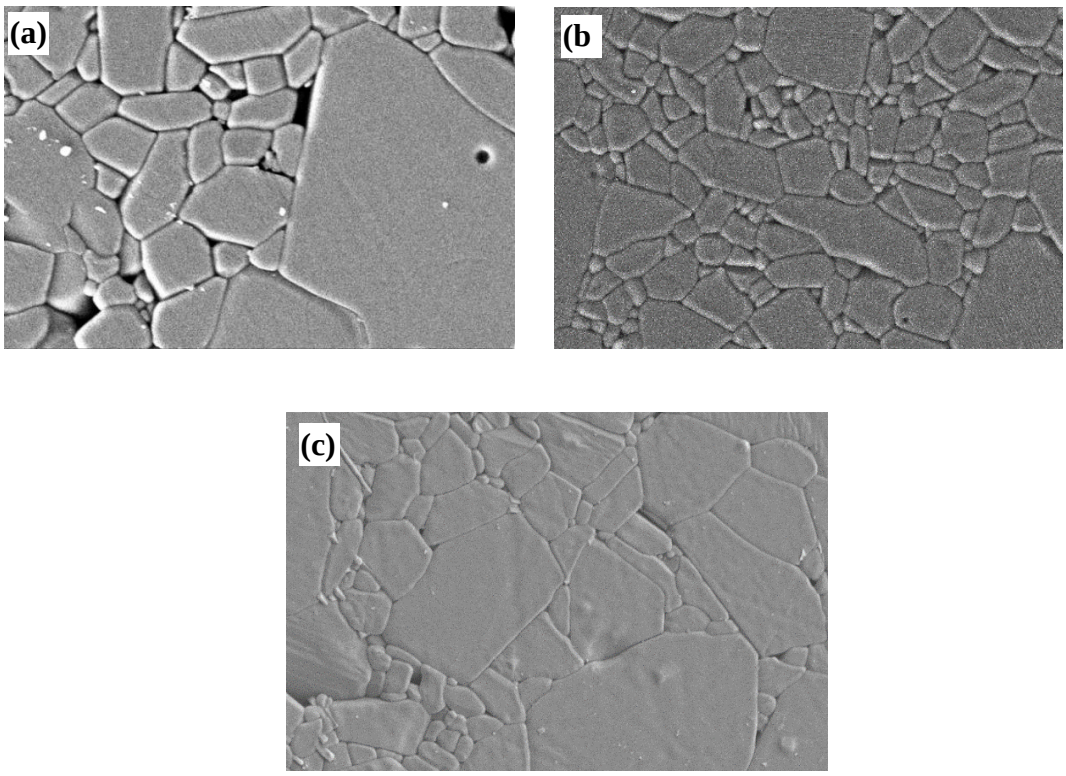

Fig. 4. 18. FESEM microstructures of sintered (a) CSC, (b) PSC and (c) CIP samples.

The effective packing caused by the choice of particle size in combination with MR-01 powder with 1.43 µm particle size act as nucleating entity during the densification process, as revealed and microstructure shown in (Fig.4.18) and Fig.4.19, the figure makes it clear that the mix powder's sinter ability has greatly improved compared to HIM-10.

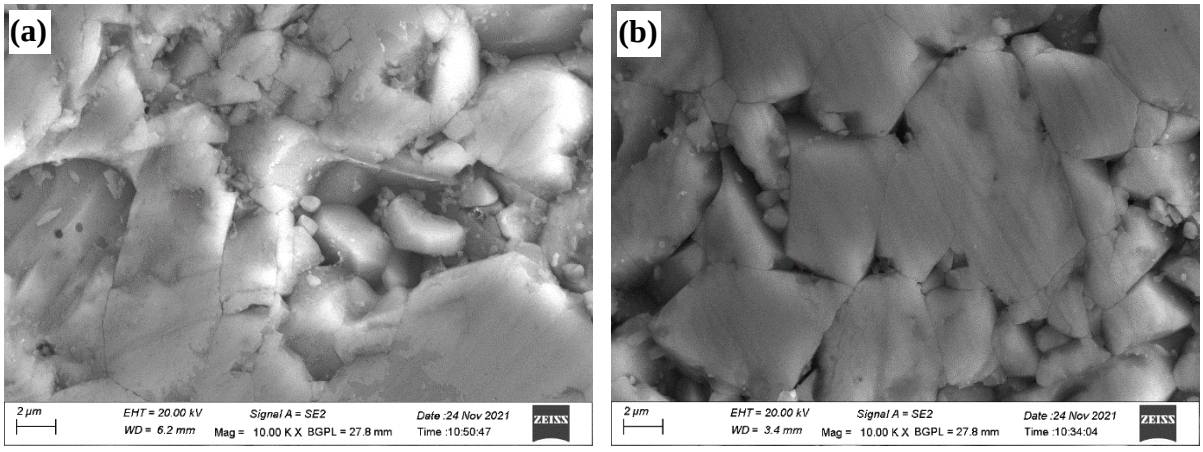

Fig. 4. 19. FESEM microstructures of sintered (a) MR-01 and (b) HIM-10 samples.

FESEM images clearly show that the PSC sample has a microstructure that is tightly packed and has finer and coarser grains interacting with each other, indicating a higher density than

that of the CSC sample, which has blemishes and pores. The micrographs make it clear that grain boundary effects lead to an improvement in mechanical properties with smaller grains. Fig.4.20. shows the grain size histogram for each of the three sintered samples. Even some cases abnormal grain growth is observed, almost close packing and for the sintered CSC, PSC and CIP Samples the average grain sizes measured which are 1.08,0.51,0.68 microns respectively attributed to evaluated mechanical properties.

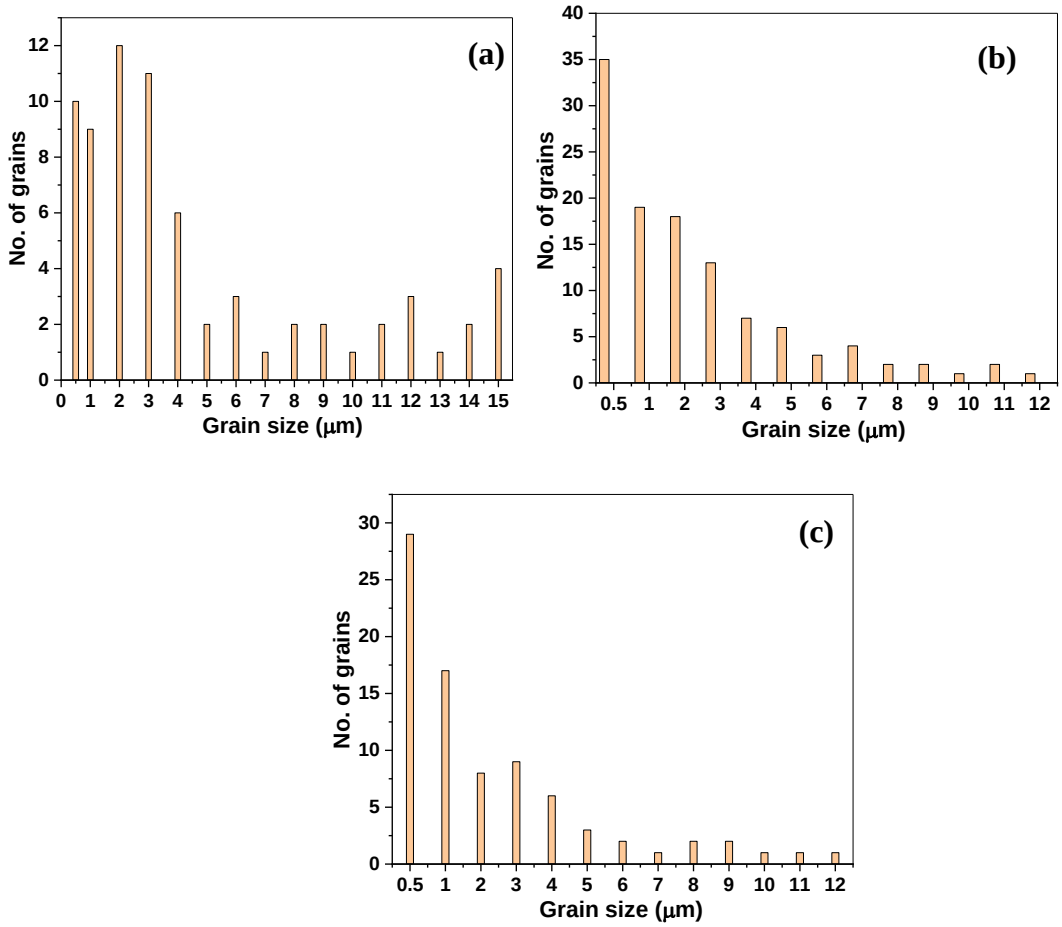

Fig.4.20: Grain size histogram of sintered (a) CSC, (b) PSC and (c) CIP Samples

4.2. Results and Discussions on Superior sliding wear characterisation of Pressure Slip Casting / Conventional Slip Cast Alumina:

4.2.1: PSC influence on wear properties:

PSC and CSC alumina samples were put through a sliding wear test against a disc made of tungsten carbide (WC). A constant load of 10N and sliding speeds ranging from 0.5 m/s to 2.5 m/s were used in experiments on sliding wear. Another set of data was completed by varying the loads from 5 to 25 N and keeping the sliding speed constant at 0.5 m/s. The normalised wear rate from each trial was computed using the weight loss information. By

performing each experiment ten times, the average wear rate and coefficient of friction (μ) for each experiment were calculated. Fig.4.21. shows the samples prepared for the sliding wear test.

Fig.4.21: Samples prepared for sliding wear test

For both CSC and PSC samples, the specific wear rate is shown in Figs.4.22a and 4.22b as a function of sliding velocity and load, respectively. The samples obtained through PSC had much lower wear rates than those obtained through CSC, regardless of sliding velocities or load. This is because the PSC samples had smaller grains and superior mechanical characteristics. The wear rate for PSC and CSC, respectively, ranges from 2.35×10^{-18} m^3/Nm to 3.11×10^{-18} m^3/Nm and from 5.97×10^{-18} m^3/Nm to 7.88×10^{-18} m^3/Nm for a sliding velocity of 0.5 m/s. With different sliding velocities, the sample showed a similar trend.

The coefficient of friction for PSC and CSC samples, respectively, for various applied loads, is shown in Figs. 4.22c and 4.22d as a function of sliding time. The severe wear loss and material removal in the case of CSC samples is what is responsible for the variations in coefficient of friction. Because of its superior mechanical properties and fine grain structure, the smooth plot in Fig.4. 22c (of PSC) (of PSC) indicates a smooth wear mechanism. When compared to PSC samples, the wear rate is higher for CSC samples, which confirms the rapid initiation of debris formation and fracturing behaviour. The worn-out samples were examined using a FESEM to better understand the wear mechanism. The low magnification SEM images of the CSC and PSC samples that were subjected to wear at 5N at 0.5 m/s are shown in Figs. 4.23a and 4.23d. The images clearly show that the smooth surface found in the PSC sample is due to smooth wear, which is consistent with the wear data shown in Fig.4.22. More details are provided by the high magnification images shown in Figs.4.23b and 4.23c for CSC and Figures 4.23e and 4.23f for PSC. For CSC and PSC samples, brittle and cleavage fractures, respectively, are the mode of fracture during sliding. Before going to steady state, most of the samples underwent to severe fluctuations, which leads to irregular worn surfaces and almost showing fractural surfaces. The smooth removal of material is indicated by the facets in

Fig.4.23f. In contrast to the images in Fig. 4.23, Figures 4.24a and 4.24d display low-magnification images of CSC and PSC samples that had been subjected to wear under high loads (25 N).

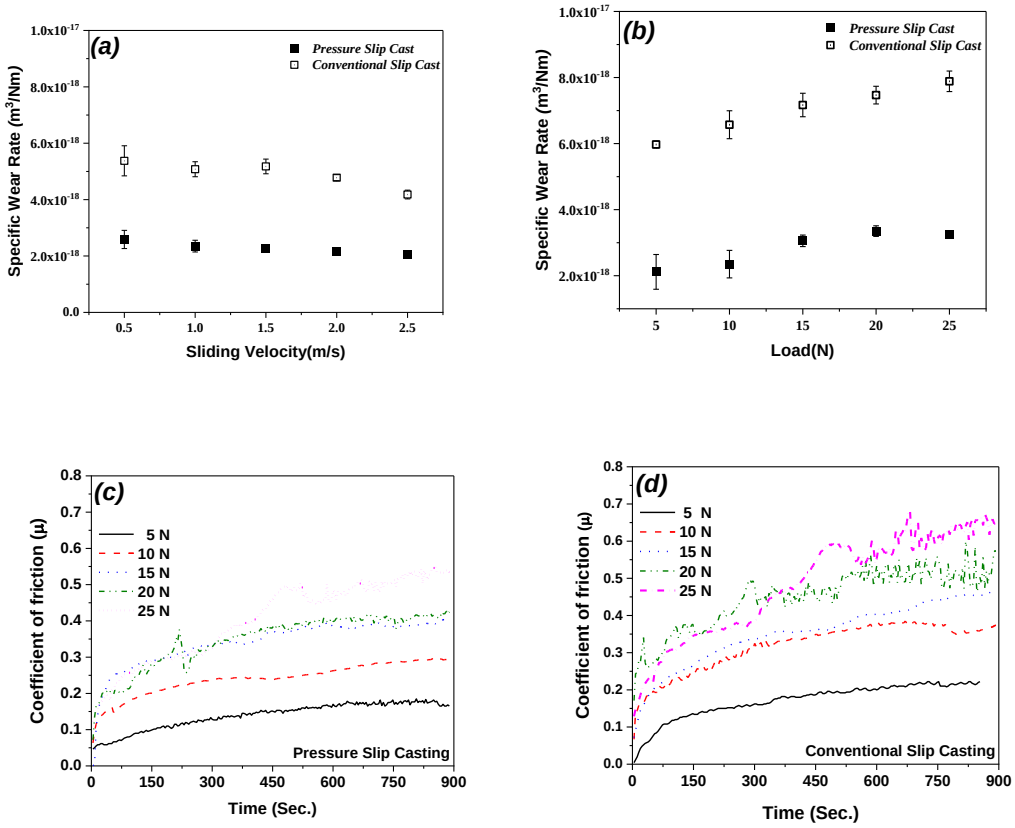

Fig.4.22: Samples specific wear rate as a function of (a) Sliding Velocity, (b) Normal load for CSC and PSC samples and as a function of time versus coefficient of friction for (c) PSC and (d) CSC samples for a varying loads.

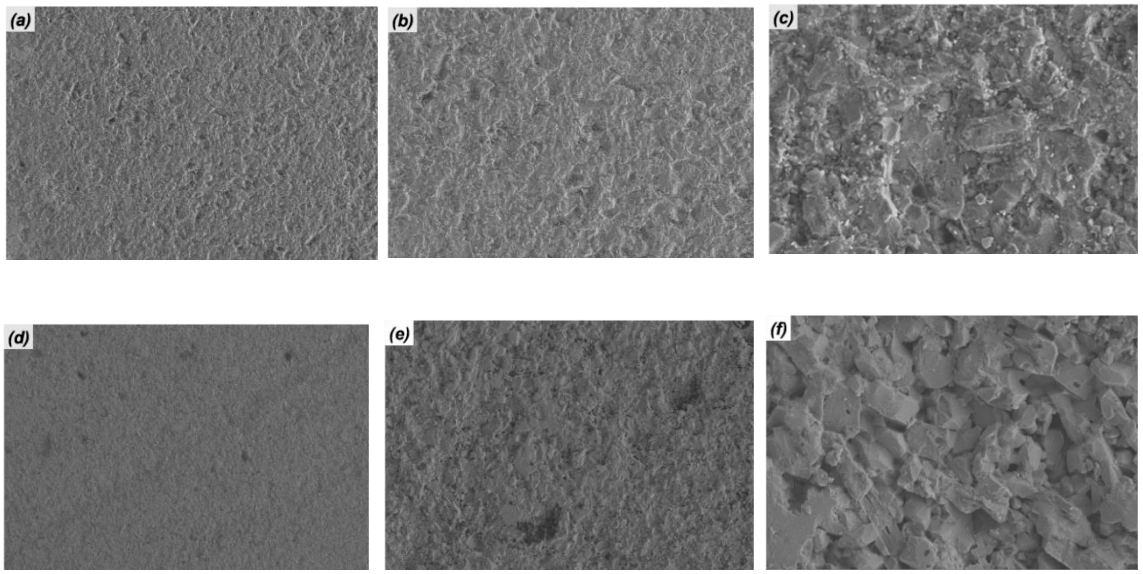

Fig.4.23: Low magnification FESEM images of the worn-out surfaces of (a) CSC and (d) PSC processed samples; High magnification images of CSC (b and c) and PSC (e and f) samples at 5N normal load and 0.5 m/s sliding velocity.

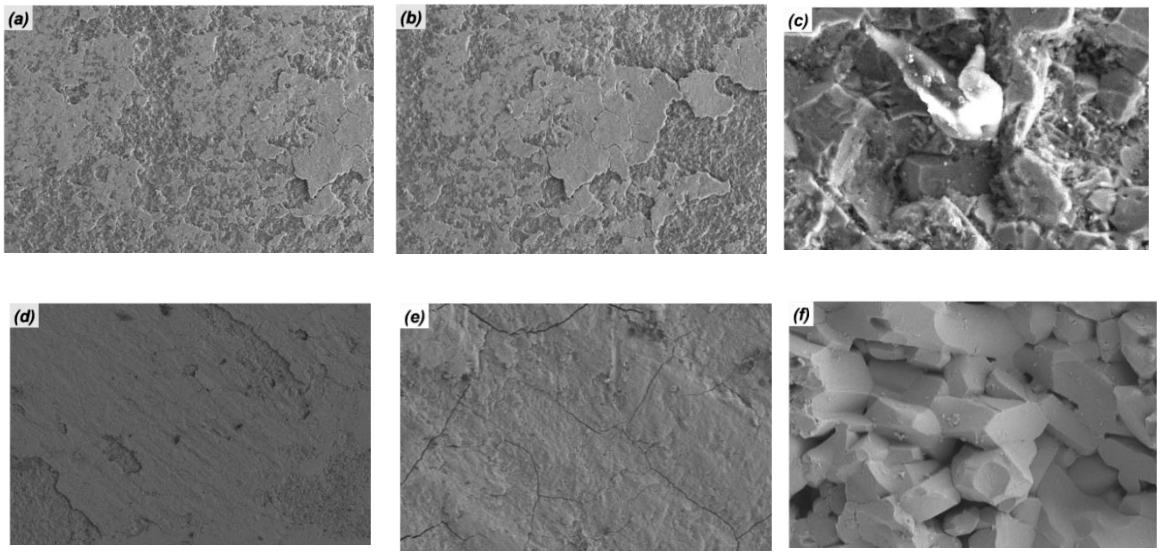

Fig.4.24: Low magnified FESEM images of the worn surfaces of (a) CSC and (d) PSC processed samples, High magnified images of CSC (b and c) and PSC (e and f) samples at 25N normal load and 0.5 m/s sliding velocity.

The layer of the adhesive film type could be seen in both samples. While the CSC sample displays highly brittle layer formation, the PSC sample exhibits continuous layering. The high-magnification image in Fig. 4.24e (PSC) displays cracks that were created at random. Still, the fact that the formed layer is still attached to the subsurface shows how well the layer adheres. The CSC and PSC failure mode is shown by further magnification in the regions where the layers were lost. The results agree with what is depicted in Fig. 4.23. CSC samples were carefully examined (Figs. 4.23c and 4.24c), and it was shown that increasing load severely eliminates the worn-out layers, leaving a roughened surface in their place. It seems that the load and roughness are inversely related. Similar to this, it is evident that the facets acquired for higher load from the high magnification SEM pictures for PSC samples are clean and devoid of debris (Figs. 4.23f and Fig 4.24f). When the normal load is low, the wear mechanism is smooth and gradual, according to the wear data of the CSC and PSC samples. In both cases, according to the FESEM images for low loads, the formation of an adhesive layer is not visible. However, during the wear test, a layer between the WC-Co disc and the surface of the alumina sample is most likely created by debris that has become trapped due to wear.

The microstructures reveal that whereas the adhesive layer is brittle in the case of CSC, it is intact in the case of PSC. PSC samples better fracture toughness is primarily responsible for their better wear resistance performance when compared to CSC samples. The deterioration of mass loss in the severe wear region of the PSC sample indicates the formation of small debris, and fracture behaviour exhibits both inter- and trans-granular behaviour. The mechanical characteristics of both samples are found to have a good correlation with wear rate, and as a result, PSC samples showed an improved wear resistance of 56% over CSC samples.

4.3. Results and Discussions on Pressure and Slip Casting of Aluminum Titanate and its Properties Evaluation:

4.3.1: Schematic representation of Aluminum Titanate cast by PSC & CSC: The overall cast processing of raw material to products preparation of Aluminum Titanate by using pressure / Pressure less (slip) casting will be represented in Fig. 4.25.

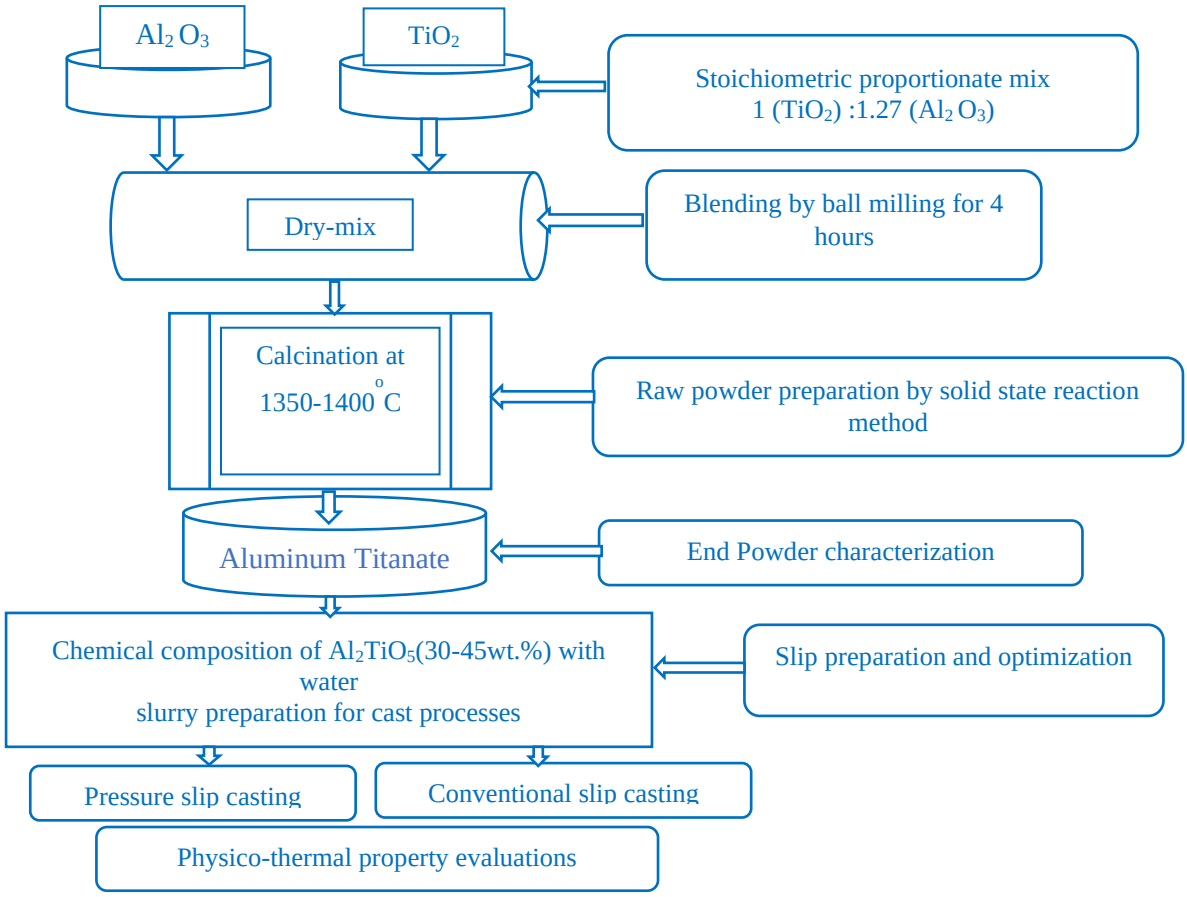

Fig.4.25: Schematic representation of Aluminum Titanate processing

4.3.2. Characterization of Raw Materials:

4.3.3. Aluminum Titanate X-ray diffraction analysis and FESEM microstructures along with its line scanning:

The powders of Alumina MR-01 and Titania were dry mixed in equimolar proportionate of 1 (TiO_2) : 1.27 (Al_2O_3) and blend for 4 hours by ball milling. After blending the dry mixed powder were kept for calcination at around 1350 -1440^oC for 2 hours soaking in-order to get the Aluminum Titanate Phase formed powder through solid - state reaction route method. The phase confirmation will be done by using the X-ray diffraction (Fig.4.26) method and also further confirmed by the line scanning of FESEM Microstructures (Fig.4.27). In line with same expectations, XRD patterns and FESEM figures detect the Aluminum Titanate confirmed phase for calcine at 1440^oC for 2 hours soaking.

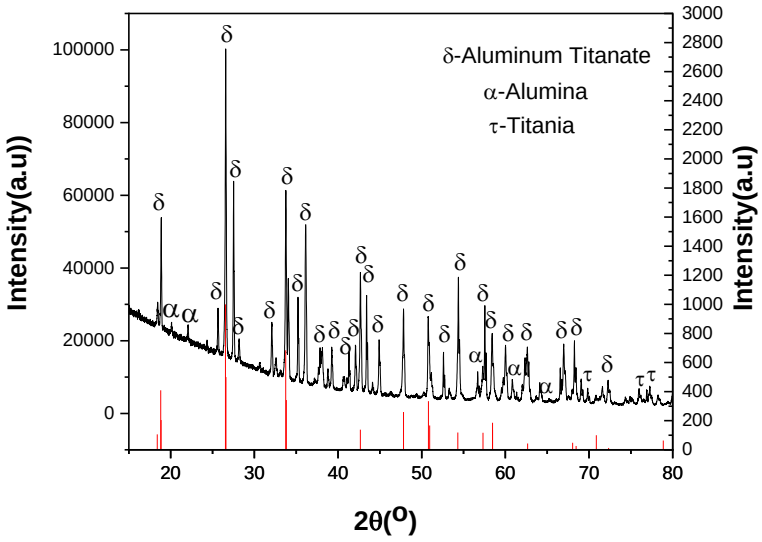

Fig.4.26 :X-ray diffraction pattern of Aluminum Titanate Phase formation

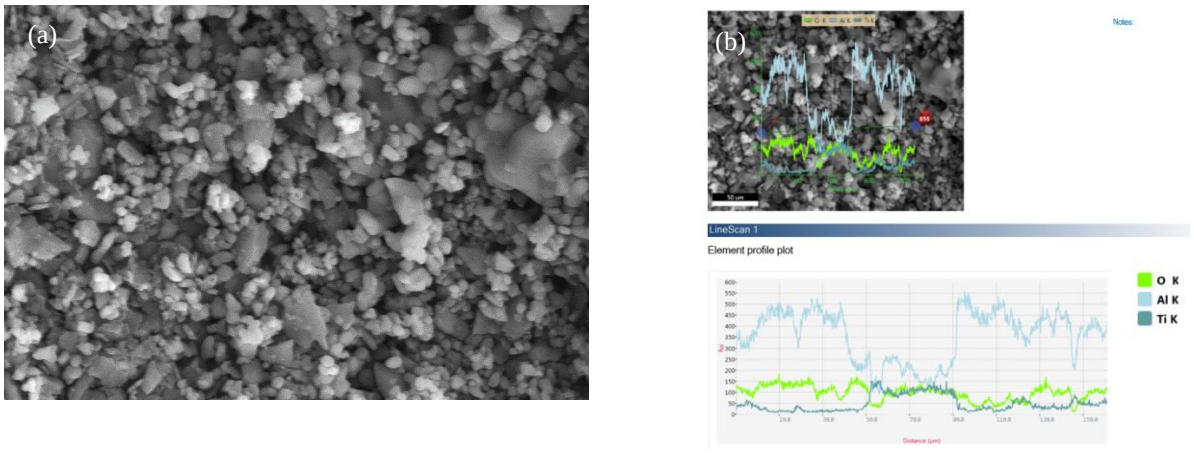

Fig.4.27: Aluminum Titanate Phase formed a) FESEM Microstructure & b) Line scanning.

4.3.4. Aluminum Titanate Particle size and TG-DTA Analysis: The particle size distributions of the measured alumina, titanium, and aluminium titanate were 1.43 mm, 0.5 mm, and 1.27 mm, respectively (Fig. 4.28).

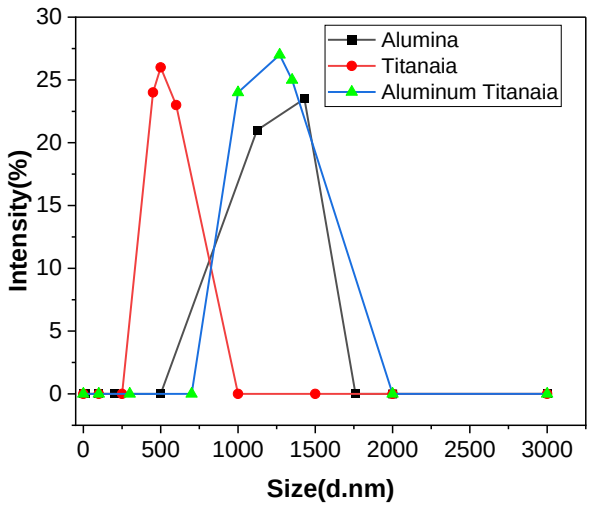

Fig.4.28: Particle size distribution of Alumina, Titania and Aluminum Titanate.

To record the thermal events taking place during sintering, calcined Aluminium Titanate powder was subjected to thermal analysis using a simultaneous thermal analyzer (Netzsch STA 449 F3, Jupiter) at a heating rate of 10°C/min. TG-DTA analysis of mixed alumina particles (Fig. 4.29) reveals two states of oxidation processes that stabilise at 1400°C.

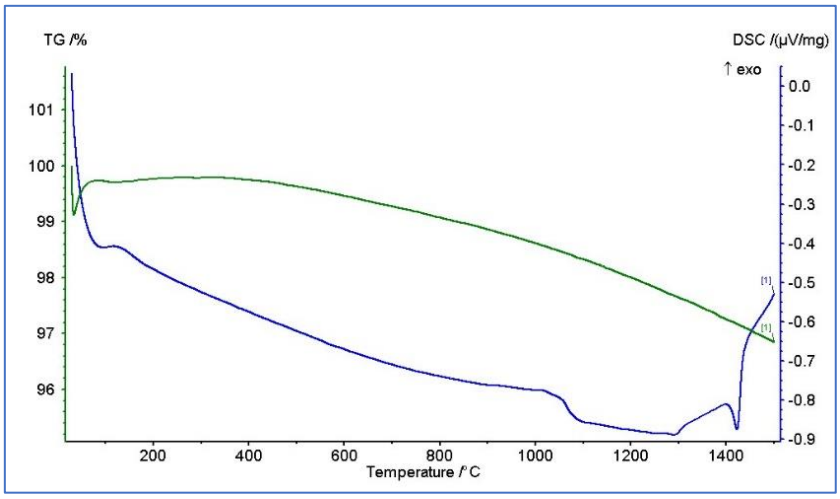

Fig.4.29.: TG-DTA Analysis of Calcined Aluminum Titanate.

4.3.5: Aluminum Titanate Slip Preparation and Optimisation for cast:

The slips have been prepared for calcined powder of Aluminum Titanate in varying proportionate ranging from 30 - 45 wt. % Solid loadings and with additions of remaining water in order to get best way of cast in both the processes. For each proportionate slips flowability condition were recorded by rheological behaviour and for suitable cast the slip should be shear thinning behaviour & shear rate exponent will be less than 1. For the 45 wt.% of solid loading its giving the better required rheological behaviours and measured shear rate exponent around 0.5. (Fig.4.30) which is the favourable for both processing techniques beyond which shear thickening will occur which is not favourable for cast.

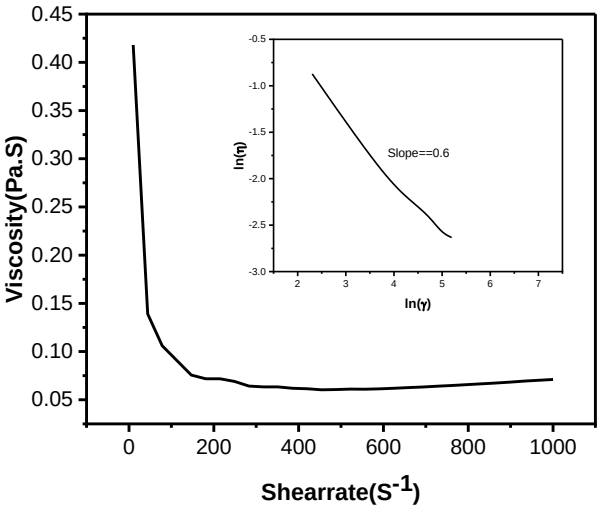

Fig.4.30: Rheology of Aluminum Titanate (Al_2TiO_5) slip.

4.3.6: Aluminum Titanate cast by PSC & CSC:

The Aluminum Titanate samples prepared from CSC & PSC of cylindrical discs (ϕ80mm) (Figs.4.31and 4.32) in the same way of Alumina samples preparation and characterized for green & sintered density, and coefficient of thermal expansion characterization to know the complete understanding of physico-thermal behaviour**.**

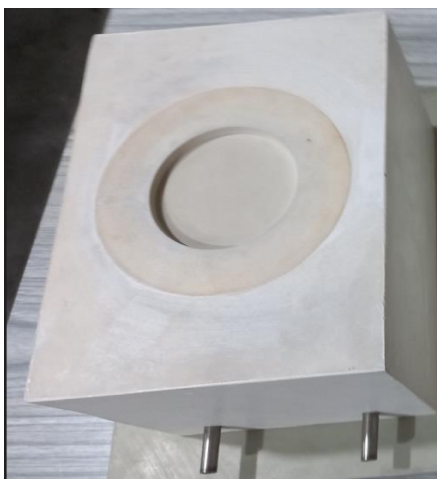

Fig.4.31: Aluminum Titanate cylindrical discs by Pressure Slip Casting

Fig.4.32: Aluminum Titanate cylindrical discs by Conventional Slip Casting.

4.3.7: Density measurement of PSC & CSC Aluminum Titanate:

In Table 4.6, the densities of sintered CSC and PSC alumina and aluminium titanate samples are listed.

Table 4.6: Green and sintered densities of CSC and PSC aluminium titanate samples

Processing technique	Composition	Green density (g/cc)	Sintered density (g/cc)
Conventional slip casting (CSC)	Aluminum-Titanate with 1 wt.% Darvan	2.02 (50.24%)	2.56(63.68%)
Pressure slip casting (PSC)		2.32(57.11%)	2.89(71.89)

PSC ceramics have a more uniform grain size distribution. Because there are no binders added to the PSC sample, mechanical interlocking under pressure in a water medium is the driving force for consolidation. As a result, in both cases of alumina and aluminium titanate, the PSC sample has a higher green density than the CSC sample when no pressure is applied. The observed green, sintered densities for Aluminum Titanate ceramics are between 50% and 57% and 63% and 71% of theoretical density, respectively.

4.3.8: CTE measurements of Aluminum Titanate:

The low thermal expansion coefficient of the Al_2TiO_5-containing sintered samples produced by CSC, and PSC is noted. PSC, with a value of 1.88 X 10^{-6} K^{-1}, has the lowest thermal expansion coefficient at 1100 °C, followed by traditional slip casting, which has a value of 2.20 X 10^{-6} K^{-1} (Fig.4.33).

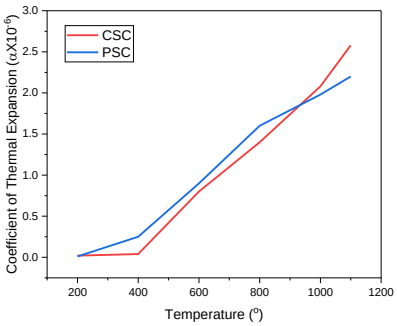

Fig.4.33: CTE measurements of CSC (2.20 x10^{-6}) /K and PSC (1.88 x10^{-6})/K.

The particle size distributions of the measured alumina, titanium, and aluminium titanate were 1.43 microns, 0.5 microns, and 1.27 microns, respectively. The average particle size of sintered samples for aluminium titanate is about 0.8 microns. Because Al_2TiO_5 sintered samples are more crystalline than other sintered samples, they have a lower thermal expansion coefficient than other sintered samples. This demonstrates the superior thermal shock behaviour of sintered samples with lower thermal expansion. Figures 4.34 (a) and 4.34 (b) display the outcomes of a microstructural investigation using FESEM on sintered aluminium titanate samples prepared using both procedures.

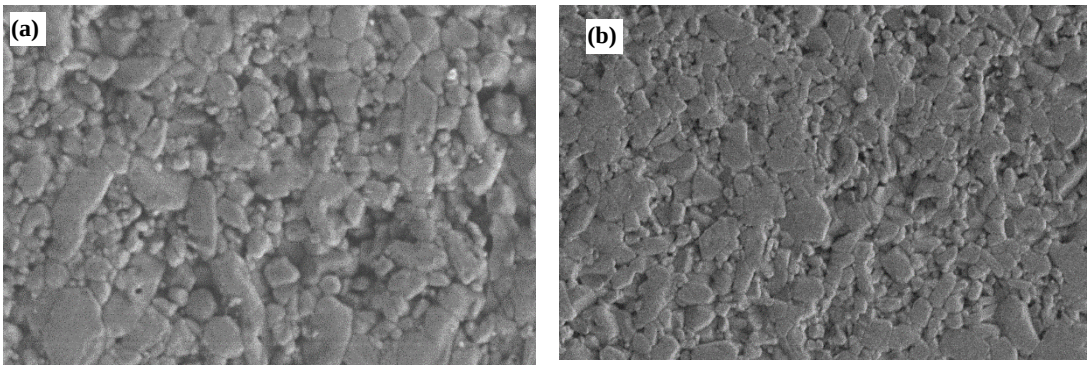

Fig.4.34: Aluminum Titanate Sintered FESEM Microstructures of (a) PSC (b) CSC.

By comparing the two SEM pictures, it is easy to see the tight packing and smaller grain sizes acquired in the pressure cast samples as well as the higher sintered densities discovered in the same. Lower values of CTE measurements of Aluminum Titanate in the case of PSC is because of the observed porosity after sintering favours low thermal coefficient.

4.4. Results and Discussions on Physico-mechanical & thermal property evaluation of Alumina and Aluminum Titanate by ceramic 3D Printing:

4.4.1: Schematic representation of Aluminum Titanate Processing through Ceramic 3D Printing: The overall ceramic 3D Printing processing of Aluminum Titanate was clearly represented in the Fig. 4.35.

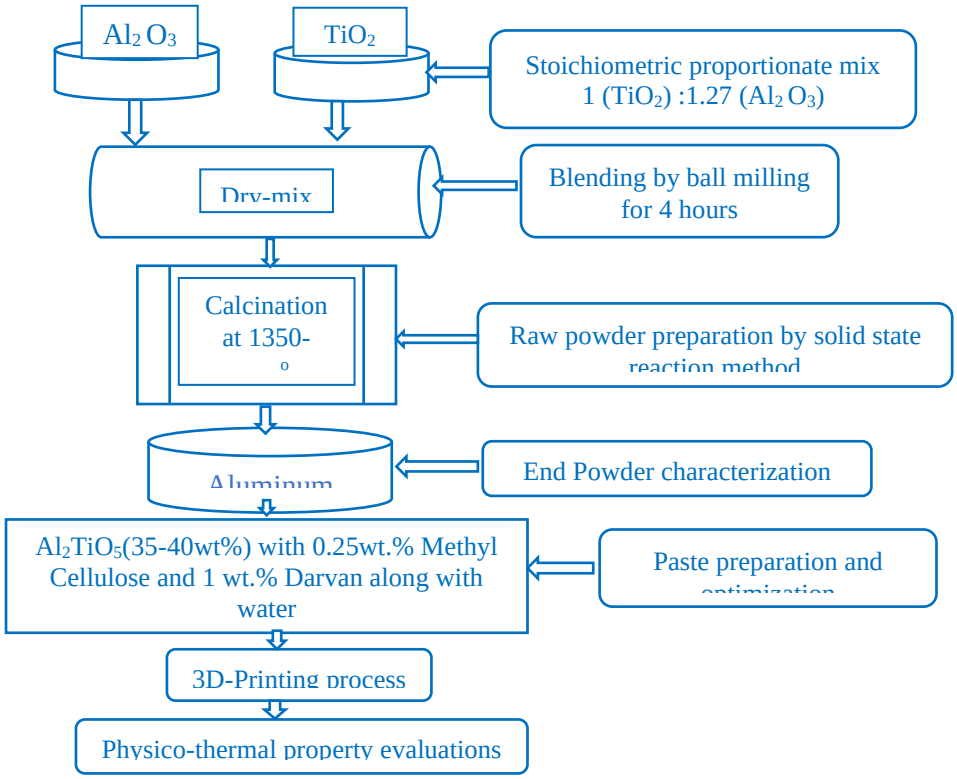

Fig.4.35: Aluminum Titanate Processing through Ceramic 3D Printing

4.4.2: Alumina paste preparation and characterisation for 3D Printing process: Alumina, 0.25 weight percent MC, and 35 weight percent water produced a homogenous, cohesive dough after 30 minutes of kneading. The agglomerates gradually dissolved and produced cohesive dough when 37 weight percent and 39 weight percent of water were incrementally added to a mixture with 0.50 weight percent and 0.75 weight percent of MC, respectively. Fig.4.36. displays a plot of apparent viscosity data against shear rate (a). Viscosity clearly decreases with shear rate, which indicates non-Newtonian behaviour, as shown by the plot. For pseudo-plastic polymeric materials, Ostwald de Wale introduced the Power Law Model, $= m \times \gamma^{n-1}$, which can be used to analyse this behaviour. In this model, the viscosity is represented by the variable, the consistency constant by the variable, the shear rate by the shear rate, and the power law index by the variable. A linear relationship with a good match can be seen in the plot of ln (η) Vs ln (γ). The characteristics of the 3D printed products within the predesigned tolerances of

the parts after shaping are determined by the pseudo-plastic or shear thinning behaviour of the alumina paste employed in the process. When using shear during printing, it is preferable for the paste's viscosity to be reduced to allow for easy paste flow. A higher viscosity, though, helps keep the form intact after printing. Additionally, the pieces must have enough handling strength to maintain their shape throughout drying and any subsequent post-heat processing. Therefore, for better end product properties, a paste with a shear rate exponent (n) of 0.6 and minimal binder (0.25 wt.%) and water (35 wt.%) additions is preferred.

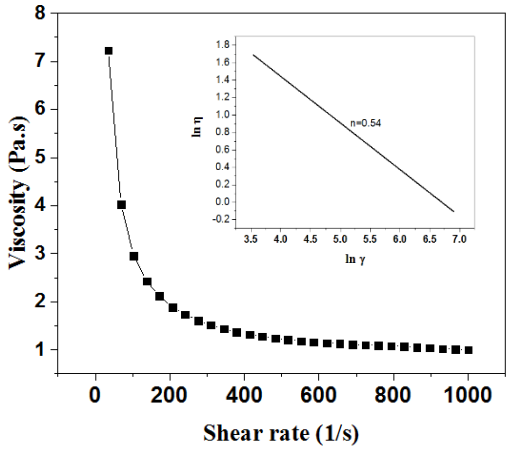

Fig.4.36: Rheological behaviour of a) Alumina paste

4.4.3: Aluminum Titanate paste preparation and characterisation for 3D Printing:

Stoichiometric mix of precursor oxide of aluminum titanate such as Alumina (Al_2O_3) and Titania (TiO_2) and solid-state synthesized aluminum titanate (ALT) were made into a paste using optimum concentration of additives. Pastes were characterized for their rheological behaviour under varying shear rates. It was observed that 3D printing of ALT paste undergo compaction under pressure however, the precursor oxides were printable. Paste compositions for Aluminum Titanate a)30 wt.% b) 35 wt.% and c) 40 wt.%+MC:0.35wt% Showing a Pseudo-plastic behaviour till 200 s^{-1}, followed by the Newtonian behaviour (Fig.4.37). Shear rate exponent of Aluminum Titanate (n)=0.2 - 0.7 is also proves shear thinning behaviour increases with solid loading and beyond 40 wt.% shear thickening occurs by which unable to process by 3D Printing.

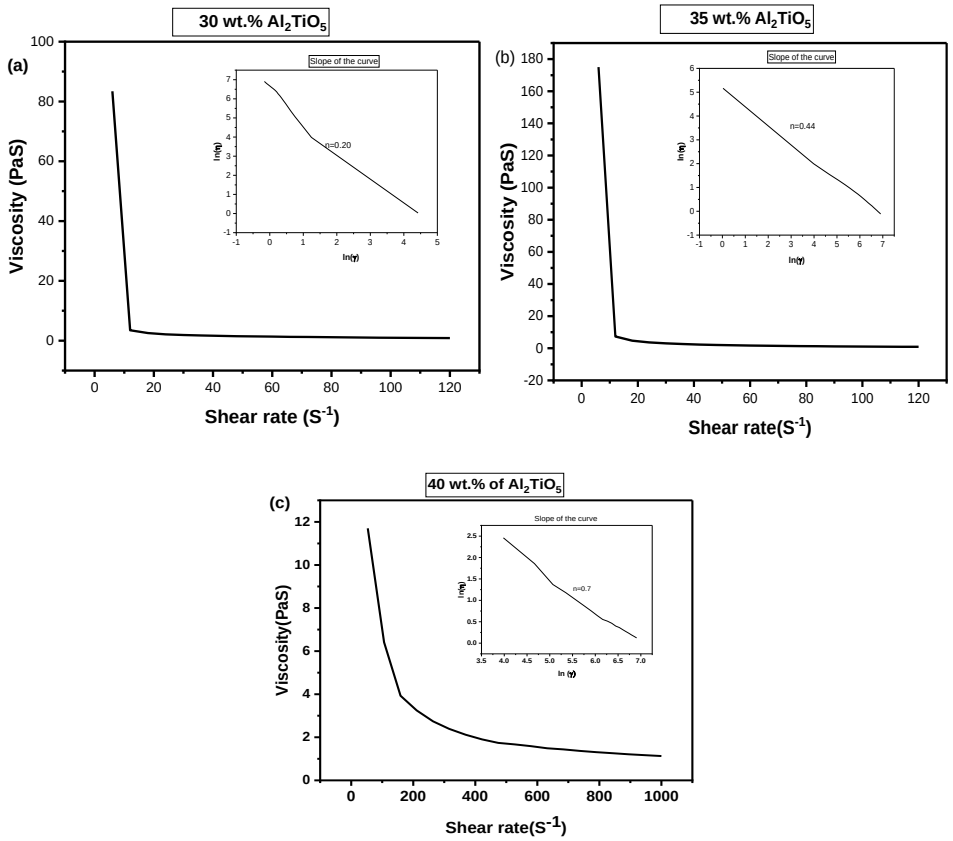

Fig.4.37: Rheological behaviour of Aluminum Titanate pastes.

4.4.4: Characterization of green and Sintered Alumina, Aluminum Titanate samples by 3D Printing:

The green densities of all the Alumina / Aluminum Titanate samples (Fig.4.38) were calculated using the dimensional method and allowed to dry at 110°C. Once the samples were further sintered for two hours at 1600 or 1400 degrees Celsius, the densities of the sintered materials were calculated using the Archimedes principle (Table 4.7).

Table 4.7: 3D Printed a) Alumina b) Aluminum Titanate Samples

Sample	Green Density (%Theoretical Density)	Sintered Density (%Theoretical Density)
Alumina	2.22(55%)	3.14 (79%)
Aluminum Titanate	2.12 (57%)	2.97 (80%)

According to ASTM D792, 2013, the density of the 3D Printed samples was assessed using the Archimedes principle and a density measuring kit (LA 120S, Sartorius AG, Germany). To fully understand physico-thermal behaviour, the samples were characterised for green and sintered density, mechanical properties and coefficient of thermal expansion measurement.

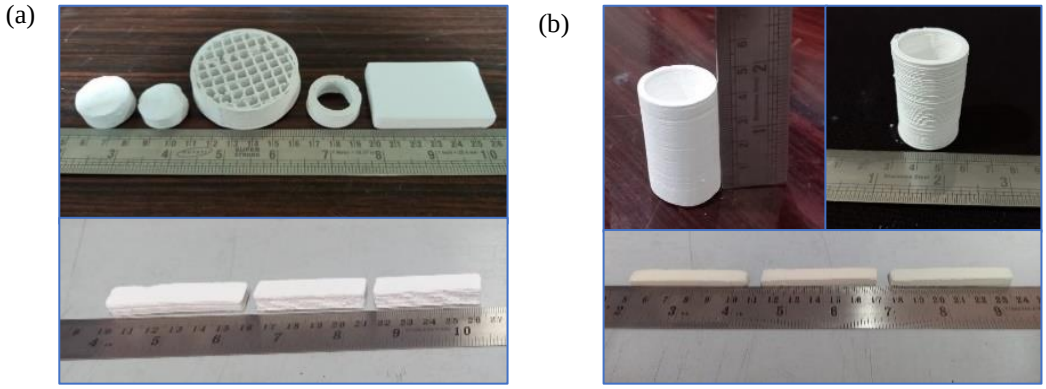

Fig.4.38: 3D Printed a) Alumina b) Aluminum Titanate samples

The observed green, sintered densities for 3D printed AL and AT ceramics are between 55 and 57% and 79 and 80% of theoretical density, respectively. It was noted from the FESEM Microstructures that the grains were arranged in layers. From the FESEM microstructures (Fig.4.39) clearly observed that the feature showing irregular and tight packing pattern of particles.

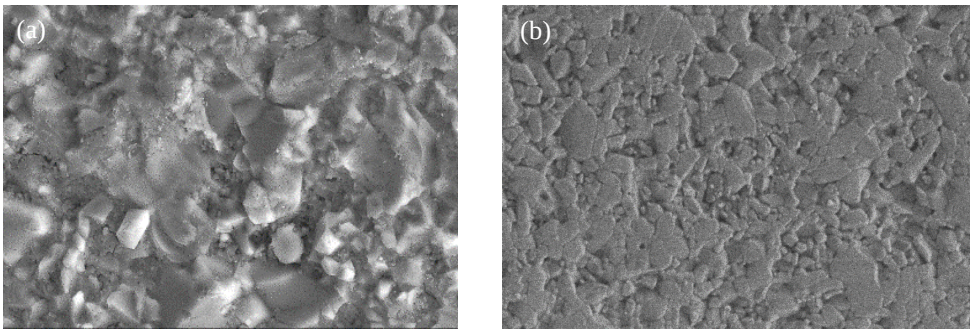

Fig.4.39: 3D Printed a) Alumina b) Aluminum Titanate FESEM samples.

4.4.5: Mechanical Characterization of Sintered Alumina Samples Prepared by 3D Printing:

In order to determine the flexural strength and compression strength of sintered samples of alumina that were 3D printed and had dimensions of 45 x 4 x 3, a three-point bend test (ASTM C1161) was carried out. Additionally, the samples' micro hardness was evaluated using a

Vickers Macro Hardness Tester (ASTMC1327). All the evaluated properties were measured and tabulated in the table 4.8.

Table 4.8: 3D Printed Alumina Mechanical properties

3D Printed	Mechanical Test (ASTM Standard)	3-Point Bending Test		Vickers Hardness Test
		Flexural Strength (MPa) (ASTMC1161)	Compression Strength (MPa) (ASTMC1424)	Hardness (GPa) (ASTMC1327)
Alumina	(ASTMC1161)	222.91	237.46	10.52±0.11

4.4.6: CTE Measurement of Aluminum Titanate Samples Prepared by 3D Printing:

The average thermal expansion coefficients (CTE) were measured in air between 100 °C and 1100°C at a constant rate of 2°C/min. A fairly typical linear thermal contraction is observed during the initial stage of cooling between 1100 and 800°C,with a CTE value of 2.58 x$10^{-6}K^{-1}$ (Fig. 4.40). CTE values that are unusually high because of the irregular way that intralayer flaws cause grains to develop in accordance with the FESEM microstructure (Fig.4.41).

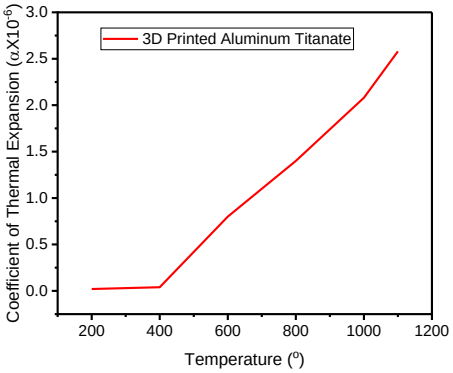

Fig 4.40: CTE Measurements of 3D Printed ALT (2.58x10^{-6})/ K

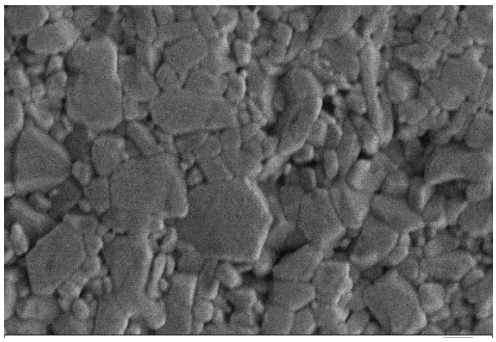

Fig 4.41: FESEM image of 3D Printed ALT

4.5: Aluminum Titanate CTE Comparison Prepared by PSC, CSC & 3D Printing:

ALTs average thermal expansion coefficients (CTE) were measured between the temperatures of 30 °C and 1100 °C at a constant rate of 2°C/min. At CTE values (Fig. 4.42) that are very

high because to the uneven grain development caused by intralayer defects, a fairly typical linear thermal contraction is seen during the initial cooling between 1100°C and 800°C.The low thermal expansion coefficient of the Al_2TiO_5 sintered samples produced by CSC and PSC is noted. PSC and traditional slip casting both have values of 1.88 X 10^{-6} K^{-1} and 2.20 X 10^{-6} K^{-1}, respectively. In terms of all the procedures involving PSC, CSC, and 3D printing processing, PSC is offering the advantageous characteristics.

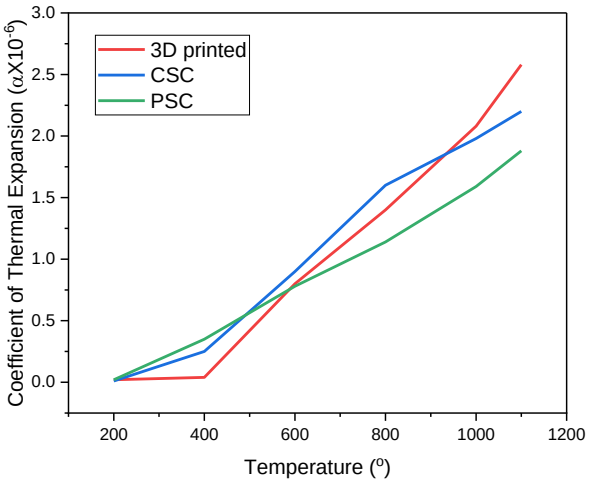

Fig.4.42: CTE Measurements of PSC, CSC and 3D Printing processed Aluminum Titanate

4.6 Summary:

Alumina powders of various particle sizes are used to compare the three processes of pressure slip casting (PSC), cold isostatic pressing (CIP), and conventional slip casting (CSC), and the cast's properties are examined. Alumina was used as an example to successfully demonstrate the application of pressure slip casting for technical ceramics, and the important issue of cast component collapse during pneumatic pressure de-molding during PSC cycle was addressed. Slip characteristics such particle size selection, engineering the percentage, and proper solid loading are crucial for efficient interlocking to retain structural integrity while de-molding. The particle size used for casting is limited by the polymer mold's pore size in PSC, but a proper mixture of larger (7 micron) and smaller (1 micron) particle sizes in the ideal proportion (65:35) has been successfully demonstrated for getting around the restriction. Due to the higher packing factor and improved nucleation, the mix has also shown improved sinterability. In contrast to the 66% achieved at 1200 bar during CIPing with granules in dray condition, PSC samples achieved a green density of 65% of theoretical density even at 35 bar pressure as the pressure is being applied to a colloidal suspension. As CSC is conducted under pressure-free conditions

and productivity was 10-15 times slower than PSC, the sample's green density was 50%. PSC and CIP samples have the same characteristics with interlocking of larger and smaller particles, according to microscopic analysis. PSC samples showed no agglomeration and complete particle merging, but CIP samples occasionally showed agglomerates. Due to the pressure-free environment, CSC samples showed loosely packed particles. Sintered densities of the PSC and CIP samples ranged from 98 to 99%, and the CSC samples displayed 96% TD in addition to the microstructure.

It is evident that the mechanical properties are better when compared to the conventional cast samples values of 3.73±0.25MPam$^{1/2}$, 242.70±2.5MPa, and 11.77±0.15GPa, respectively. These values correspond to the fracture toughness, flexural strength, and Vickers hardness of the pressure cast sample. The microstructure indicates that the interlocking of elongated grains (3.786 µm major axis, 1.452 µm minor axis) with smaller grains, on average 0.514 µm in the intergranular spaces between th elongated grains, is what enhances the mechanical capabilities of PSC samples. The optimised slip and machine settings have been further proven by casting 60mm alumina solid spheres with >98.5% density for the applications as grinding balls, which were sintered at 1600^{o}C.The pilot scale machine has been used in the current study to show how 12-14 grinding balls can be produced per hour. Multiple cavities can be added to the mould, which is currently being investigated, to further boost productivity. Pressure slip cast (PSC) alumina with a solid loading of 75% has a theoretical density of 98.5%, which is higher than the theoretical density of standard casting, which is only 97%. This material also demonstrates structural integrity. The mechanical properties of hardness, flexural strength, and fracture toughness, which are measured at 14.92±0.15 GPa, 294.40±2.5 MPa, and 4.06±0.25 MPa m$^{1/2}$ respectively, are improved by the PSC- achieved refined grain structure with minimal defects/pores, making them suitable for wear resistance applications. In comparison to the CSC samples, the PSC samples are found to have 56% less wear, with wear rates as low as 2.35 x 10^{-18} m^3/Nm (at 0.5 m/sec under 5N load). Successful correlations exist between all of the results and the corresponding mechanical and microstructural behaviour. Aluminum titanate (Al_2TiO_5) green bodies were created using a 60mm diameter disc produced from a mixture of titania and alumina powders with various particle sizes, and the green densities were determined. Green densities in the case of alumina significantly increase when 25-35 bar of pressure are applied with PSC, reaching up to 60% TD. The most crucial factors in CSC are particle size distribution and solid loading, but pressure is also crucial for producing higher green densities in PSC. It is noted that the Al_2TiO_5-containing sintered samples made by CSC

and PSC have a low thermal expansion coefficient. PSC, with a value of 1.88×10^{-6} K^{-1}, and conventional slip casting, with value of 2.20×10^{-6} K^{-1}, have the lowest thermal expansion coefficients at 1100°C.Successfully demonstrated that the physic-thermal properties of Alumina and Aluminum Titanate were measured for a variety of geometrical shapes. The observed green, sintered densities in the cases of 3D-printed AL and AT ceramics are in the ranges of 55-57% and 65-70% of theoretical density, respectively and also the samples of AT by 3D printed with a value of CTE is 2.58×10^{-6} K^{-1}.

CHAPTER 5

Conclusions and Future Scope

This chapter concludes the results of the research work done and presents the potential for future work and summarises the key findings.

1. According to the findings of the ongoing research programme, the mechanical properties restrictions on advanced ceramics have been successfully overcome by modern ceramic processing techniques that allow for customised microstructures.
2. Colloidal processing techniques like pressure slip casting and conventional slip casting are employed for the successful production of advanced ceramics, and they are even compared to non-colloidal processing techniques like cold isostatic pressing.
3. Alumina was used as an example to successfully demonstrate the application of pressure slip casting for technical ceramics, and the important issue of cast component collapse during pneumatic pressure de-molding during PSC cycle was handled.
4. The key elements for effective interlocking to maintain the structural integrity while de-molding are slip parameters like particle size selection, engineering the proportion, and optimal solid loading. In contrast to the relatively low density of 97% obtained through conventional casting, pressure casting of Alumina slip with 75 weight percent solid loading prepared with a mixture of powders having d_{50} of 1 & 7 microns in a 30:70 ratio has demonstrated structural integrity with a higher density of 98.5% of TD.
5. By comparing the fracture toughness, flexural strength, and Vickers hardness of the pressure cast sample to the conventional cast sample's respective values of 3.73 ± 0.25 MPa $m^{1/2}$, 242.70 ± 2.5 MPa, and 11.77 ± 0.15 GPa, it is clear that the mechanical properties are improved.
6. According to the microstructure, the interlocking of elongated grains (3.786 µm major axis, 1.452 µm minor axis) with smaller grains, on average 0.514 µm in size, in the intergranular spaces between the elongated grains is what contributes to the improvement in mechanical properties of PSC samples.
7. By casting 60 mm alumina solid spheres that reached > 98.5% density during sintering at 1600^{o}C for the purposes of serving as grinding balls, optimised slip and machine parameters have been further confirmed. In the current study, a pilot-scale machine was used to show how 12-14 grinding balls could be produced per hour. By adding multiple

cavities to the mould, which is currently being researched, productivity can be increased even more.

8. With a theoretical density of 98.5%, pressure slip cast (PSC) alumina with a solid loading of 75% demonstrates structural integrity as compared to a relatively low density of 97% obtained through conventional casting (CSC).
9. PSC and CSC alumina samples were subjected to a sliding wear test against a tungsten carbide (WC) disc. The experiments on sliding wear involved varying the sliding speed from 0.5 m/s to 2.5 m/s while maintaining a constant load of 10 N. A different set of data was filled out by altering the loads, which ranged from 5 to 25 N while maintaining a sliding velocity of 0.5 m/s.
10. The PSC processed samples with refined grain structure and minimal imperfections/pores is found to improve the mechanical properties such as hardness, flexural strength, and fracture toughness, which are measured to be 14.92±0.15 GPa, 294.40 ± 2.5 MPa, and 4.06 ± 0.25 MPa $m^{1/2}$ respectively.
11. and suitable for wear resistance applications. It is observed that the wear rate in PSC sample is as low as 2.35 x 10-18 m^3/Nm (with 0.5 m/sec at 5N load), which is 56% lower than that in CSC samples. Results are correlated with their corresponding mechanical and microstructural behaviour and are then explained.
12. In order to compare pressure slip casting (PSC), cold isostatic pressing (CIP), and conventional slip casting (CSC), starting alumina powder was made by mixing two powders with different average particle sizes (1.43 and 7 m) in a ratio of 65:35. In contrast to the 66%TD achieved at 1200 bar during CIP with granules in dry condition, the green density of the PSC samples was achieved at only 35 bar, a pressure that is much lower than that of CIP. When CSC was performed under pressure-free conditions, the sample's green density was 50%TD, and productivity was 10-15 times lower than with PSC.
13. The PSC and CIP green samples had the same characteristics, including interlocking of larger and smaller particles, when examined under a microscope. The PSC samples showed no agglomeration and complete alumina particle merging. However, because of the absence of pressure, the CIP samples occasionally exhibited agglomerates while the CSC samples exhibited loosely packed particles.
14. The PSC-produced alumina with improved mechanical properties is anticipated to be a better option for such applications since alumina is typically used in wear-resistant applications such as ceramic lining, ceramic grinding media, and high temperature ceramic parts.

15. Successfully showed that measurements of the physic-thermal characteristics of aluminium titanate and alumina were made for a range of geometrical geometries by 3DPrinting. In the cases of 3D-printed AL and AT ceramics, the observed green, sintered densities are in the ranges of 55-57% and 65-70% of theoretical density, respectively. AT Samples of sintered materials via 3D printing also have a value of CTE of 2.58 10^{-6} K^{-1}.

16. The Synthesis of high-density sintered alumina through colloidal and non-colloidal processing techniques we can concluded that the PSC-produced alumina with improved mechanical properties and for low thermal expansion aluminium titanate is anticipated to be a better option to CSC, CIP, also 3D printing process. Complete comparison has done for the samples of Alumina and Aluminium Titanate with respect to property evaluation and correlations.

5.1 Future scope

1. With the help of the results mentioned above, it is clear that using colloidal processing techniques with the same impact will allow us to enhance the mechanical qualities in high-temperature environments.

2. We will be able to expand our existing study in order to increase the rupture modulus under various high temperature environmental circumstances. We are capable of extending and replacing even metallic materials when high temperature conditions call for mechanical properties.

3. As the feasibility with respect to additives, rheology, and printing conditions to produce various simple and complicated ceramic components is established, there is a good opportunity to extend the work to various oxide ceramic formulation by Ceramic 3D Printing.

References

[1] W.D. Kingery, H.K. Bowen and D.R. Uhlmann, “Introduction to Ceramics”, John Wiley & Sons, Inc., (1976), ISBN 0-471-47860-1.

[2] M.W. Barsoum, “Fundamentals of Ceramics”, McGraw-Hill Co., Inc., (1997), ISBN 978-0-07- 005521-6.

[3] D.W. Richerson, “Modern Ceramic Engineering”, 2nd Ed., Marcel Dekker Inc., (1992), ISBN 0-8247-8634-3.

[4] M.N. Rahaman, “Ceramic Processing and Sintering”, 2nd Ed., Marcel Dekker Inc., (2003), ISBN 0-8247-0988-8.

[5] John B. Wachtman, “Ceramic Innovations in the 20th century”, J. Am. Ceram. Soc., (1999), ISBN 978-1-57498-093-6.

[6] W.D. Callister, “Materials Science and Engineering: An Introduction”,5th Ed., John Wiley &Sons, Inc.,(2000).

[7] W.F. Smith, “Principles of Materials Science and Engineering”,3rd Ed., McGraw-Hill, Inc.,(1996).

[8] W.E. Lee and W.M. Rainforth, “Ceramic microstructures: property control by processing”, Springer, (1994).

[9] K. J. Morrisey, K. K. Czanderna, R. P. Merrill, and C. B. Carter, ‘‘Transition Alumina Structures Studied Using HREM,’’ Ultramicroscopy, 18(1985)379-6.

[10] S. Lamouri, M. Hamidouche, N. Bouaouadja, H. Belhouchet, V. Garnier, G. Fantozzi, J. Fran, O. Trelkat, “Control of the γ-alumina to α-alumina phase transformation for an optimized alumina densification”, Bol. Soc. Esp. Ceram. Vidre. 56(2017)47-54.

[11] I. Levin and D. Brandon, “Metastable Alumina Polymorphs: Crystal Structures and Transition Sequences”, J. Am. Ceram. Soc., 81 [8] (1998)1995-2012.

[12] P. Souza Santos, H. Souza Santos, S.P. Toledo, “Standard Transition Alumina’s. Electron Microscopy Studies”, Mater. Res., 3(2000)104 -114.

[13] H. Saalfeld, “The Structures of Gibbsite and of the Intermediate Products of its Dehydration”, Neues. Jahrb. Mineral. Abhandl., 95 (1960) 1-87.

[14] G.L. Messing and M. Kumagai. “Low-temperature sintering of alpha-alumina seeded boehmite gels”, Ame. Ceram. Soc. Bull., 73(1994)88-91.

[15] I. Levin, L. A. Bendersky, D. G. Brandon, and M. Ruhle, “Cubic to Monoclonic δ-Phase Transformations in Alumina”, Acta Metall. Mater., 45 [9] (1997) 3659-69.

[16] I. Levin and D. G. Brandon, “A New Alumina Polymorph with Monoclinic Symmetry”, Philos. Mag. Lett., 77 [2] (1998) 117-24.

[17] I. Levin, T. Gemming, and D. G. Brandon, “Some Metastable Phases and Transient Stages of Transformation in Alumina”, Phys. Status Solidi, A, 166 [1] (1998)197-218.

[18] D. Mo, Y.N. Xu, and W. Y. Ching, “Electronic and Structural Properties of Bulk δ-Al_2O_3”, J. Am. Ceram. Soc., 80 [5] (1997)1193-97.

[19] B. E. Yoldas, “Hydrolysis of Aluminum Alkoxides and Bayerite Conversion”, J. Appl. Chem. Biotech., 23(1973) 803-809.

[20] G. Yamaguchi, I. Yasui and W. C. Chiu, “A New Method of Preparing α-Alumina and the Interpretation of its X-ray Powder Diffraction Pattern and Electron Diffraction Pattern”, Bull. Chem. Soc. Jap., 43(1970) 2487-2491.

[21] S. Iijima, “Ultra-Fine Spherical Particles of δ -Alumina: Electron Microscopy of Crystal Structure and Surface Morphology at Atomic Resolution”, Jpn. J. Appl. Phys., 23 [6] (1984) 347-350.

[22] Y. Takeuchi, H. Umezaki and H. Kadokura, “High Puriy Alumina Derived from Aluminum Alkoxide”, Sumitomokagaku, 1993-I (1993) 4-14.

[23] G. Tiloca,“Thermal stabilization of aluminium-titanate and properties of aluminium-titanate solid solutions”, J. Mater. Sci. 26(1991) 2809-2814.

[24] J.J.M. Martonez, M.J. Melendo, “High temperature mechanical behavior of aluminium titanate ± mullite composites”, J. Eur. Ceram. Soc. 21(2001) 63-70.

[25] J. H. Park, W.J. Lee, and I. Kim, “Al_2TiO_5-machinable Ceramics Made by Reactive Sintering of Al_2O_3 and TiO_2”, J. Korean Ceram. Soc. Vol. 47(2010)498-502.

[26] Hamanok, “Effect of TiO_2 on sintering of alumina ceramic”, J. Am. Ceram. Soc. 94(1986)505.

[27] A.B. Serkan, “Effect of TiO_2 doping on microstructural properties of Al_2O_3-based single crystal Ceramics” J.Ceram.Process.Res.,12(2011) 21-25.

[28] R. Yılma, A.O. Kurt, “Effects of TiO_2 on the mechanical properties of theAl_2O_3-TiO_2 plasma sprayed coating”, J. Eur. Ceram. Soc. 271(2007)319-32.

[29] C. J. Wang, C.Y. Huang, “Effect of TiO_2 addition on the sintering behavior, hardness and fracture toughness of an ultrafine alumina”, Mater. Sci. Eng. A 492(2008)306-310.

[30] F.J. Parker, “Al_2TiO_5-$ZrTiO_4$-ZrO_2 composites: a new family of low thermal expansion ceramics,” J. Am. Ceram. Soc. 73 (1990) 929-932.

[31] I.J. Kim, H.C. Kim, “Zero level thermal expansion materials based on $ZrTiO_4$-Al_2TiO_5 ceramics synthesized by reaction sintering”, J. Ceram. Process. Res. 5 (2004) 308-312.

[32] S.K. Jha, J.M. Lebrun, R. Raj, “Phase transformation in the alumina-titania system during flash sintering experiments”, J. Eur. Ceram. Soc. 36 (2016) 733-739.

[33] M. Nagano, S. Nagashima, H. Maeda, A. Kato, “Sintering behavior of Al_2TiO_5 base ceramics and their thermal properties”, Ceram. Int. 25 (1999) 681-687.

[34] C.H. Chen, H. Awaji, “Mechanical properties of Al_2TiO_5 ceramics”, Key Eng. Mater. 336-338 II (2007) 1417-1419.

[35] S. Bueno, R. Moreno, C. Baudín, “Reaction sintered Al_2O_3/Al_2TiO_5 microcrack-free composites obtained by colloidal filtration”, J. Eur. Ceram. Soc. 24 (2004) 2785-2791.

[36] Y. Ohya, Z. Nakagawa, “Measurement of crack volume due to thermal expansion anisotropy in aluminium titanate ceramics”, J. Mater. Sci. 31 (1996) 1555-1559.

[37] A. Tsetsekou, “A comparison study of tialite ceramics doped with various materials and tialite-mullite composites: microstructural, thermal and mechanical properties,” J. Eur. Ceram. Soc. 25 (2005) 335-348,

[38] H.A.J. Thomas, R. Stevens, “Aluminium titanate a literature review. Part 1, Micro. Phenom”, Br. Ceram. Trans. J. 88 (1989) 144-151.

[39] H.C. Kim, K.S. Lee, O.S. Kweon, C.G. Aneziris, I.J. Kim, “Crack healing, reopening and thermal expansion behaviour of Al_2TiO_5 ceramics at high temperature”, J. Eur. Ceram. Soc. 27 (2007) 1431-1434.

[40] I.M. Low, D. Lawrence, R.I. Smith, “Factors controlling the thermal stability of aluminum titanate ceramics in vacuum”, J. Am. Ceram. Soc. 88 (2005) 2957-2961.

[41] N.M. Rendtorff, G. Suárez, E.F. Aglietti, “Non isothermal kinetic study of the aluminium titanate formation in alumina-titania mixtures”, Ceramica 60 (2014) 411-416.

[42] C.H. Chen, H. Awaji, “Temperature dependence of mechanical properties of aluminum titanate ceramics,” J. Eur. Ceram. Soc., 27(2007)13-18.

[43] S. Anathakumar, K.G.K. Warrier, “Extrusion Characteristics of alumina-aluminum titanate composite using boehmite as a reactive binder,” J. Eur. Ceram. Soc., 21(2001) 71-78.

[44] B. Freudenberg, and A. Mocellin, “Aluminium titanate formation by solid state reaction of coarse alumina and titania powders”, J. Am. Ceram. Soc.,71(1988)22±28.

[45] H.A.J. Thomas, and R. Stevens, “Aluminium titanate the literature review. Part I: microcracking phenomena”. Br. Ceram. Soc. Trans. J., 88(1989)144±151.

[46] J.L. Runyan and S.J. Bennison, Fabrication a of flaw tolerant aluminium titanate reinforced alumina”. J. Eur. Ceram. Soc.,7(1991)93±99.

[47] R. Baghizadeh R, H.R. Rezaie, F. Golestani-fard, "The influence of composition, cooling rate and atmosphere on the synthesis and thermal stability of aluminum titanate", Mater. Sci. Eng.B157(2009) 20-25.

[48] T. Tambas, Z.E. Erkmen and S. Ozgen, "Improvement on the Slip Casting of Bayer-Processed Alumina", Am. Ceram. Soc. Bull., 86 (2007)9201-9213.

[49] I. Ganesh, G. Sundararajan, M.O. Susana, P.M.C. Torres, J.M.F. Ferreira, "A novel colloidal processing route to alumina ceramics" Ceram. Inter., 36 (2010) 1357-1364.

[50] S.T. Alweendo, O.T.Johnson, B.M. Shongwe, F.P. Kavishe, J. O. Borode, "Microstructural and Mechanical Properties of Alumina (Al_2O_3) Matrix Composites Reinforced with SiC from Rice Husk by Spark Plasma Sintering", J. Mater. Res. 23(2020)1.

[51] A.Rafferty, A.M. Alsebaie, A.G. Olabi, T.Prescott, "Properties of zirconia-toughened-alumina prepared via powder processing and colloidal processing routes", J. Colloid. Interface. Sci. 329 (2009) 310-315

[52] T. Carolina, G.V. Frank, "Recent trends in shape forming from colloidal processing: A review", J. Ceram. Soc. Jpn., 119 (2011) 147-160.

[53] A.G. Evans, "Perspective on the Development of High-Toughness Ceramics", J. Am. Ceram Soc., 73(1990) 187-205.

[54] Z. R. Ismagilov, R. A. Shkraabina, N. A. Koryabkina, "New Technology for Production of Spherical Alumina Supports for Fluidized Bed Combustion" Catalysis Today, 47 (1999) 51-71.

[55] S.Schaffoner, C.G. Aneziris, "Pressure Slip Casting of Coarse Grain Oxide Ceramics," Ceram. Inter., 38 (2012)417–422.

[56] C.H. Schilling and I.A. Aksay, "Slip casting. In Engineered Materials Handbook of Ceramics and Glasses", American Technical Publishers, Herts, 4(1991) 153±160.

[57] J. M. F Ferreira, and O. Lyckfeldt, "Influence of the stabilizing mechanism and solid loading on slip casting of alumina". J. Eur. Ceram. Soc.,18 (1988) 479±486.

[58] J.H.D. Hampton, S.B. Savage and R.A.L. Drew, "Experimental analysis and modeling of slip casting". J. Am. Ceram. Soc.,71 (12) (1988)1040±1045.

[59] J.M.F. Ferreira, "Role of the clogging effect in the slip casting process", J. Eur. Ceram. Soc., 18 (1998) 1161±1169.

[60] F.F. Lange, "Powder processing science and technology for increased reliability". J. Am. Ceram. Soc.,72 (1) (1989)3±15.

[61] N.S. Bell, T.C. Monson, D Antonio, C.B.Wu, “Practical colloidal processing of multication ceramics”, J. Ceram. Sci. Tech.,7 (2016)1-28.

[62] N. S. Yuzbasi, T. Graule, “colloid casting processes: slip casting, centrifugal casting, and gel casting”, encyclopedia of materials: technical ceramics and glasses,1 (2021)146-153.

[63] S. Schaffoner, C.G. Aneziris, “Pressure Slip Casting of Coarse Grain Oxide Ceramics”, Ceram. Inter., 38 (2012)417-422.

[64] Y.S. Rao and R. Johnson, “Pressure Slip Casting: A novel process for Producing Alumina Bodies with Superior Green Density”, Interceram-Refractories Manual 1 (2013)218-220.

[65] A. Salomani, I. Stamenkovic, “Pressure Casting Offers Possibilities for Technical Ceramics” Am. Ceram. Soc. Bull., 79 (2000)49-53.

[66] E. Mohamed, M. Ewais, “Rheological Properties of Concentrated Alumina slurries: Influence of Ph and dispersant agent”, TESCE 30 (2004)2.

[67] E.G. Blanchard, “Pressure Casting Improves Productivity,” Am. Ceram. Soc. Bull.67 (1988)1680-1683.

[68] C.S Hogg, “A Comparison of Plaster Casting and Pressure Casting of Sanitary Ware with Particular Reference to Clay Properties”, Ceram. Inter., 11(1985) 32.

[69] A.W. Hey, A. Bresciani, L.A. Correia, R. Moreno, and A. Salomoni, “Industrial Pressure Casting of High Alumina Ceramics”, Key Engineering Materials 132(1997)350-353.

[70] R. Boulesteix, A. Goldstein, C. Perriere, A. Maitre, M. Katz, C. Coureau, “Transparent ceramics green-microstructure optimization by pressure slip-casting: Cases of YAG and $MgAl_2O_4$”, J. Euro. Ceram. Soc., 41(2021)2085-2095.

[71] S.J.L, Zhang et al. “Compaction and sintering behaviour of bimodal alumina powder suspension by pressure filtration”, J. Am. Ceram. Soc.,83(2000)737-742.

[72] K. E. Ravi, A. Lusin, S. Kumar, R.M. German, V. Sundar, “Effects of lubricant on green strength, compressibility and ejection of parts in die compaction process”, Pow. Tech., 233(2013)22-29.

[73] R. Moreno, A. Salomoni & I. Stamenkovic, “Rheology of Pressure Casting of Slips with Different Alumina Contents”, Ceramic Transactions, Ceramic Processing Science and Technology, (Eds H. Hausner, S. Hirano & G. L. Messing) Am. Ceram. Soc., Westerville, Oho. 51(1998) 379-383.

[74] Y. Ergun, C. Dirier, M. Yılmaz, C. Tokman, M. Tanoglu, “Microstructure Performance Relation in PMMA-Based Open-Cell Porous Materials for High Pressure Ceramic Sanitaryware Casting”, Key Engineering Materials 12 (2007)270-273.

[75] Y. Ergun, C. Dirier, M. Tanoglu, “Polymethyl Methacrylate Based Open-Cell Porous Plastics for High-Pressure Ceramic Casting”, Mater. Sci. Eng. A 385 (2004) 279-285.

[76] O.D. Neikov, S.S. Naboychenko and A. Nikolay, “Handbook of Non-Ferrous Metal Powders: Technologies and Applications,” Second Edition, ISBN 978-0-08-100543-9, (2019).

[77] Y. Liu, J. Zhu, “Fabrication of transparent $MgAl_2O_4$ ceramics by gel casting and cold isostatic pressing,” Ceramics International, 46(2020) 4154-4158.

[78] K. J. Morris, “Tooling for Isostatic Pressing Technology”, edited by P.J. James. Applied Science Publishers, UK, 12(1983)91-112.

[79] J.F. Harvey, “Theory and Design of Pressure Vessels”, Van Nostrand Reinhold, New York, USA, (1991)61.

[80] H.C. Jackson, “Progress in Powder Metallurgy” Int. J. Eng. Sci. 20(1964)159-168.

[81] E.L.J. Papen, “Cold Isostatic Pressing, processes and equipment”, edited by P. J. James, Applied Science Publishers, (1983)47-91.

[82] K.J. Morris, “Cold Isostatic Pressing: Encyclopedia of Advanced Ceramic Materials” (1991) 84-88.

[83] E.L.J. Papen, “Isostatic Pressing Technology”, ed. P. J. James. Applied Science Publishers, London, UK, (1983) 47-90.

[84] K.J. Morris, “In Isostatic Pressing Technology”, ed. P. J. James. Applied Science Publishers, London, UK, (1983)91-112.

[85] B.P. Bewlay, “Consolidation dynamics of tungsten powder during dry bag cold isostatic pressing”, Int. J. Refract. Met. Hard Mater.,1(1992)165-174.

[86] H. Lloyd and Symonds, “International journal of powder metallurgy”, 6 (1960)170-188.

[87] E.M. Sachs, J.S. Haggerty, M.J. Cima, P.A. Williams, “Three-dimensional printing techniques”, Google Patents, (1993).

[88] J. Deckers, J. Vleugels, J.P. Kruth, “Additive manufacturing of ceramics: a review”, J. Ceram.Sci.Technol.,5(2014)245-260.

[89] B. Utela, D. Storti, R.Anderson, M. Ganter, “A review of process development steps for new material systems in three-dimensional printing (3DP)”, Journal of Manufacturing Processes, 10(2008)96-104.

[90] H.Yang, S.Yang, X.Chi, J.R.Evans, “Fine ceramic lattices prepared by extrusion free forming”, Journal of Biomedical Materials Research Part B: Applied Biomaterials, 79(2006)116-121.

[91] Z. Xianwei, H.E.Zhang, W.Chunwei, Z.Zexiong, W.Enhui, C.Yiqing, “Hectorite modified 3D printing ceramic clay and preparation method thereom”. Chinese Patent application 108840662A, (2018).

[92] M.J. Cima, E.M.Sachs, “Three-dimensional printing: Forms, materials and performance”, SFF symposium, Texas, (1991).

[93] B.H. King, D. Dimos, P.Yang,S.L.Morissette, “Direct-write fabrication of integrated, multilayer ceramic components”, J. Electroceram., 3[2](1999)173-178.

[94] J. Kruth, M. Leu, T. Nakagawa, “Progress in additive manufacturing and rapid prototyping”, CIRP Ann-Manuf. Techn., 47[2](1998)525-540.

[95] C.M. Gomes, A.P.N. Oliveira, D. Hotza, N. Travitzky, P. Greil, “LZSA glass-ceramic laminates: Fabrication and mechanical properties,” J. Mater. Process. Tech., 206(2008)194-201.

[96] E.M. Sachs, J.S. Haggerty, M.J. Cima, P.A. Williams, “Three-dimensional printing techniques”, United States patent 5.204.055(1993).

[97] H.H. Tang, “Method and apparatus for making three-dimensional parts”, Google Patents, (2010).

[98] H.H. Tang, “Direct laser fusion to form ceramic parts”, Rapid Prototyping Journal., 8 [5] (2002) 284-289.

[99] H.H. Tang, H.C. Yen, W.H. Lin, “On ceramic parts fabricated rapid prototyping machine based on ceramic laser fusion”, SFF Symposium, Texas, 2003.

[100] L. I. Osayande and I.O. Okenwa, “Fracture Toughness Enhancement for Alumina Systems: A Review” Int. J. Appl. Ceram. Technol., 5 [3] (2008)313-323.

[101] D. Kovar, J. B. Stephen and J.R. Michael, “Crack stability and strength variability in alumina ceramics with rising toughness-curve behaviour” Acta Mater.48 (2000) 565-578.

[102] Y. Wu, Y. F. Zhang, X. Huang, J. Guo, “Microstructural development and mechanical properties of self-reinforced alumina with CAS addition” *J. Eur. Ceram. Soc.,* 21(2001) 581-587.

[103] W. Yao, J. Liu, T. B. Holland, L. Huang, Y. Xiong, J. M. Schoenung and A. K. Mukherjee, “Grain size dependence of fracture toughness for fine grained alumina”, Scr.Mater. (2011) 65.

[104] S.T. Alweendo, O.T. Johnson, B.M. Shongwe, et al. “Microstructural and mechanical properties of alumina (Al_2O_3) matrix composites reinforced with sic from rice husk by spark plasma sintering”, J. Mater. Res. (2020) 23.

[105] S. Mohantya, A. P. Ramesh babu, S. Mandal, et al. “Critical issues in near net shape forming via green machining of ceramics: A case study of alumina dental crown”, J. Asian Ceram. Soc. 1(2013)274-281.

[106] N.A. Fleck, V.S. Deshpande, M.F. Ashby, “Micro-architectured materials: past, present and future”, Proceedings of the Royal Society A: Mathematical, Physical and Engineering Sciences 466 (2010) 2495-2516.

[107] T.A. Ring, “Fundamentals of Ceramic Powder Processing and Synthesis”, Academic Press, San Diego, CA, 1996.

[108] T. Carolina, G.V. Frank, “Recent trends in shape forming from colloidal processing: A review”, J. Ceram. Soc. Jpn., 119 (2011) 147-160.

[109] C. Tallon, G. V. Franks, “Recent trends in shape forming from colloidal processing: A review”, J. Ceram. Soc. Jpn., 119 (2011) 147-160.

[110] K. Sugita, “The colloidal process-a new approach to advanced ceramics”, Adv. Mater., 4, 9(1992) 582-586.

[111] J. Binner, B. Vaidhyanathan, “Processing of bulk nanostructured ceramics”. *J. Eur. Ceram. Soc*., 28 (2008) 1329-1339.

[112] A. Cascales, N. Tabares, J. F. Bartolome et al. “Processing and mechanical properties of mullite and mullite–alumina composites reinforced with carbon nanofibers”. *J. Eur. Ceram. Soc*..35 (2015) 3613-3621.

[113] F.F. Lange, “Colloidal processing of powder for reliable ceramics” J. Am. Ceram. Soc., 72, (1989) 315.

[114] J Alzukaimi, R Jabrah, “Development of high strength large open porosity alumina ceramics using the sacrificial phase route: The role of the sacrificial phase fineness”, Ceram.Int.49(2023) 2923-2933.

[115] R.L. Coble, W.D. Kingery, “Effect of Porosity on Physical Properties of Sintered Alumina”, J. Am. Ceram. Soc., 39(11) (1956)377-385.

[116] K.S. Mazdiyasni, R.T. Dolloff, J. S. Smith II, “Preparation of High-Purity Submicron Barium Titanate Powders”, J. Am. Ceram. Soc., 52(10) (1969) 523-526.

[117] Dr. Kiyoshi Sugita, “The colloidal process: A new approach to advanced ceramics” J. Adv. Mater. 4(9) (1992) 582-586.

[118] J.A. Lewis. “Colloidal processing of Ceramics”, J. Am. Ceram. Soc 83 (2000) 2341-2359.

[119] J.S. Reed, “Introduction to the Principles of Ceramics Processing”, book, Wiley, ISBN:978-0-471-59721-6 New York, 1995.

[120] I.A. Aksay, J.A. Mangels and G.L. Messing, “Microstructure control through colloidal consolidation, in Advances in Ceramics”, American Ceramics Society, Columbus, OH, (9) (1984) 94-104.

[121] W.M. Sigmund, N.S. Bell, L. Bergstrom, “Novel powder-processing methods for advanced ceramics”. J Am Ceram Soc., (83) (2000)1557-1574.

[122] S. Rangarajan, N. Venkataraman, A. Safari, S.C. Danforth, “Powder processing, rheology, and mechanical properties of feedstock for fused deposition of Si_3N_4 ceramics”. J Am Ceram Soc. 83 (2000) 1663-1669.

[123] M. Almeida, J. Vieira, “Processing of Ceramics by Direct Coagulation Casting”, Encyclopedia Mater: Tech. Ceram. Glasses., 1 (2021) 154-161.

[124] D. Sihamoummadi, B.N. Ali, A. Alzina, O. Siham, J.L. Victor, Y. Launay, M. Mirdrikvand, W. Dreher, K. Rezwan, S. David, “Distribution of water in ceramic green bodies during drying”, J. Eur. Ceram. Soc.,19 (2009) 3164-3172.

[125] F.F. Lange, “Powder Processing Science and Technology for Increased Reliability,” J. Am. Ceram. Soc., 72 (1989) 3-15.

[126] L. Bergstrom, K. Holmberg, Ed John, “Colloidal processing of ceramics. In: Handbook of applied science and colloid chemistry”, book, Wiley & Sons, Ltd., 2001.

[127] L. Bergstrom, C.H. Schilling, I.A. Aksay, “Consolidation behaviour of flocculated alumina suspensions”, J. Am. Ceram. Soc.,75(1992)3305-3314.

[128] J. Guo and J. A. Lewis, “Aggregation Effects on Compressive Flow Properties and Drying Behaviour of Colloidal Silica Suspensions,” J. Am. Ceram. Soc., 82 [9] (1999) 2345-2358.

[129] N.S. Bell, T.C. Monson, D.C. Yiquan, “Practical colloidal processing of multication ceramics”, J. Ceram. Sci. Tech., 7 (2015) 2190-9385.

[130] S. Mende, F. Stenger, W. Peukert, J. Schwedes, “Mechanical production and stabilization of submicron particles in stirred media mills”, Powder Technol. 132 (2003) 64 -73.

[131] L. Bergstrom, CH. Schilling and I.A. Aksay, “Consolidation Behaviour of Flocculated Alumina Suspensions” Journal of the American Ceramic Society 75 (1992) 3305.

[132] F. Stenger, S. Mende, J. Schwedes, W. Peukert, “The influence of suspension properties on the grinding behaviour of alumina particles in the submicron size range in stirred media mills”, Powder Technol., 156 (2005) 103 -110,

[133] F. Stenger, W. Peukert, “The role of particle interactions on suspension rheology-application to submicron grinding in stirred ball mills”, Chem. Eng. Technol. 26 (2) (2003) 177-183.

[134] S. Blackburn, “New processes or old: Complex shape processing of advanced ceramics” Advances in applied ceramics 104 (2005) 97-102.

[135] G.V. Frank, T. Carolina, A.R. Studart, “Colloidal Processing: Enabling Complex Shaped Ceramics with Unique Multiscale Structures”, J. Am. Ceram. Soc., 2 (2016) 100-112.

[136] T.A. Otitoju, P.U. Okoye, G. Chend, L. Yang, M.O. Sanxi, “Advanced ceramic components: materials, fabrication, and applications”, Ind. Eng. Chem.,85 (2020) 34-65.

[137] R.W. Rice, ‘‘Ceramic Processing: An Overview,’’ A.I. Ch.E. J., 36 [4] (1990) 481-510.

[138] L.C. Lim, P.M. Wong, J. Ma. “Colloidal processing of sub-micron alumina powder compacts”, J. Mater. Process. Technol. 67 (1997) 137-142.

[139] I. Ganesh, G. Sundararajan, M. Susana et al. “A novel colloidal processing route to alumina ceramics”, Ceram. Int.36(2010) 357-1364.

[140] T. Tambas, Z. E. Erkmen and S. Ozgen, “Improvement on the Slip Casting of Bayer-Processed Alumina”, American Ceramic Society Bulletin, 86 (2007) 9201-9213.

[141] Z.R. Ismagilov, R.A. Shkraabina, N.A. Koryabkina, “New Technology for Production of Spherical Alumina Supports for Fluidized Bed Combustion” Catalysis Today, 47 (1999) 51-71.

[142] P.A. Badkar, “Alumina ceramics for high temperature applications. Key Engineering Materials”, 57 (1991) 45±58.

[143] C.M. Lambe, W.D. Kingery, “Preparation and use of plaster moulds. In Ceramic Fabrication Processes”, American Ceramic Society, Columbus, OH, (1874)31±40.

[144] D.S. Adcock, & I. C. Mcdowall, “Mechanism of filter pressing and slip casting”, J. Am. Ceram. Soc., 40 (1957) 355±362.

[145] M. Murfin et al. “Slip casting is a time- and energy-consuming process that is ideal for producing large components and thin-walled bodies with complex shapes”, Sci. Res. Essays 11 (2009) 302-314.

[146] I.A. Aksay & S.H. Schilling, “Mechanics of colloidal filtration” American Ceramic Society, Columbus, 9(1984).

[147] A. Evcin, “Investigation of the effects of different deflocculants on the viscosity of slips”, Sci. Res. Essays 6 (11) (2011) 2302-2305.

[148] H. Sarraf, J. Havrda, “Rheological behaviour of concentrated alumina suspension: effect of electro steric stabilization”, Ceramics 51 (3) (2007) 147-152.

[149] K. Shqau, “Electrosteric Dispersants Used in Colloidal Processing of Ceramics, Literature Review”, The Ohio State University/Group Inorganic Materials Science, (2005)1-17.

[150] I. Sever, I. Zmak, L.Curkovic, Z. Svageli, “Stabilization of highly concentrated alumina suspension with different dispersants”, Trans. FAMENA XLII-3 (2018) 61-70.

[151] A. Papo, L. Piani, “Rheological properties of alumina slurries: effect of deflocculant addition”, Part. Sci. Technol. 25 (2007) 375-380

[152] C. Tallon, M. Limacher, G.V. Franks, “Effect of particle size on the shaping of ceramics by slip casting*”, J. Eur. Ceram. Soc.*.30 (2010) 2819-2826.

[153] R.J. Hunter, “Foundations of Colloid Science”, Vol. 1, book Oxford University Press, 1995.

[154] P.C. Heimenz, “Principles of Colloid and Surface Chemistry”, 2nd edn, Marcel Dekker, New York, 1986.

[155] A. Tonck, J.M. Georges and J.L. Loubet, “Measurements of the in termolecular forces and rheology of dodecan between alumina surfaces”. J. Coll. Interf. Sci., 126 (1988) 151±163.

[156] P.F. Luckham, “The measurement of interparticle forces. Powder Techn”, 58 (1989) 75±91.

[157] W.E. Lee and W.M. Rainforth, “Ceramic Microstructure-Property Control by Processing”, ed. Chapman & Hall, London, 1994.

[158] P.F. Luckham, M.A. Ansarifar, and L. Costello, “The relationship between interparticle forces and the bulk rheology of suspensions,” Powder. Techn. 65 (1991) 371±379.

[159] R.G. Horn, “Surface forces and their action in ceramic materials”. J. Am. Ceram. Soc, 73 (1990)1117±3115.

[160] D.S. Adcock & I.C. Mcdowall, “Mechanism of filter pressing and slip casting”, J. Am. Ceram. Soc., 40 (1957) 355±362.

[161] G. Tari, J.M.F. Ferrerira, O. Lyckfeld, “Infuence of the Stabilising Mechanism and Solid Loading on Slip Casting of Alumina” *J. Eur. Ceram. Soc.*.18 (1998) 479±486.

[162] F.M. Tiller, C.D. Sao et al. “Theory of filtration of ceramics: 1. slip casting,” J Am Ceram Soc. 69(1986)882-887.

[163] I.T. Sao & R.A. Haber, “The effect of dispersant concentration on the cast structure and rheology”. In Ceramics Transactions, Vol. 26, ed. M. Cima. American Ceramic Society, Columbus, 1992.

[164] F.M. Tiller & N.B. Hysing, “Theory of filtration of ceramics: II. Slip casting on radial surfaces”. J. Am. Ceram. Soc., 74(1) (1991) 210±218.

[165] B. Kostic, D. Kicevic & M. Gasic, “Mathematical modelling of ceramic slip casting”, Ceramics International, 16 (1990) 281±284.

[166] A.O. Boschi, “Effects of different forming processes on the sinterability of rutile”. Ph.D. thesis, Leeds University, 1986.

[167] P.H. Dal & W. Deen, “The forming of ceramic bodies during the slip casting process”. 6th International Ceramic Congress, Wiesbaden, 1958.

[168] T.J. Fennelly, and J.S. Reed, “Mechanics of Pressure Slip Casting”, Journal of the American Ceramic Society, 55(1972)264-268.

[169] F.F. Lange and K.T. Miller, “Pressure Filtration: Consolidation Kinetics and Mechanics”, American Ceramic Society Bulletin, 66(1987)498-1504.

[170] R. R. Rowlands, “Review of the Slip Casting Process,” Amer. Ceram. SOC. Bull., 45 (1966)16-19.

[171] W. E. Hauth, “Slip Casting of Aluminum Oxide,” J. Amer. Ceram. SOC., 32 [12] (1949)394-98.

[172] M.P. Greene “Pressure casting sanitaryware”. cfi–Ceramic Forum International 81(11) (2004) E37-E38.

[173] J. Kraus, “High pressure casting of hollow articles – also with a more complex shape”, cfi–Ceramic Forum International 86(8) (2009) E54-E55.

[174] H. P. Grace, “Resistance and Compressibility of Filters,” Chern. Eng. Progr., 49 [6] (1953)303-318.

[175] R. Moreno, A. Salomoni, I. Stamenkovic, S.M. Castanh, “Colloidal filtration of silicon nitride aqueous slips, Part II: Slip casting and pressure casting performance”, J. Eur. Ceram. Soc., 19 (1999) 49-59.

[176] R. Moreno, A. Salomoni I. Stamenkovic, “Influence of slip rheology on pressure casting of alumina”, 17(1997)327-331.

[177] R. Buscall, L.R. White, “The consolidation of concentrated suspensions: Part 1. The theory of sedimentation”. J. Chem. Soc., Faraday Trans. 83(1987) 873-891.

[178] D. Kretser, R.G. Usher, S.P. Scales, P.J. Boger, “Rapid filtration measurement of dewatering design and optimization parameters”. AIChE, 47(2001)1758-1769.

[179] R. Papitha, M.B. Suresh, Y.S. Rao, B.P. Saha, D. Das, R. Johnson, “Pressure slip casting and cold isostatic pressing of aluminum titanate green ceramics: A comparative evaluation” Processing and Application of Ceramics 7 [4] (2013) 159-166.

[180] S. Maleksaeedi, M.H. Paydar, S. Saadat, H. Ahmadi, “In situ vibration enhanced pressure slip casting of submicrometer alumina powders”, J. Eur. Ceram. Soc., 28 (2008) 3059-3064.

[181] T.J. Fennelly, J.S. Reed, “Compression permeability of Al_2O_3 cakes formed by pressure casting”, J. Am. Ceram. Soc., 55 [8] (1972) 381-383.

[182] A. Solomoni, R. Moreno, E. Rastelli, I. Stamenkovic, L. Esposito, “Correlation between rheological behaviour of alumina slip and characteristics of pressure cast bodies”, Key Eng. Mater., 132 (1997) 346-349.

[183] A.W Hey, A. Bresciani, L. Correia, R. Moreno, “Industrial pressure casting of alumina ceramics”, Key Eng. Mater.,136 (1997) 350-353.

[184] Y.S. Rao and R.Johnson, “Pressure Slip Casting: A novel process for Producing Alumina Bodies with Superior Green Density, Interceram-Refractories Manual 1 (2013) 218-220.

[185] Y Ma, Z Wang, Y Qin, “Impact of characteristic length and loading rate upon dynamic constitutive behavior and fracture process in alumina ceramics”, Ceram. Inter.,49(2023) 4775-4784.

[186] A. Tsetsekou, C. Agraotis, A. Milias, “Optimization of the rheological properties of alumina slurries for ceramic processing applications Part I: Slip-casting” *J. Eur. Ceram. Soc.,* 21 (2001) 363±373.

[187] S.M. Olhero, J.M.F. Ferreira, “Influence of Particle Size Distribution on Rheology and Particle Packing of Silica-Based Suspensions”, Powder Technol., 139(1) (2014)69-75.

[188] D. Bourcier, J.P. Fraud, D. Colson et al. “Influence of particle size and shape properties on cake resistance and compressibility during pressure filtration,” Chem. Eng. Sci. 144(2016)176-187.

[189] L. Bergstrom, “Colloidal processing of ceramics-technology and science”, in: H. Hausner, G.L. Messing, S. Hirano (Eds.), Ceramic Processing Science and Technology, Ceramic Transactions, vol. 51, The Am. Ceram. Soc., Westerville, Ohio, (1995) 341-348.

[190] G.K. Khoe, T.L. Ip, J.R. Grace, “Rheological and fluidisation behaviour of powders of different particle size distribution”, Powder Technol. 66 (1991) 127-141.

[191] D.C.H. Cheng, A.P. Kruszewski, J.R. Senior, “The effect of particle size distribution on the rheology of an industrial suspension,” J. Math. Sci. 25 (1990) 353-373.

[192] T. Dabak, O. Yucel, “Modelling of the concentration and particle size distribution effects on the rheology of highly concentrated suspensions”, Powder Technol. 52 (1987) 193-206.

[193] P.A. Smith, R.A. Haber, “Effect of particle packing on the filtration and rheology behaviour of extended size distribution alumina suspensions”, J. Am. Ceram. Soc. 78 (7) (1995) 1737-1744.

[194] B.V. Velamakanni, F.F. Lange, “Effect of interparticle potentials and sedimentation on particle packing density of bimodal particle distributions during pressure filtration”, J. Am. Ceram. Soc. 74 (1) (1991) 166-172.

[195] S. Raha, K.C. Khilar, P.C. Kapur, “Regularities in pressure filtration of fine and colloidal suspensions,” Inter J Miner Process, 84 (2007) 348-360.

[196] G V Frank, T Carolina, A R Studart, “Colloidal Processing: Enabling Complex Shaped Ceramics with Unique Multiscale Structures”, J. Am. Ceram. Soc., 12 (2016) 100-112.

[197] C Wu, Q Liu, R Chen, J Wang, W Liu, S Yao, Y Ma, “Mechanism of grain refinement and growth for the continuous alumina fibers by MgO addition”, Ceramics International 94(2022)60-82.

[198] R. Bai, C. Tien, “Further work on cake filtration analysis”, Chem. Eng. Sci. 60 (2005)301-313.

[199] S.M.H. Banda, K.S.E. Forssberg, “Structure variation in filter cakes from flocculated slurries”, Scand. J. Metal. 17(1988)57-60.

[200] L. Besra, D.K. Sengupta, S.K. Roy, “Flocculation and dewatering of kaolin suspensions in the presence of polyacrylamide and surfactants.” Int. J. Miner. Process. 66(2002)203-232.

[201] U. Klippel, C.G. Aneziris, A.J. Metzger, “Shaped coarse-grained refractories by pressure slip casting,”Adv. Eng. Mater. 13 (2011) 68-76.

[202] N. Gerlach, C.G. Aneziris, F.F.Lange, H. Grote, “Coarse-grained ceramic heat shields made by pressure slip casting” , Ceram. Forum. Int. 93 (3) (2016) 1-15.

[203] G. Cordoba, R. Moreno, A. Salomoni, & I. Stamenkovic, “Rheology of pressure casting of slips with different alumina contents. Ceramic Transactions, vol. 51: Ceramic

Processing Science and Technology," eds H.Hausner, S. Hirano & G. L. Messing. The American Ceramic Society, Westerville, OH, (1995)379-383.

[204] A. Salomoni, I. Stamenkovic, A. Tucci. & L.Esposito, "Sintering of alumina and zirconia greens obtained via slip casting and pressure slip casting. Ceramic Transactions: Forming Science and Technology for Ceramics", J. Cima. Am. Ceram. Soc., (1992)178.

[205] K. Moritz, N. Gerlach, J.Hubalkova, C.G.Aneziris, "Pressure slip casting of coarse-grained alumina-carbon materials" Int. J. Appl. Ceram.Technol. 16(2019)14-22.

[206] S. Schafföner, L. Freitag, J. Hubálkova, C.G. Aneziris, "Functional composites based on refractories produced by pressure slip casting" J. Eur. Ceram. Soc.,36 (2016) 2109-2117.

[207] H.C. Weerasinghe, P.M. Sirimanne, G.P. Simon, Y.B. Cheng, "Cold isostatic pressing technique for producing highly efficient flexible dye-sensitised solar cells on plastic substrates", Prog. Photovolt.: Res. Appl. 20 (3) (2012) 321-332.

[208] J. Shao, F. Liu, W. Dong, R. Tao, Z. Deng, X. Fang, S. Dai, "Low temperature preparation of TiO2 films by cold isostatic pressing for flexible dye-sensitized sol cells", Mater. Lett. 68 (2012) 493-496.

[209] H.C. Yang, J.K. Kim, K.T. Kim, "Rubber isostatic pressing and cold isostatic pressing of metal powder", Mater. Sci. Eng.: A 382 (1-2) (2004) 41-49,

[210] Y. Gu, R.J. Henderson, H.W. Chandler, "visualizing isostatic pressing of ceramic powders using finite element analysis", J. Eur. Ceram. Soc., 26 (12) (2006) 2265-2272.

[211] C.Y. Huang, G.S. Daehn, "Densification of composite powder compacts in pressure cycling", Acta Mater. 44 (3) (1996) 1035-1045.

[212] G. Jiang, G.S. Daehn, R.H. Wagoner, "Observations on densification of Al-Al_2O_3 composite powder compacts by pressure cycling, Pow. Metall. 46 (1) (2003) 78-82.

[213] A. Tavakoli, A. Simchi, S.S. Reihani, Study of the compaction behavior of composite powders under monotonic and cyclic loading, Compos. Sci. Technol. 65 (14) (2005) 2094-2104,

[214] S. Schafföneraa, J. Fruhstorfer, S. Ludwig, C.G. Aneziris, "Cyclic cold isostatic pressing and improved particle packing of coarse grained oxide ceramics for refractory applications" Ceram. Inter., 8(44) (2018) 9027-9036.

[215] Y. Fu, Z. Tao, X. Houn, "Weibull distribution of the fracture strength of 99% alumina ceramic reshaped by cold isostatic pressing" Ceram. Inter., 40 (2014) 7661-7667.

[216] B. Utela, D. Storti, R.Anderson, M. Ganter, “A review of process development steps for new material systems in three-dimensional printing (3DP)”, J. Manuf. Process.10 (2008) 96-104.

[217] E.M. Sachs, J.S. Haggerty, M.J. Cima, P.A. William s, “Three-dimensional printing techniques,” Google Patents, (1993).

[218] J. Deckers, J. Vleugels, J.P. Kruth, “Additive manufacturing of ceramics: a review,” Journal of Ceramic Science and Technology, 5(2014) 245-260.

[219] I. Gibson, D. Rosen, B. Stucker, “Additive manufacturing technologies: 3D printing, rapid prototyping, and direct digital manufacturing,” Springer, 2014.

[220] P. Colombo, G. Mera, R. Riedel, G.D. Soraru, “Polymer-derived ceramics: 40 years of research and innovation in advanced ceramics,” J. Am. Ceram. Soc., 93(2020)1805-1837.

[221] U. Scheithauer, E. Schwarzer, T. Moritz, A. Michaelis, “Additive Manufacturing of Ceramic Heat Exchanger: Opportunities and Limits of the Lithography-Based Ceramic Manufacturing (LCM),” J. Mater. Eng. Perform., 27(2018)14-20.

[222] H.L. Marcus, J.J. Beaman, J.W. Barlow, D.L. Bourell, “Solid freeform fabrication powder processing,” American Ceramic Society Bulletin 69 (6) (1990) 1030-1031.

[223] E. Sachs, M. Cima, J. Cornie, “Three-dimensional printing: rapid tooling and prototypes directly from a CAD model”, CIRP Annals-Manufacturing Technology 39 (1) (1990) 201-204.

[224] M. Zhou, W. Liu, H. Wu, X. Song, Y. Chen, L. Cheng, F. He, S. Chen, S. Wu, “Preparation of a defect-free alumina cutting tool via additive manufacturing based on stereolithography -Optimization of the drying and debinding processes”, Ceram. Inter., 42(2016) 11598-11602.

[225] Z. Chen, Z. Li, J. Li, C. Liu, C. Lao, Y. Fu, C Liu, Y. Li, P. Wang, Y. He, “3D printing of ceramics: A review*”, J. Eur. Ceram. Soc.,* 4 [39] (2019)661-6870.

[226] U. Scheithauer, E. Schwarzer, H-J Richter, T. Moritz, “Thermoplastic 3D printing- an additive manufacturing method for producing dense ceramics”, International Journal of Applied Ceramic Technology,12(2015)26-31.

[227] R. Hea, W. Liua, Z. Wua, D. An, M. Huang, H. Wu, Q. Jiang, X. Ji, S. Wu, Z. Xie, “Fabrication of complex-shaped zirconia ceramic parts via a DLP stereolithography-based 3D printing method”, Ceramic International, 44(2018)3412-3421.

[228] H. Wu, D. Li, Y. Tang, B. Sun, D. Xu, “Rapid fabrication of alumina-based ceramic cores for gas turbine blades by stereolithography and gel casting”, Journal of Materials Processing Technology, 209(2009)5886-5891.

[229] M.C. Leu, L. Tang, B. Deuser, R.G. Landers, G. E. Hilma, S. Zhang, J. Watts, “Freeze-form extrusion fabrication of composite structures”, Reviewed article 09(2011).

[230] M.L. Griffith, J.W. Halloran, “Freeform fabrication of ceramics via stereo-lithography”, Journal of the American Ceramic Society, 79(1996)2601-2608.

[231] J.W. Halloran, V. Tomeckova, S. Gentry, S. Das, P. Cilino, D. Yuan, R. Guo, A. Rudra raju, P. Shao, T. Wu, “Photopolymerization of powder suspensions for shaping ceramics*”, J. Eur. Ceram. Soc.*.31(2011)2613-2619.

[232] C.J. Bae, A. Ramachandran, J.W. Halloran, “Quantifying particle segregation in sequential layers fabricated by additive manufacturing”, *J. Eur. Ceram. Soc.*.38(2018)4082-4088.

[233] H. Xing, B. Zou, S. Li, X. Fu, “Study on surface quality, precision and mechanical properties of 3D printed ZrO_2 ceramic components by laser scanning stereolithography”, Ceram. Inter., 43(2017)16340-16347

[234] C.J. Bae, “Integrally cored ceramic investment casting mold fabricated by ceramic stereolithography”, University of Michigan, (2008).

[235] W.Z. Zhou, D. Li, Z. W. Chen, S. Chen, “Direct fabrication of an integral ceramic mould by stereolithography”, Proceedings of the Institution of Mechanical Engineers Part B-J.Manuf.Eng.,224(2010)237-243.

[236] Z. Chen, D. Li, W. Zhou, “Process parameters appraisal of fabricating ceramic parts based on stereolithography using the Taguchi method, Proceedings of the Institution of Mechanical Engineers”, Part B: J.Manuf.Eng.,226(2012)1249-1258.

[237] N.T. Nguyen, N. Delhote, M. Ettorre, D. Baillargeat, L. L. Coq, R. Sauleau, “Design and characterization of 60-GHz integrated lens antennas fabricated through ceramic stereolithography”, IEEE Transactions on Antennas and Propagation, 58(2010)2757-2762.

[238] S.J. Leigh, C. Purssell, J. Bowen, D.A. Hutchins, J.A. Covington, D. Billson, “A miniature flow sensor fabricated by micro-stereolithography employing a magnetite/acrylic nanocomposite resin”, Sensors and Actuators A: Physical, 168(2011)66-71.

[239] Q. Lian, W. Sui, X. Wu, F. Yang, S. Yang, “Additive manufacturing of ZrO_2 ceramic dental bridges by stereolithography”, Rapid Prototyp. J., 24(2018)114-119.

[240] C.J. Bae, J.W. Halloran, “Influence of residual monomer on cracking in ceramics fabricated by stereolithography”, Int. J. Appl. Ceram., 8(2011)1289-1295.

[241] T. Huang, M.S. Mason, G.E. Hilmas, M.C. Leu, “Freeze-form extrusion fabrication of ceramic parts”, Virtual and Physical Prototyping, 1(2006)93-100.

[242] M.C. Leu, B.K. Deuser, L. Tang, R.G. Landers, G.E. Hilmas, J.L. Watts, “Freeze-form extrusion fabrication of functionally graded materials”, CIRP Ann Manuf. Technol. CIRP ANN-MANUF TECHN, 61(2012)223-226.

[243] R. Gmeiner, G. Mitteramskogler, J. Stampfl, A.R. Boccaccini, “Stereolithographic ceramic manufacturing of high strength bioactive glass”, Int. J. Appl. Ceram., 12(2015)38-45.

[244] M. Schwentenwein, P. Schneider, J. Homa, “Lithography-based ceramic manufacturing: a novel technique for additive manufacturing of high-performance ceramics”,J.Adv.Sci.Technol.,88(2014)60-64.

[245] U. Scheithauer, E. Schwarzer, G. Ganzer, A. Kornig, W. Becker, E. Reichelt, M. Jahn, A. Hartel, H. Richter, T. Moritz, “Micro-Reactors Made by Lithography-Based Ceramic Manufacturing (LCM), Additive Manufacturing and Strategic Technologies in Advanced Ceramics”, Ceram. Trans. 258(2015)31-41.

[246] A. Bose “Advances in Particulate Materials”, Boston: Butterworth Heinemann, (1995).

[247] Y.M. Chiang, D. P. Birnie, and W. D. Kingery. “Physical Ceramics: Principles for Ceramic Science & Engineering” New York: John Wiley & Sons, (1997).

[248] Asthana, Rajiv, “Materials Processing and Manufacturing Science, Powder Metallurgy and Ceramic Forming”, (2006).

[249] R.M. German, “Powder Metallurgy Science. Princeton”, NJ: Metal Powder Industries Federation (MPIF), (1994).

[250] I. Chang, Y. Zhao, “Advances in powder metallurgy: properties, processing and applications”, UK, (2013).

[251] J.M. Torralba, “Comprehensive Materials Processing, Improvement of Mechanical and Physical Properties in Powder Metallurgy”, (2014) 281-294.

[252] K. S. Esamael, A. Fatalla, “Evaluation on processing parameter’s effects on some mechanical properties of pure magnesium bulk prepared by powder metallurgy” Materials Today: Proceedings 57 (2022) 622-629.

[253] H. Merkus, “Particle Size Measurements”, Dordrecht: Springer Netherlands, (2009)259-285.

[254] H.C. Hulst, “Light scattering by small particles”, Dover; New York, (1957).

[255] C. Bohren and D.Huffman, “Absorption and Scattering of Light by Small Particles”, Weinheim Wiley-VCH Verlag GmbH & Co. KGaA, (2007)381-428. 3.ISO 13320:20009.

[256] H.C. Hulst, “Light scattering by small particles”, Dover; New York,(1957).

[257] Kerker, Milton, “The scattering of light, and other electromagnetic radiation Physical chemistry”, 16(1969) Academic Press; New York.

[258] B.J. Berne, R. Pecora, “Dynamic light scattering” John Wiley & Sons, Inc.; New York, (1976).

[259] B.E. Dahneke, “Measurement of suspended particles by quasi-elastic light scattering” Wiley-Interscience; New York, (1983).

[260] I H. Merkus, “Particle Size Measurements”, Dordrecht: Springer Netherlands, (2011)759-779.

[261] Schmitz, S. Kenneth, “An introduction to dynamic light scattering by macromolecule”, Academic Press; Boston (1990).

[262] K. Thamaphat, P. Limsuwan, B. Ngotawomchai, “Phase Characterization of TiO_2 Powder by XRD and TEM. Nat. Sci.42(2008)357-361.

[263] G.W. Brindley, G. Brown, “Crystal Structures of Clay Minerals and Their Identification”, Mineralogical Society: London(1980).

[264] J.R. Connolly, “Introduction to X-Ray Powder Diffraction” Spring (2007).

[265] S.S. Iyengar, V.E. Buhrke, R. Jenkins, D.K. Smith, “Sample Preparation for Clays in Preparation of Specimens for X-ray Fluorescence and X-ray Diffraction Analysis” Wiley-VCH: New York (1997).

[266] R.J. Pugh and L. Bergstrom, ¨ Surface and Colloidal Chemistry in Advanced Ceramics Processing”, Marcel Dekker, New York (1994).

[267] J.S. Reed, “Introduction to the Principles of Ceramics Processing”, Wiley, New York (1988).

[268] I.A. Aksay, “Microstructure control through colloidal consolidation, in Advances in Ceramics”, Am. Ceram. Soc., Columbus19(1984) 94-104.

[269] W.B. Russel., D.A. Saville, and W.R. Showalter, “Colloidal Dispersions, Rheology of Concentrated Suspensions in Surfaces and Conoid Chemistry in Advanced Ceramics Processing", Surfactant Science Series, Marcel Dekker, New York. 51(1994) 193-244.

[270] H. Myung, Kim and James, L. White, “A Non-Newtonian Model Of Flow In Forward And Backward Pumping Screw Regions Of A Modular Tangential Counter-Rotating Twin Screw Extruder”, Journal of Non-Newtonian Fluid Mechanics, 37(1990)37-53.

List of the publications from the current research work

1. “Pressure Slip Cast Processing of Alumina (Al_2O_3) Products and Comparative Evaluation of Mechanical Properties” P Raju, Asit kumar khanra, Y S Rao, Roy Johnson, Journal of Advances in Applied Ceramics, 2022 accepted and published.
2. “Investigations on colloidal and dry formed alumina parts under pressure and pressure-less conditions” P Raju, Asit Kumar Khanra, Papiya Biswas, Y S Rao, Roy Johnson, Journal of Processing and Applications of Ceramics, 2022 accepted and published.
3. “Superior sliding wear performance of pressure slip cast Alumina bodies” P Raju, Asit Kumar Khanra, S Kumar, YS Rao, Roy Johnson, Journal of Material Sciences, 2022 accepted and published.

About the author

The author was born in Nashkal, nearby Warangal in Telangana State, India on 23rd August 1986. After completion of his B. Tech in Mechanical engineering in the year 2009 from G Pulla Reddy Engineering College, he worked as faculty for a period of 4 years and then he joined for his M. Tech in Materials Technology discipline at National Institute of Technology, Warangal (NITW), Telangana, India in the year 2013. After completing his M. Tech in 2015, the author worked as faculty for a period of 2 years. Then after joined as Senior Research Fellow in Centre for Advanced Ceramic Materials at International Advanced Research Centre for powder Metallurgy and New Materials (ARCI) Hyderabad. Also as external candidate he registered his PhD at National Institute of Technology Warangal, Telangana, India. The author published several papers in international journals and presented his research work at international conferences**.**